NUMERICAL SIMULATIONS OF FLOW THROUGH MODEL PAPER MACHINE FORMING FABRICS

by

Zhaolin Huang

B.S., Peking University, 1987

M.S., Peking University, 1990

A THESIS SUBMITTED IN PARTIAL FULFILLMENT OF

THE REQUIREMENTS FOR THE DEGREE OF

MASTER OF APPLIED SCIENCE

in

THE FACULTY OF GRADUATE STUDIES

DEPARTMENT OF MECHANICAL ENGINEERING

We accept this thesis as conforming

to the required standard

THE UNIVERSITY OF BRITISH COLUMBIA

August 2003

In presenting this thesis in partial fulfillment of the requirements for an advanced degree at the University of British Columbia, I agree that the Library shall make it freely available for reference and study. I further agree that permission for extensive copying of this thesis for scholarly purposes may be granted by the head of my department or by his or her representatives. It is understood that copying or publication of this thesis for financial gain shall not be allowed without my written permission.

Zhaolin Huang
Department of Mechanical Engineering
The University of British Columbia
Pulp and Paper Centre
2385 East Mall
Vancouver, Canada
V6T 1Z4

Date: Aug 20th, 2003

Abstract

In the manufacture of high quality paper, it is of vital importance that the fiber distribution in the web be as uniform as possible so that the best formation is attained. In order to provide for uniform dewatering and uniform fibre distribution, a uniform velocity profile is desired upstream of the paper side fabric layer. To understand the factors that affect the flow upstream of the forming fabric, a computational model has been applied to study the flow details through paper machine forming fabrics.

The flow through the forming fabric is three-dimensional and involves interaction with wood fibers and fines, and is therefore extremely complicated to model in full. To avoid these difficulties, simplified model was proposed. The flow through forming fabrics was modeled as two-dimensional laminar water flow around cylinder arrays of unequal sizes. All calculations are done using FLUENT™, a commercially available CFD software.

A systematic study on both an existing forming fabric i.e., the commercial 73 x 75 mesh triple-layer fabric, and a hypothetical triple-layer fabric was performed. Under their current configurations, there is little variation of the flow upstream of the fabric caused by the machine side mesh.

The effect of several design parameters of the two fabrics were investigated, such as the z direction separation between the paper side and machine side layers, the diameter ratio of two-row cylinders, the second row spacing between two adjacent cylinders, and variable second row spacing between two adjacent cylinders. The simulations showed that upstream flow was non-uniform and may cause formation problems for several conditions. First, when the forming fabric has fine mesh in both paper and machine sides, changes in z direction separations of the two layers, diameter ratios, or offsets between two layers appear to have little impact on the velocity profiles upstream. Second, when the fabric has a fine mesh in the paper side and a coarse mesh in the machine side, the z direction separation between the paper side and machine side layers has the most significant effect on the flow non-uniformity. When this separation is greater than approximately $2d$, where d is the diameter of filaments on the paper side layer, the variations on the velocity profile are negligible. Third, the steady simulation gives the

same trend of the impact on flow upstream as the unsteady simulation. Fourth, the unequal cross-machine direction (CD) separations of the machine side layer also have a significant impact on the flow upstream. The CD separation of the machine side layer should be kept as constant as possible; otherwise a larger z direction separation between the two layers is required to eliminate the impact on flow upstream. As a rough rule of thumb, provided the fine layer is more than L upstream of the coarse layer, where L is the scale of the largest irregularity in the downstream fabric (e.g. the width of two grouped filaments), then the flow above the fine layer is unaffected by the coarse layer.

This two-dimensional model can only address the wire marks in the cross direction, not in the machine direction. It cannot distinguish double-layer fabrics from single-layer ones or different triple-layer fabrics among many configurations of CD filaments. Developing a three-dimensional model is thus recommended for future work.

Table of Contents

List of Tables

List of Figures

List of Symbols

a	x-coordinate of the center of the vortex cores divided by the diameter D
b	y-distance between the vortex cores divided by the diameter D
Cd	drag coefficient
Cl	lift coefficient
d	cylinder diameter (m)
D	cylinder diameter (m)
f	vortex shedding frequency
g	gap between the cylinder centers divided by the diameter d
$G1$	gap between the first-row cylinder centers (m)
$G2$	gap between the second-row cylinder centers (m)
k	permeability of a fibre mat
L	length of separation bubbles divided by the diameter D
p	pressure (Pa)
R	roll radius (m)
Re	Reynolds number
St	Strouhal number
t	time (s)
T	vortex shedding period (s)
T_f	fabric tension (N/m)
u, U	x velocity (m/s)
U_o	free stream velocity (m/s)
v, V	y velocity (m/s)
x	x coordinate (m)
y	y coordinate (m)
Y	offset of the second row (m)
z	center-to-center separation between the two rows (m)
z/d	two-row's center-to-center separation to first-row cylinder diameter ratio
Z	perimeter separation between the two rows (m)
Z/d	two-row's surface-to-surface separation to first-row cylinder diameter ratio
θ	separation angle(°)
λ	blockage ratio
ν	kinematic viscosity (m^2/s)
ρ	fluid density (kg/m^3)
Δp	pressure difference across the mat
Δt	time step

Acknowledgements

I would like to express my gratitude to all those who offered me support and assistance throughout my studies at UBC, especially to my supervisors, Dr. Sheldon I. Green, Dr. James A. Olson and Dr. Richard J. Kerekes for their advice, encouragement and patience.

Dr. Carl F. Ollivier-Gooch provided helpful discussions at the beginning of my studies. The time he invested and the courses he offered were greatly appreciated.

I would also like to thank Alan Steeves and Jay Zhao of UBC Mechanical Engineering computer networks for their help with software applications.

Thanks to Leonard Drakes and Doug Yuen of the UBC Mechanical Engineering machine shop for their contributions to the experimental apparatus.

Deserving of special mention are my friends and fellow students at UBC, especially Edmond Young, Monica Feng, Jean-Louis Iaconis, Karl Davis, Mark Epp, Barbara Dalpke, Hildur Ingvarsdóttir, and Michelle Corinne Straver.

Thanks are also due to people at Pulp and Paper Center for their continuous assistance and support.

I would like to express my sincere thanks to AstenJohnson and NSERC for their financial support.

On a more personal level, I would like to thank my family for their unstinting support. I could never finish my work without their continuous encouragement.

Chapter - 1 Introduction

The significance of paper and paper products in modern life is obvious. Paper provides the means of recording, storage and dissemination of information; virtually all writing and printing is done on paper. It still has a key role in communication and is needed in many areas of our society. It is the most widely used wrapping and packaging material, and is important for structural applications.

Paper has traditionally been defined as a felted sheet formed on a fine screen from a water suspension of fibers. Current paper products generally conform to this definition except that most products also contain non-fibrous additives. The fine screen here is the forming fabric.

The function of the paper machine is to transform a pulp suspension into a uniform, dry sheet of fibres. The requirements are efficient operations at high speed.

One essential requirement is that the formed paper web is uniform in its structure. This requirement applies to machine-direction, cross-direction, and z-direction material distribution and composition. This requires certain designs in all sections of the machine. The forming section and the press section are the most critical from this point of view. Our study addresses the design of forming fabrics in the forming section.

1.1 Paper machine and papermaking

The first historical mention of paper was in 105 A.D. in China [1]. The original inventor is believed to be Chinese, Cai Lun, who indeed became the god of paper makers.

The oldest method of paper making in China was with a floating mold. The principle involves pouring a fixed amount of fibre suspension onto a mold partially submerged in water. The mold consists of a wooden frame with coarsely woven cloth stretched across it. The water draining through the cloth leaves the fibre web on top. The cloth with the paper on top is dried, and the sheet is pulled off when dry. This coarsely woven cloth is what is now called forming fabric.

Paper continued to be made by hand up to the beginning of 19th century. Nicolas-Louis Robert (1761-1828) has gone down in history as the inventor of a continuous

moving belt of wire cloth on which the fibre suspension was spread and the water was allowed to drain away, leaving an endless sheet of paper on the wire. His patent was granted in 1799.

Since the days of Nicolas-Louis Robert, the paper machine has undergone continual development, making it possible to produce wider webs of paper at ever increasing speeds. The first machine ever to be built and successfully operated was started up in England in 1803. The Fourdrinier brothers had acquired all patents by 1807 and the machine eventually became known as the Fourdrinier machine [2]. A schematic drawing of a Fourdrinier machine is given in Figure 1.1. The paper machine consisted of a headbox adding paper stock to a moving wire supported between two rolls. The wet sheet was pressed once on the wire and then taken to a felt and run through another press nip before being accumulated on a roll for eventual drying in sheet form.

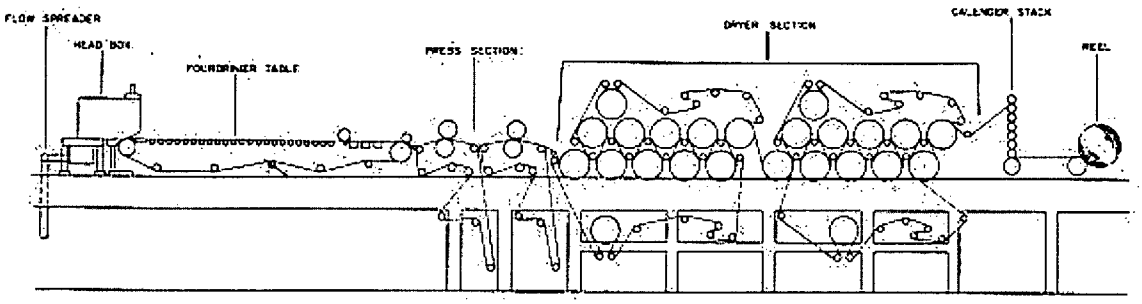

Figure 1.1 Fourdrinier paper machine [2]

Twin-wire formers were developed in order to drain the water from top and bottom of the web simultaneously, allowing paper to be made at higher speed. Since the invention of the first modern twin-wire roll former by David Webster in 1953, a number of two-wire designs, such as the blade former, gap former and hybrid former, have been introduced and used for various applications. A photograph of a twin-wire paper machine is shown in Figure 1.2. Twin-wire forming differs from the single-wire Fourdrinier in that the pulp suspension is pumped between two forming fabrics. It allows dewatering through two wires and has a high dewatering capacity.

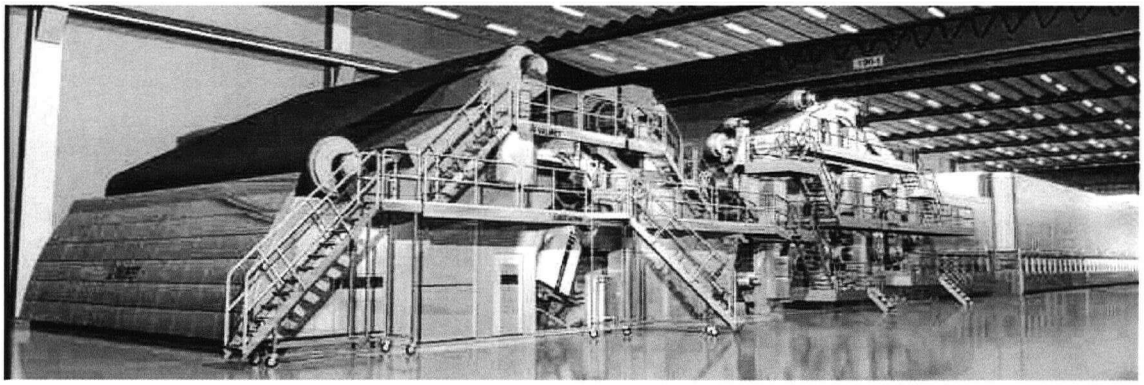

Figure 1.2 Twin wire paper machine (Valmet)

In general, from the headbox to the reel, a paper machine, either Fourdrinier or twin-wire, consists of three main sections: the forming section, the press section and the dryer section. A uniform fiber suspension is jetted onto the forming fabrics. The fiber mat is formed on the moving fabrics while the water is drained through forming fabrics. The sheet is then pressed to consolidate the web and remove more water. After pressing, the fiber web is conveyed through the dryer section where the residual water is removed by evaporation.

1.2 Web forming and forming fabrics

The forming section is critical in almost every paper process, because the structure of the fibrous web is mainly determined here and in the web pressing process. During the forming process, the basic structure of the final paper product is created.

The water is drained from the pulp suspension in wire section, and a wet web is formed. In principle, the dewatering process can be of two different kinds, filtration or thickening.

In Fourdrinier forming, downward dewatering of the mix takes place through a horizontal 'wire' or 'fabric'. Originally, all dewatering was produced by gravity and supporting rolls were introduced only to keep the wire horizontal, while causing a minimum of friction drag. Today, dewatering devices, such as blades, are applied below the Fourdrinier wire with the purpose of creating dewatering effects and also of providing a means for controlling the degree of fiber flocculation in the sheet formed.

Twin wire forming (TWF), or 'gap forming', was first introduced in the 1950's. In TWF, the pulp suspension discharges from the headbox into the gap between two moving, permeable fabrics. The resulting jet leaving the headbox impinges on one or both wires, at which location some dewatering of the suspension occurs, and the fabrics (or 'wires') trap the pulp suspension and convey it downstream. The fabrics are under tension and wrap around either fixed obstacles ('blades' and 'suction boxes') or rotating cylinders ('rolls'), where additional dewatering occurs through both wires.

In twin wire roll forming, the forming fabrics pass over rotating cylinders. Measurements in the suspension between the two fabrics show that the pressure is nearly constant, attaining a value on the order of

$$p = T_f/R \tag{1-1}$$

where T_f is the fabric tension, and R is the roll radius. Because dewatering in a roll former occurs fairly gradually, roll formers have high retention [3,4]. The implication of this high retention is that the paper has large numbers of fines, which improve the sheet opacity, brightness and smoothness. A second implication of gradual dewatering is that fibre flocs, which are present in the pulp suspension downstream of the headbox, are not disrupted in the forming section. The resulting paper therefore may have poor formation (spatial uniformity), and therefore higher printing dot-skip and low paper strength.

In twin wire blade forming, the forming fabrics pass over fixed blades. Careful measurements in blade formers have shown that the pressure in the gap is sharply spiked, with (typically) a region of high pressure just upstream of both the blade leading and trailing edges, separated by regions of near-zero gauge pressure. As a consequence of this spiked pressure distribution, the pulp suspension experiences rapid acceleration and deceleration, and is thus sheared by the velocity gradient between it and the adjacent wire [5-7] The high peak pressures associated with blade forming produce rapid local dewatering, and thus poor retention. The combined effects of the large shearing and the rapid dewatering is to produce paper with good formation (indicating that the fibre flocs have been disrupted) but comparatively poor sheet smoothness, opacity and brightness.

A paper machine forming fabric is basically a cloth woven from polyester and polyamide monofilaments, formed into a continuous belt by a seam. It is composed of

machine direction filaments (warp) and cross-machine direction filaments (weft, shute or filling). The individual filaments (yarns) of a forming fabric are a few tenths of millimeters in diameter. The fine mesh of the fabric permits dewatering while retaining the fibers.

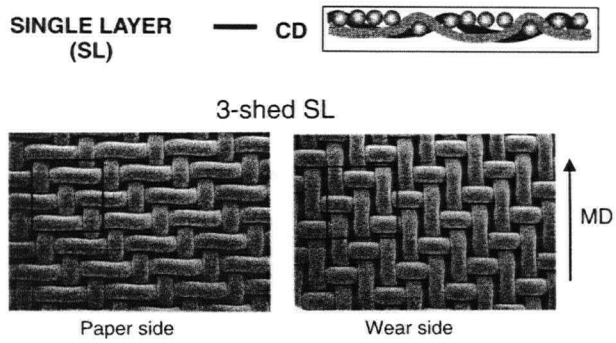

Figure 1.3 Single-layer forming fabric [1]

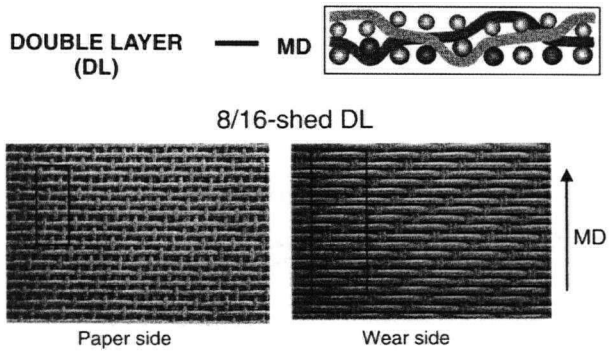

Figure 1.4 Double-layer forming fabric [1]

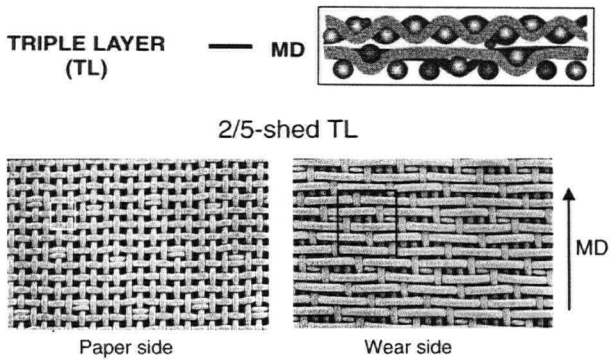

Figure 1.5 Triple-layer forming fabric [1]

There are typically three forming fabric structures in use; they are single-layer, double-layer and triple-layer [1]. A single-layer fabric is a fabric made of one machine direction (MD) yarn system and one cross-machine direction (CD) yarn system as illustrated in Figure 1.3. A double-layer fabric is a fabric made of one MD yarn system and two CD yarn systems as illustrated in Figure 1.4. A triple-layer fabric is a fabric made of two or more MD yarn systems and two or more CD yarn systems as illustrated in Figure 1.5. The construction typically consists of two cloths that are woven together with a binding yarn either in the cross or in the machine direction. Forming fabrics have two distinct surfaces, the forming surface (paper side) and the wearing surface (machine side). The actual structure of a forming fabric is quite complex and three-dimensional, with fabric filaments oriented in both the machine and cross directions. Not only are there filaments running in two orthogonal directions, but the filaments are woven together such that they also zig-zag in the z-direction.

The fabric functions as a filtration media and as a smooth support base for the fiber suspension flowing from the headbox; at the same time, it also transfers the web to the press section. The most important properties of a forming fabric, depending on the application, are drainage, sheet support and mechanical stability, wear resistance, and nonmarking structure. Water is removed through the fabric with the help of various dewatering elements. Forming fabrics typically provide rapid drainage in order to run the paper machine fast. However, depending on the paper grade requirements, slow drainage may be desired. The fabric's drainage properties must be matched to the paper machine and the paper grades produced. Sheet support refers to the ability to retain fibers for strong paper, which is strong enough to make it through press section, and to retain fines for good opacity. Mechanical stability refers to its ability to run for long periods on the paper machine without excessive stretching or wrinkling. Another important requirement of the forming fabric is that the paper is smooth and free of markings that are sometimes caused by the fabric ("wire marks, shadow marks").

The design of polymer fabrics was developed from single-layer to double-layer, to triple-layer and then to multi-layer. To simultaneously provide a fine, high draining paper side surface and at the same time a coarser, wear-resistant bottom surface, multi-layer

designs are increasingly being used. There is still much development taking place within this area.

From a paper quality point of view, the three-dimensional fabric surface structure has a large impact on paper surface structure and on dewatering resistance. The distribution of open area for dewatering and the fabric surface structure variations due to knuckles, etc. has a large impact on the web formation and thus on paper surface structure.

To generate a smooth paper surface, a flat fabric surface would be preferable. However, a certain degree of surface three-dimensionality facilitates dewatering, since it makes it possible for individual fibers to bridge the dewatering openings, without causing complete blockage.

1.3 Project Objective

Forming fabrics play an integral part in the physics of drainage and in finished sheet qualities. It has been known for many years that details of the forming fabric structure affect the retention of the paper sheet. Modern double and triple layer fabrics produce paper with higher retention than do single layer fabrics [8]. This higher retention is caused by the convoluted path taken by water passing through a multi-layer fabric. It is less well known that details of the forming fabric structure affect paper qualities such as wire mark and the local fibre distribution near fabric pores [9,11]. The reason for this is believed to be the same as for the inhomogeneous flow through a network of simulated pulp fibres [10]; the dewatering flow cannot pass through fabric knuckles, but rather must travel between the fabric filaments, which causes local flow anisotropy.

Important properties of paper, such as wire mark and fines retention, are known to depend on details of the three-dimensional flow through the forming fabric. It is perhaps surprising that not only the filaments in direct contact with the paper, but also the arrangement of coarser filaments beneath the fabric surface, affect the paper surface [9,11]. In addition to its impact on paper surface characteristics, the forming fabric plays a key role in the jet impingement process. In particular, jet impingement is strongly influenced by the fabric drainage resistance, which itself is a function of the three-dimensional structure of the fabric. Presently, forming fabric manufacturers know almost nothing about the "paper surface finish" or drainage characteristics of a new fabric until

after it has been manufactured. Also the forming fabric industry wants to understand the details of the flow through the forming fabric because the flow details affect the quality of the paper.

The purpose of this study is to model the flow through forming fabrics using modern computational fluid dynamic techniques, and to gain better physical insight into how the flow details affect the quality of the paper, with the ultimate goal of assisting the design of improved forming fabrics.

1.4 Approach

The actual structure of a forming fabric is quite complex and three-dimensional, with fabric filaments oriented in both the machine and cross directions. Not only are there filaments running in two orthogonal directions, but the filaments are woven together such that they also zig zag in the z-direction. The flow through the forming fabric is three-dimensional and involves with interaction with wood fibers and fines. The flow details are therefore quite complicated.

To avoid some of the difficulties in modeling the complex three-dimensional flow of a fibre suspension through a forming fabric, a simplified model system that captures the essential physics is proposed. First, a two-dimensional model representation of the wire is developed and second, the presence of fibres in suspension and a fibre web is ignored.

From this simplified system some insight into the flow through a forming fabric may be gleaned. For example, the cross flow velocity profile indicates whether uniform drainage is achieved. The cross-direction velocity profile indicates whether or not the fibres distribute uniformly in cross machine direction. The forming fabric is thus simplified to many parallel filaments located in two planes. Each filament is approximately circular in cross section and therefore the geometry is modeled as cylinder arrays. The jet to wire ratio is approximately 1 in simplification for normal incidence, thus the flow is simplified to two-dimensional flow through cylinder arrays. This simplification can address the shadow marks in the cross direction but not in the machine direction.

The individual filaments of a forming fabric are a few tenths of millimeters in diameter, and characteristic flow velocities through a fabric are a few tenths of a metre

per second. The characteristic flow velocities are the cross flow velocities at the jet to wire ratio of approximately 1. Therefore, the flow through a forming fabric occurs at a Reynolds number based on filament diameter on the order of or below a hundred. The flow can be assumed to be laminar. This assumption may be justified on two grounds. First, it is well known that for a uniform flow approaching a cylinder array at low Reynolds number, the flow, including the wake, is laminar. Second, although the flow out of a headbox is turbulent, fibres present in the flow cause the turbulent eddies of the scale of the fibre length (a few millimeters) or smaller to be dissipated. Thus only turbulent eddies a few millimeters in length should remain when the jet strikes the fabric. Since we are only interested in the flow behavior on scales on the order of a fabric filament (a tenth of a millimeter), these long-lived eddies are not relevant.

In summary the following assumptions are made to simplify the problem [11]:

- The CD filaments are neglected and flow is simplified to two-dimensional cross flow around cylinder arrays.
- The fibre suspension is very dilute and therefore can be modeled as pure water.
- The fibre web has not built up on the fabric and therefore does not affect the flow.
- Laminar flow is assumed because the Reynolds number based on filament diameter is below 100.

Chapter - 2 Literature Review

Although there are no computations or analysis on the detailed flow through a forming fabric, various researchers have worked on related fluid mechanical problems. In particular, flow through a forming fabric may be simplified to two-dimensional flow through cylinder arrays of unequal sizes [11]. Many studies can be found on flow around cylinders in the literature; however, in such studies the cylinders are usually of equal sizes.

Studies on the characteristics of a forming fabric and a review of research on flow around multiple cylinders are discussed in the following sections.

2.1 Forming fabrics characteristics and drainage

Unfortunately the forming fabric industry, has so far, been unable to come up with a relevant method to characterize the drainage behavior of a forming fabric [1]. It is believed that the forming surface plays a critical role as fibers are retained or lost in the initial dewatering stage. McCumsey *et al.* [12] analyzed the influence of the forming fabric on sheet characteristics and properties achieved in the converting operation. They described some of the forces acting between the headbox, wire, and drainage elements in the Fourdrinier, gap former, and top wire processes. They related characteristics developed on the wet end of paper machine to their impact on converting operation. The initial drainage was very dependent on the support network. Then, at a transition point, the fiber network became more of the limiting factor than the fabric. Jet impact on the forming fabric surface could have drastic impact on the MD and CD marking. Details of how the fabric was woven caused flow patterns in the base sheet that could influence marking.

Drainage rates have been difficult to quantify at industrial significant conditions. A new drainage apparatus that permitted accurate estimation of the drainage resistance of headbox and other papermaking stock samples under industrial significant conditions was introduced by Paradis et al. [13]. The drainage rate was determined by a conductance measurement in the stock remaining in the shear cell. Their flow resistance data for the

forming fabric agreed with the Ergun equation [14]. Therefore, if the equivalent diameter, thickness, and the void fraction of forming fabric were known, the flow resistance of the wire could be predicted. This relationship might be of use in designing fabrics for papermaking applications. Their drainage apparatus permitted drainage resistance coefficients to be determined under a known shear condition at high drainage rates and at short times. At low drainage rates, the drainage resistance increased with increasing shear rate. At higher drainage rates, the drainage resistance decreased with increasing shear rate.

A new device to measure permeability under simulated forming conditions was developed by Duplantis and Green [15]. The apparatus was similar in appearance to one cylinder of an engine. The cylinder head comprised a forming fabric through which the dewatering took place. A flush-mounted sensor in the piston read the total pressure (fluid pressure and interfibre forces) inside the pulp suspension, while a sensor protected by a handsheet fabric measured the water pressure only. A combined position/velocity sensor measured the motion of the cylinder. The permeability of a fibre mat adhering to a forming fabric was thus given by $k = V/\Delta p$, where k was the permeability, V was the superficial velocity through the fibre mat, and Δp was the fluid pressure difference across the mat. The variables tested were different forming fabrics and pulp types. The results showed the type of pulp had a greater influence over permeability than the type of forming fabric.

Jong et al. [16] developed an experimental method for the estimation of the screen coefficient and mat resistance coefficient. The basic assumption was that when the fiber mat was formed, there was a pressure difference across the fiber mat and the screen as the water passed through. The screen and the fiber mat were treated as two different mechanisms, so the total pressure drop was assumed to be the superposition of the two. The screen coefficient was introduced to represent the pressure drop across the screen. The effect of the forming fabric was less than 5% once 20 gsm or more of basis weight was accumulated.

All the above studies address the pressure drop across the fibrous mat and the screen. No research has been done on the detailed flow through a forming fabric.

2.2 Flow around cylinder arrays

Flow through a forming fabric may be simplified to two-dimensional laminar flow around cylinder arrays of unequal sizes at low Reynolds numbers [11]. Although no research could be found on the detailed flow through a forming fabric, numerous researchers have studied the flow around a series of cylinders. Cylinder-like structures can be found, both alone and in groups, for example in the designs for heat exchangers, cooling systems for nuclear power plants, offshore structures, buildings, chimneys, power lines, struts, grids, screens, and cables, in both air and water flow. One of the principal operational problems in heat exchangers is that they are prone to flow-induced vibration. The periodic shedding of Karman vortices is responsible for problems with flow-induced vibration and noise. As a result, much of the research literature on flows past circular cylinder arrays aims to explain vibration of the cylinders [17-22]. For a similar reason, there is also much research on heat transfer from such an array of cylinders [23-25]. Most industrially relevant flows (e.g. in tube bundles) are at very high Reynolds numbers (typically greater than 10^5 or 10^6), and thus much research has been conducted on the turbulent flow past cylinder arrays at high or moderate Reynolds numbers [26-38].

Some researchers [39-44] have studied the flow past an array of circular cylinders at low Reynolds numbers; however, all these authors investigated cylinders of uniform diameter. No previous research has been found related to the flow at low Reynolds number around cylinder arrays of varying diameter.

By virtue of its common occurrence in many forms and in different applications, both in nature and technology, fluid flow around a circular cylinder has been well studied, and is one of the classical problems of fluid dynamics. A complete understanding of the fluid dynamics for the flow around a circular cylinder encompasses such fundamental subjects as boundary layer separation, vortex formation and vortex shedding, and also vortex induced oscillation.

Flow around two circular cylinders has been investigated extensively and appears in review articles by Zdravkovich [29] and Ohya et al. [33]. The arrangement of two parallel cylinders positioned at a certain incident angle to the approaching flow direction is called a staggered arrangement. There are two special arrangements under staggered arrangements when the incidence is 0° or 90° that may be identified: first, the cylinders

are in tandem arrangements (also called in-line arrangements), one behind the other at any transverse spacing (i.e. the incidence is 0°); and second, the cylinders face the flow side by side at any transverse spacing (i.e. the incidence is 90°).

A Schlieren visualization technique was used by Ishigai et al. [26] to visualize the flow behind two side-by-side cylinders for Reynolds number of about 4×10^4. They observed a remarkably symmetric vortex formation and shedding for center-to-center spacing ratio $g = 2.5$ and 3.0, but a biased flow for $1.5 < g < 2.0$. The biased flow was bistable and intermittently changed over from one side to another, forming two asymmetric vortex streets of different frequencies. Bearman and Wadcock [27] have made a similar observation in their experiments.

The frequency of vortex shedding from two circular cylinders of the same diameter in staggered arrangements was experimentally investigated at a Reynolds number of 1.58×10^4 by Kiya et al. [30] using hot-wire anemometry. Some of his conclusions are:

- When the distance between the cylinders is less than 1.4 diameters, the pair of cylinders behaves as a single body with regard to the vortex shedding.
- The bistable side-by-side arrangement represents a transition from the upstream to the downstream stagger with regard to one of the two cylinders. This transition brings about a large change in the Strouhal number for the cylinder.
- There exists an island like region in which the Strouhal number for the upstream cylinder is much higher than that for the single cylinder.
- The Strouhal number for the downstream cylinder is generally lower than that for the single cylinder except the case where the distance between the cylinders is less than about 1.4 diameters in tandem arrangements.
- The gap flow between the cylinders is biased to the side of the upstream cylinder, thus forming a much narrower wake behind the upstream cylinder than that behind the downstream cylinder. Narrower wakes correspond to higher Strouhal numbers and wider wakes to lower Strouhal numbers.

Based on flow visualization of a laminar wake at low Reynolds numbers (100 – 200) behind a pair of side-by-side cylinders in the range of $g = 1.7$ to 6.0, Williamson [40] suggested that the two different frequencies, observed in the asymmetric flow regime ($1.5 < g < 2.0$), were due to the existence of harmonic vortex shedding modes. He also noted

that, as a result of interaction, the wakes of the two cylinders could amalgamate to form a single wake. He suggested that the ratio of shedding frequencies might be nearly integral. On the other hand, the measurements of Kim and Durbin [32] at Reynolds number of 3300 did not support this. Therefore, the mechanism for the two distinct frequencies in the asymmetric flow regime has yet to be properly understood.

Peschard and Le Gal [44] proposed a dynamical system which modeled the behavior of the coupled wakes of a pair of cylinders placed side by side in a constant flow at low Reynolds numbers (100 – 130). This model was constituted by two coupled Landau equations whose coefficients were estimated from experimental observations. The model was able to reproduce most of the experimental features such as in phase locked states, phase opposition locked states, and asymmetric bistable locked states. They also presented some new experiments which completed previous observations of locked and unlocked wakes depicted in Figure 2.1.

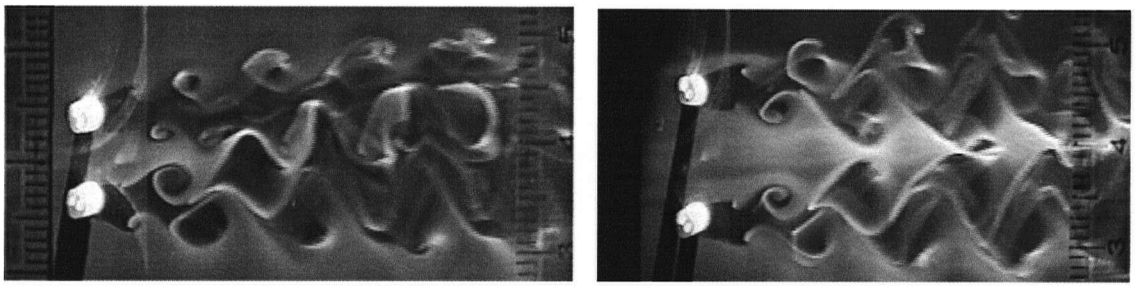

Figure 2.1 In phase locked states and phase opposition locked states of two side-by-side cylinders [44]

Recently Sumner et al. [35,36] investigated the flow around two circular cylinders in various arrangements using dye injection flow visualization, hot-film anemometry and particle image velocimetry for center-to-center spacing ratio g in the range of 1.0 to 6.0, and Reynolds number from 500 to 3000. Nine flow patterns were identified, and processes of shear layer reattachment, induced separation, vortex pairing and synchronization, and vortex impingement, were observed. New insight was gained into previously published Strouhal number data, by considering the flow patterns involved. The study revealed that vortex shedding frequencies were more properly associated with individual shear layer than with individual cylinders; more specifically, the two shear layers from the downstream cylinder often shed vortices at different frequencies.

In summary, it is now well established that for flow around two side-by-side cylinders, when the cylinder center-to-center spacing ratio g is less than 1.2, the two cylinders act like a single bluff body, forming a single Karman vortex street. For g between 1.2 and 2, the gap flow between the cylinders is asymmetric about the plane of geometric symmetry, thus generating one narrow and one wide wake. The deflected gap flow is bi-stable, that is, the deflection can change its direction in a random way and stay in the same direction for a while. Two dominant frequencies have been identified, although the mechanism for the two distinct frequencies in the asymmetric flow regime is still not understood. Most researchers believe that the higher and lower frequencies are associated with the narrow and wide wakes, respectively. For g greater than 2, two coupled vortex streets occur, either in-phase or anti-phase.

It is worth mentioning that one of the earliest computational studies of interactive vortex shedding was undertaken by Chang and Song [41]. Two cases, on either side of the critical spacing, were considered for the side-by-side arrangement at Re = 100. Using a hybrid finite element/finite difference vorticity-stream function formulation they found that it was possible to simulate many of the phenomena associated with this arrangement of equal diameter cylinders. Even a flipping between the in-phase and anti-phase shedding modes for the synchronized shedding regime was observed in the computation. Furthermore, the numerical scheme produced accurate resolution of the flow features near the cylinders, using the finite element method together with a computationally inexpensive finite difference procedure for the far-field flow. The use of the finite element method eased the problems of generating a mesh around, and in between, the two cylinders. The asymmetric vortex shedding had two different Strouhal numbers because of its bistable nature; however, those two Strouhal numbers were somewhat scattered around two different values.

Farrant et al. [45] used the cell boundary element method to solve flows around two cylinders of equal diameter side by side and in tandem. For computations involving side-by-side cylinder arrangements, vortex shedding occurred typically in the anti-phase modes. A small perturbed inlet flow could be applied to induce the in-phase shedding that would continue indefinitely. Each mode continued for large numbers of cycles (>20), unless perturbed by changing the boundary conditions. Particle streak line simulations,

generated from the cell boundary element method velocity fields, had similarities with the smoke visualization photographs of Williamson [40].

Investigations of flow past multiple cylinders are reported far less in the literature. Thus the fluid dynamics of more circular cylinders that are placed in close proximity to one another are less well studied and understood. The flow pattern around a tube in a bank is influenced by the following parameters: the arrangement and geometrical parameters of the bank, and the Reynolds number. Nishimura [31] has reviewed the earlier works on flow pattern and localized flow characteristics, such as surface pressure, shear stress, and velocity distribution around a tube in a bank. Unfortunately his definitions of the flow regimes such as the laminar flow regime, mixed flow regime, and turbulent flow regime no longer seem valid.

The turbulent near-wake of three side-by-side circular cylinders with equal or unequal spacing has been experimentally investigated by Zhang and Zhou [24] using various techniques, including the hot wire, laser Doppler anemometer, and laser-illuminated flow visualization. The flow patterns behind three side-by-side circular cylinders bore similarity to the two side-by-side cylinders, such as multiple dominant frequencies and the gap flow deflection and flopping.

Some of the earliest systematic research on flow structures in tube banks was done by Ishigai and Nishikawa [31]. They used the Schlieren optical method to visualize the flow in single column, single row, and double row tube banks at Reynolds number of 1300 to 33000. Several flow patterns were revealed such as:

- In single row tube banks, when the center-to-center spacing ratio is $g < 2.5$, a larger wake and a smaller wake take place in a strictly alternate order one after another.
- For double row tube banks, each tube in staggered arrangements sheds Karman vortices at any tube spacing. There are two types of spacing, i.e., the center-to-center separation between two rows, z/d, and the center-to-center gap between adjacent cylinders in each row, g. While under in-line arrangements, the vortex formation region occurs only behind the tube in the downstream row when $g \geq 2$, $z/d \leq 3$. At tube spacing with $g \leq 1.5$, $z/d \geq 3$, however, Karman vortices are formed also in the wake between two rows.

The flow visualization of Polak and Weaver [34] showed that first-row alternate vortex shedding occurred in every pitch ratio, except g = 1.14. They experimentally studied the vortex shedding in normal triangle tube banks over a pitch ratio range g = 1.14 - 2.67, and Reynolds number range 760 – 49000 based on the upstream velocity. For $g \geq 2.0$, second-row vortex shedding occurred at a lower Strouhal number than that from the first row. Their experimental observations of Strouhal number depended on the pitch ratio, location of measurements in the array, and Reynolds number. The higher frequency observed in the array always had a phase difference of about 180°, at the minimum gap of the second tube row, in the near wake of the first row tubes. This was caused by alternate vortex shedding from the first row tubes. The lower frequency found in the array always had a phase difference of about 180°, at the third row minimum gap. Apparently, this was caused by second row alternate vortex shedding.

Braun and Kudriavtsev [42] performed numerical simulations of flow in one row and seven rows of cylinders at Reynolds numbers ranging from 86 to 869 based on the mean flow velocity in the pitch (or from 43 to 434 based on the upstream velocity). Because they presented only flow patterns in the U velocity distribution, it is hard to compare their simulations with experimental studies.

Le Gal et al. [43] experimentally studied the collective behavior of wakes downstream of a row of parallel cylinders placed side by side, perpendicular to an incoming flow at low Reynolds numbers (100 – 160) based on the velocity in the minimum area. When the distance separating the cylinders was small compared to their diameter, two instability mechanisms, associated with different patterns and dynamics competed. A first spatial symmetry breaking appeared when the stationary wakes behind each cylinder were deviated towards one side or the other and formed large clusters containing from 2 to sometimes more than 10 wakes. These clusters were separated by intense recirculating zones. When the Reynolds number was increased, the wakes belonging to the widest clusters experienced a secondary temporal oscillatory bifurcation. Classical Benard-Von Karman vortex streets were thus shed in phase by these cylinders (acoustic mode), by contrast with the wakes outside these cells which stayed stationary. However, the primary instability did not occur in the flow around the far apart cylinders and a more uniform mode of vortex shedding, with neighbours in phase opposition, took

place in the flow. The two flow patterns are shown in Figure 2.2 and Figure 2.3 at $g = 3$ and $g = 1.5$ respectively.

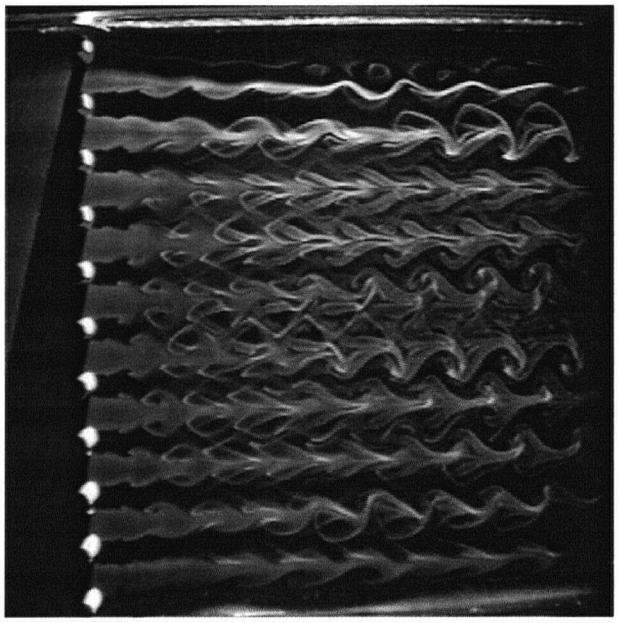

Figure 2.2 Anti-phase flow behind the row of 11 cylinders at $Re = 120$, $g = 3$ [43]

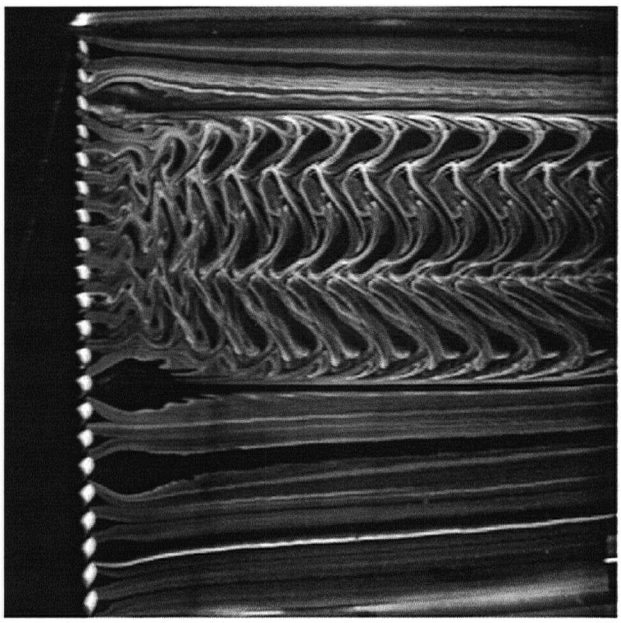

Figure 2.3 In-phase flow behind the row of 21 cylinders at $Re = 115$, $g = 1.5$ [43]

In conclusion, previous studies were mostly concerned with the behavior of the wake flow and the flow pattern, the flow-induced vibration, and heat transfer characteristics. We could find no previous studies of the flow around multiple rows of cylinders for which the cylinders are of unequal sizes. There are also few studies at the range of Reynolds numbers (roughly, 50-200) of interest in papermaking and few numerical studies on cylinder arrays. No research has been done of direct relevance to papermaking, for which one is interested primarily in the flow upstream of the cylinders, not in the cylinder wake.

Chapter - 3 Computations and Validation

As described in the first chapter, modeling of flow through forming fabrics was simplified to a two-dimensional cross flow around cylinder arrays, assuming a single-phase of pure water in laminar flow. The flow is steady if the Reynolds number is very small; however, for moderate Reynolds numbers, it is generally unsteady. A commercial CFD software package, FLUENT^{TM}, is used for all computations.

3.1 CFD Modeling

FLUENT uses a control-volume-based technique [46] to solve the governing integral equations for the conservation of mass and momentum. It converts the governing equations to algebraic equations that can be solved numerically. This control volume technique consists of integrating the governing equations about each control volume, yielding discrete equations that conserve each quantity on a control volume basis. A second-order upwind scheme is selected to achieve higher-order of accuracy. The segregated solver is used, i.e., the governing equations are solved sequentially. In this sequential procedure, the continuity equation is used as an equation for pressure. When the segregated solver is used, a second-order pressure interpolation scheme is selected. For pressure-velocity coupling in the segregated solver, SIMPLEC [46,47] is selected for steady-state calculations, while PISO [46,48,49] is used for transient calculations. The SIMPLEC (SIMPLE-Consistent) and PISO (Pressure-Implicit with Splitting of Operators) belong to the SIMPLE (Semi-Implicit Method for Pressure-Linked Equations) family of algorithms [46,50], which is used for introducing pressure into the continuity equation. The SIMPLE algorithm family uses a relationship between velocity and pressure corrections to enforce mass conservation and to obtain the pressure field.

A second order implicit time advance scheme is used to simulate unsteady flow. The laminar viscous model is selected because of low Reynolds number. The geometric complexity of the two-dimensional geometry will likely necessitate the use of an unstructured mesh. A purely unstructured mesh and a combined structured and unstructured mesh is used in our simulations, where unstructured mesh is used near the

cylinders, while choosing structured mesh in the other areas to save memory usage and computing time. A typical mesh is shown in Figure 3.1.

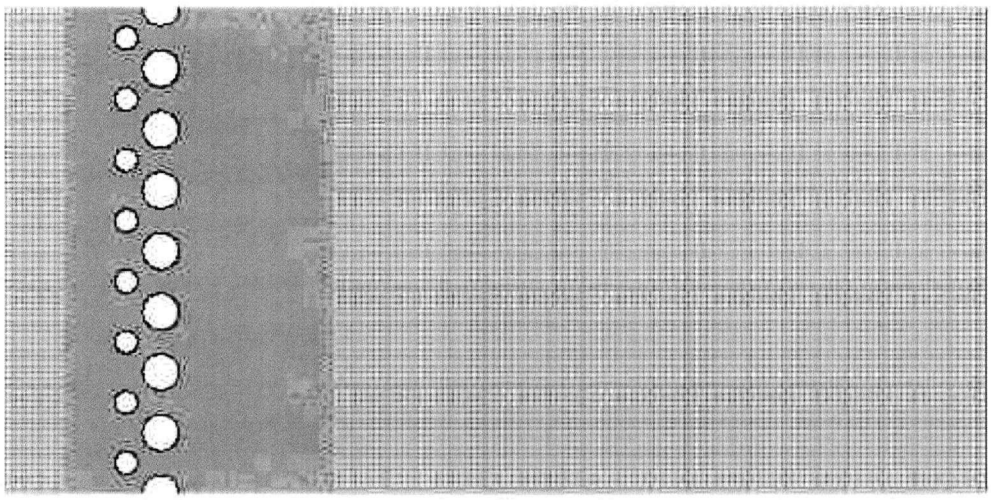

Figure 3.1 Combined structured and unstructured mesh

3.2 Flow around a single cylinder

The fundamental fluid dynamics problem of a circular cylinder in uniform flow has been examined extensively in both computational and experimental studies and is considered a stringent test for flow solvers. Also this is a very good test case for our problems.

For flow around a circular cylinder at very low Reynolds numbers, $0 < Re < 4$, the streamlines are symmetrical, and the flow is attached. This regime of viscous flow is called Stokes flow. Figure 3.2 shows our simulation of the stream function of flow around a circular cylinder at $Re = 1$. The drag coefficient (pressure drag and friction drag) is 20.53, obtained from computation, which is much higher than 9.94 that the following curve-fit formula [51] to experimental results predicts for flow around a cylinder in an infinite stream.

$$Cd \approx 1.18 + \frac{6.8}{\mathrm{Re}^{0.89}} + \frac{1.96}{\sqrt{\mathrm{Re}}} - \frac{0.0004\,\mathrm{Re}}{1 + 3.64\times10^{-7}\,\mathrm{Re}^2} \quad (10^{-4} < \mathrm{Re} < 2\times10^{5}) \qquad (3\text{-}1)$$

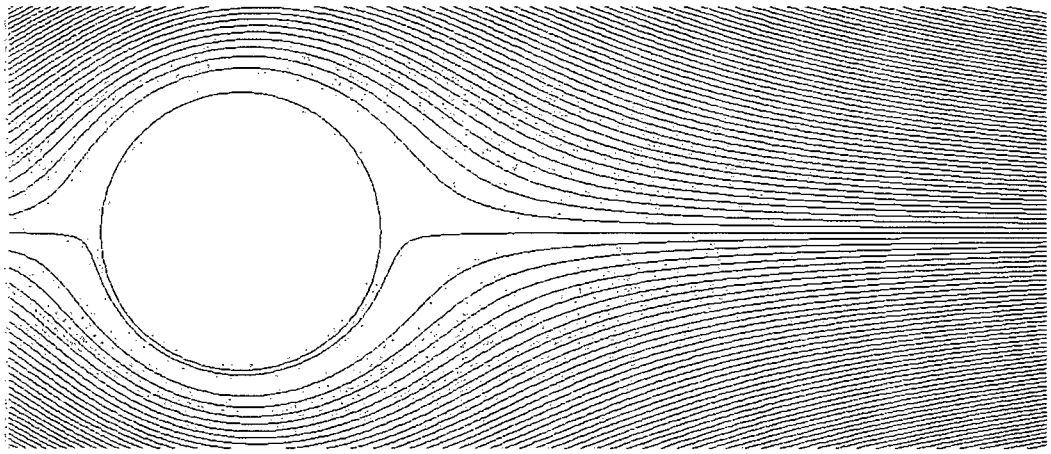

Figure 3.2 Stream function of flow around a cylinder at $Re = 1$

For a cylinder in an infinite stream, the experimental measurements of drag coefficient is around 10 at $Re = 1$. However, in our calculation, it is not a cylinder in an infinite stream, but rather in a channel. The blockage ratio, λ, is 0.0625. Flow past a cylinder in a channel tends to increase the drag dramatically at very low Reynolds number, comparing with the flow past a cylinder in an infinite stream. This effect is demonstrated in Figure 3.3. The drag coefficient will tend to 11.84 as λ tends to zero, obtained from the following curve-fit formula to calculated values, which is still higher than experimental value 10 for flow around a cylinder in an infinite stream.

$$Cd = 11.84 + 104.75\lambda + 489.54\lambda^2 \tag{3-2}$$

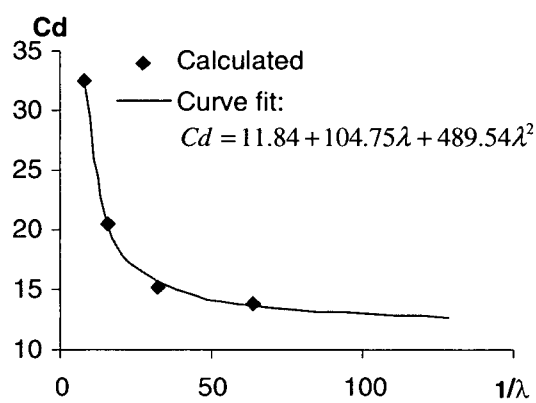

Figure 3.3 Effect of blockage ratio on drag for flow around a cylinder at $Re = 1$

For $4 < Re < 40$, the flow becomes separated on the back of the cylinder, forming two distinct, stable vortices. Our simulation of this type of flow is given in Figure 3.4, where $Re = 30$.

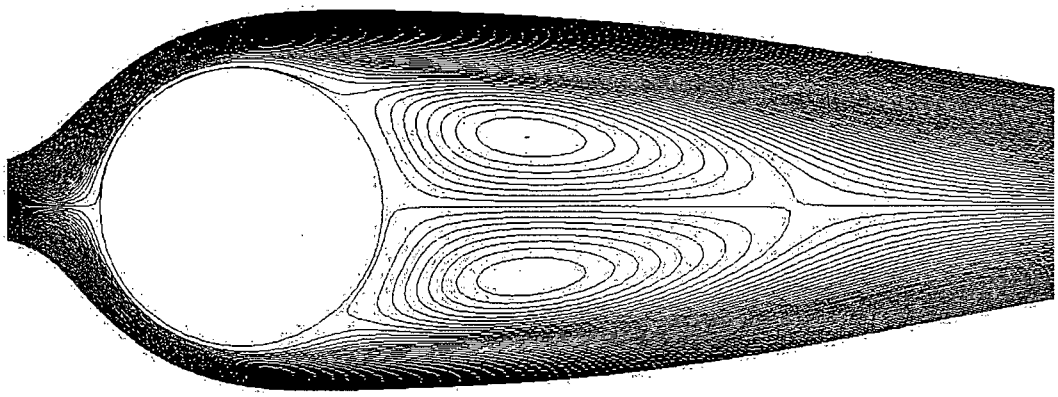

Figure 3.4 Stream function of flow around a cylinder at $Re = 30$

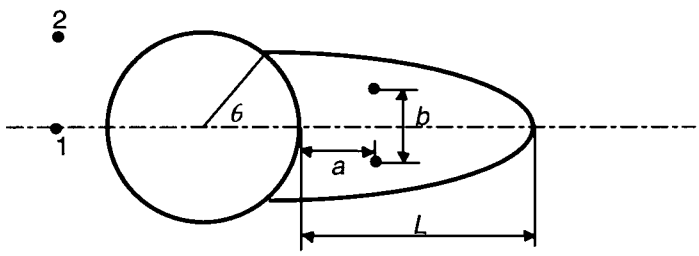

Figure 3.5 Geometrical parameters of the closed wake

The point at which the flow separates from the wall depends on the Reynolds number. The higher the Reynolds number, the sooner the flow separates, and the larger the recirculating bubbles [52]. At $Re = 30$, our calculation shows that the separation angle is 49.2° and the length of the attached wake is $1.45D$. The calculated parameters of the vortices are compared with previous experimental and numerical studies [53,54] in Table 3.1 and show good agreement. The definition of the geometrical parameters is given in Figure 3.5. Point 1 and Point 2 are where we will do our grid convergence studies later. The reason that we compare the velocity at Point 1 and Point 2 is because it is the region that we are most interested in; i.e., for our simplified model of forming fabrics, it is where

we monitor the velocity profile to indicate the uniform drainage and uniform fiber distribution.

***Re* = 30**	Present results (λ =0.0625)	Coutanceau and Bouard [53] (λ =0)	Coutanceau and Bouard [53] (λ = 0.07)	Saiki and Biringen [54] (λ = 0.1)
Length of separation bubbles (*L*)	1.453	1.53	1.31	1.7
x-coordinate of the center of the vortex cores (*a*)	0.513	0.55	0.48	0.62
y-distance between the vortex cores (*b*)	0.505	0.54	0.5	0.5625
Separation angle (θ)	49.22°	50.1°	49°	48°

Table 3.1 Comparison of the wake properties of flow past a cylinder at *Re* = 30 with experimental and numerical results

In the steady-state flow situation the streamlines around the circular cylinder are symmetrical or nearly symmetrical so that only one component of the force is present: the drag. Our results give a lift coefficient of –0.002 and the drag coefficient (pressure drag and friction drag) of 1.906 (λ =0.03125), which agrees with the value, 1.855, that the empirical formula (3-1) predicts. Again, putting a cylinder in a channel tends to increase the drag, relative to that of a cylinder in an infinite stream. When the blockage ratio, λ, is 0.0625, the drag coefficient is 2.064, which is a little higher than 1.855.

As *Re* is increased above 40, the flow behind the cylinder becomes unstable; the vortices, which are in a fixed position in Figure 3.4, now are alternately shed from the body in regular fashion and flow downstream, which form a Karman vortex street. Figure 3.6 and Figure 3.7 show this type of flow, where *Re* = 150.

The frequency with which the vortices are shed from the cylinder can be made dimensionless with the flow velocity and the cylinder diameter. The Strouhal number (*St*) depends only on the Reynolds number:

$$St = \frac{f \times D}{U_o} = \frac{D}{U_o \times T} \tag{3-3}$$

where U_o is free stream velocity, D is cylinder diameter, and f and T are vortex shedding frequency and period respectively.

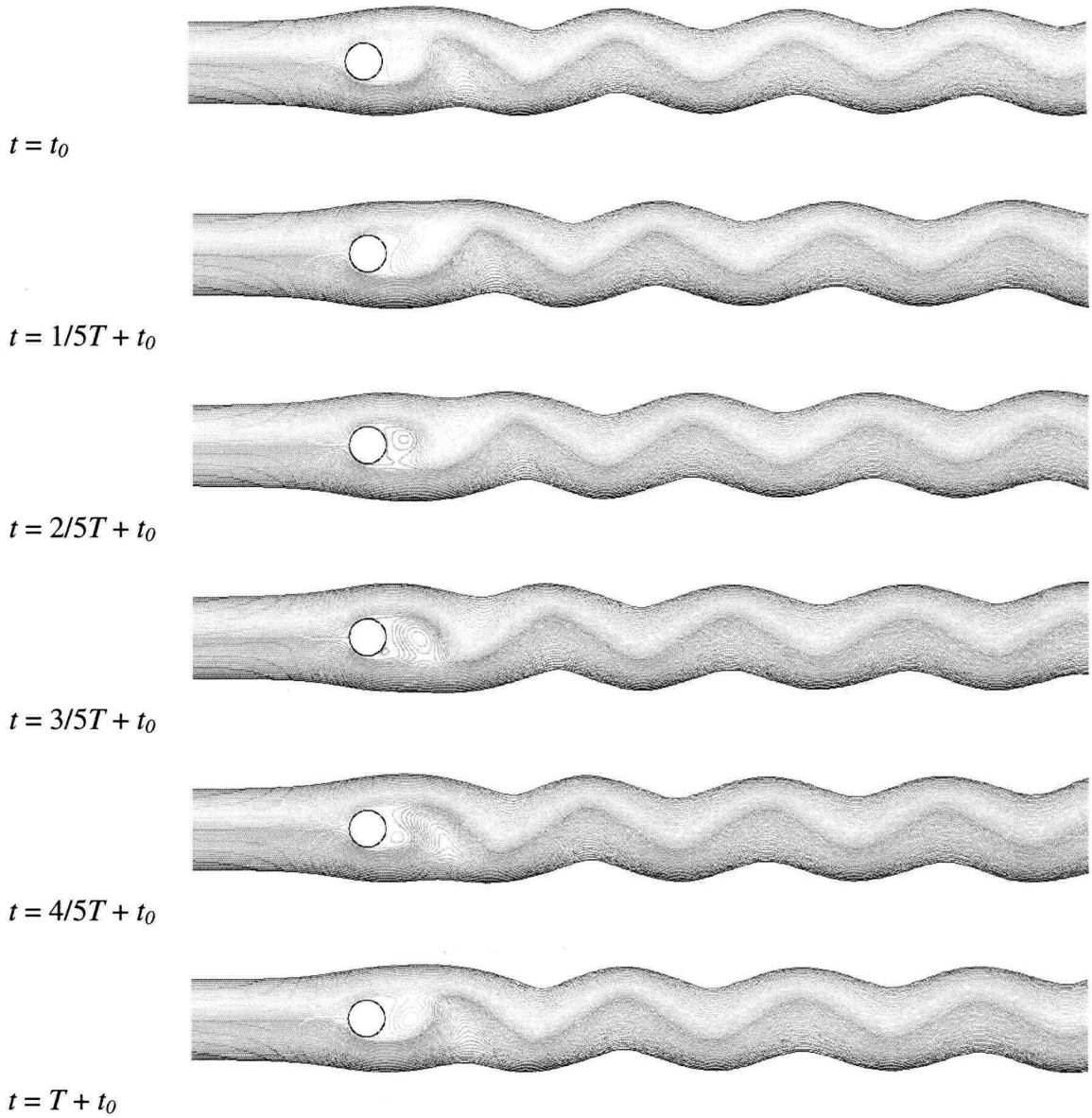

Figure 3.6 Time evolution of stream function of flow around a cylinder at $Re = 150$

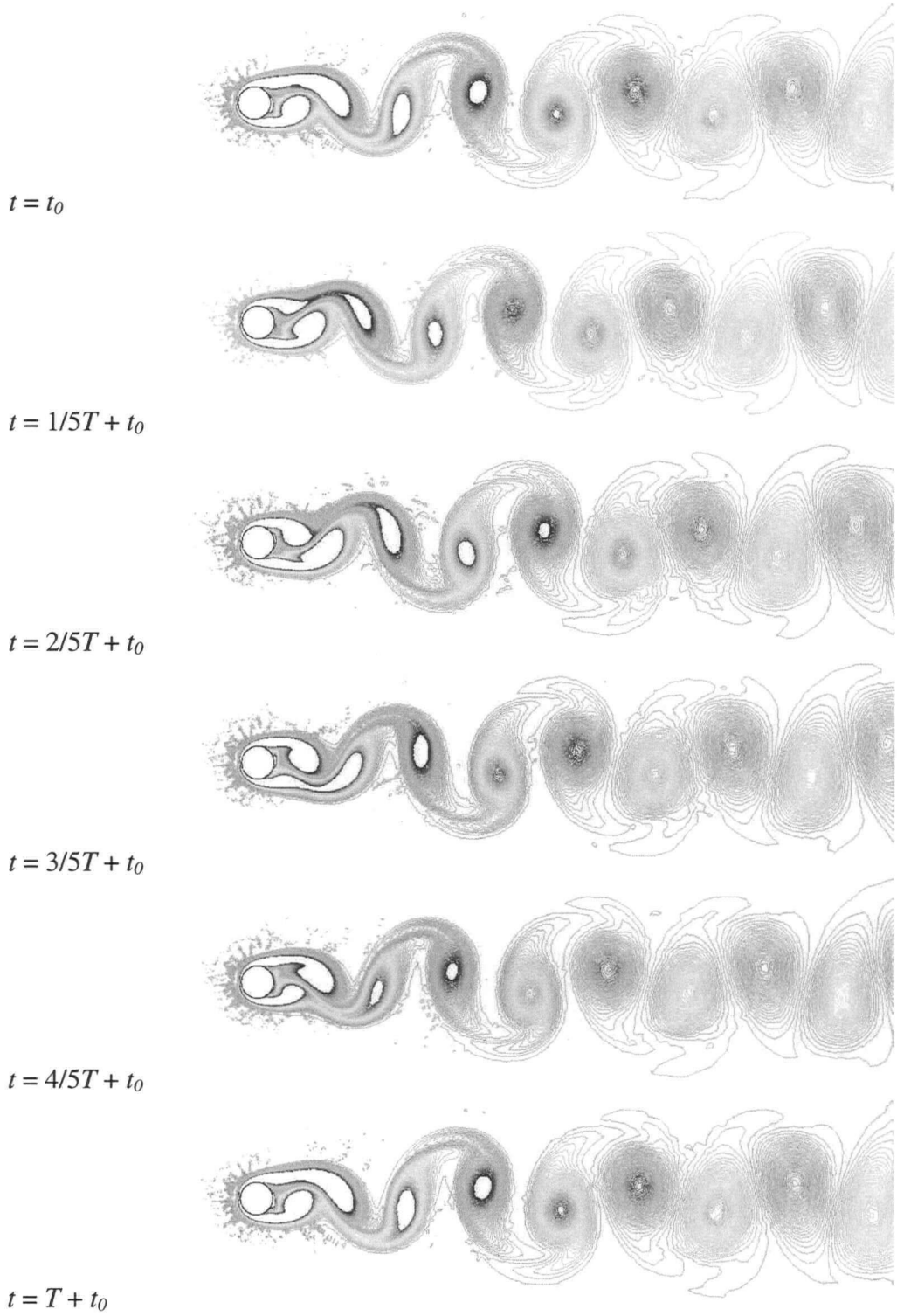

Figure 3.7 Time evolution of vorticity magnitude contours of flow around a cylinder at $Re = 150$

Due to vortex shedding, both the drag and lift forces oscillate. Figure 3.8 shows the time evolution of lift coefficients, while Figure 3.9 shows the oscillation of drag and lift coefficients. The lift coefficient oscillates around zero, but the drag coefficient oscillates around 1.410 (λ =0.03125), which agrees with the value 1.359 formula (3-1) predicts.

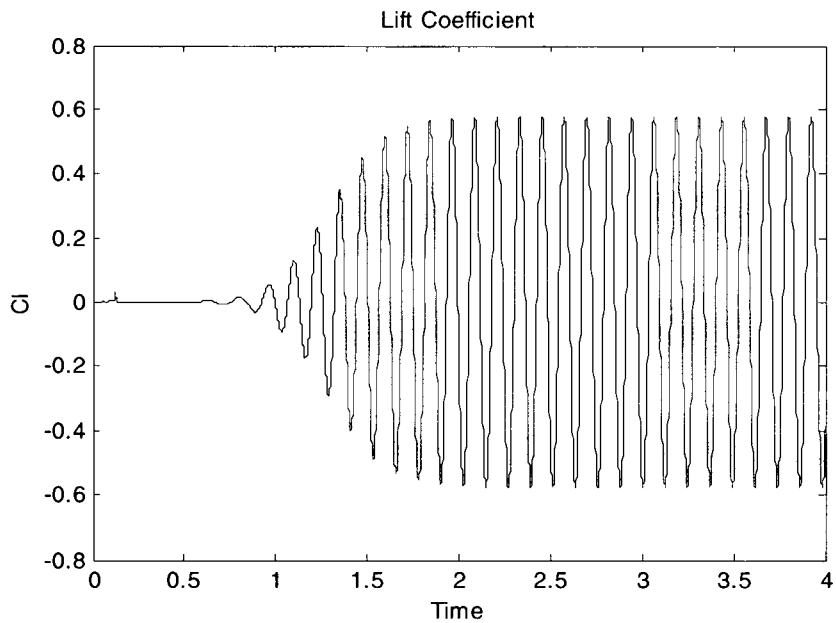

Figure 3.8 Time evolution of lift coefficients of flow around a cylinder at Re = 150

The drag and lift coefficients oscillate at different frequencies: the drag has twice the frequency of the lift. The reason for two frequencies is that the drag force has one maximum and one minimum during the growth and shedding of each of the vortex pairs, while the sign of the lift force depends on the location of the vortex pairs, i.e. whether it is above or below the cylinder. Thus the frequency of the lift oscillation gives the Strouhal number, which represents the shedding frequency of the vortex pairs. A FFT (Fast Fourier Transform) of lift coefficient is illustrated in Figure 3.10. The FFT result gives a Strouhal number of 0.1935 (λ =0.03125), while a FFT of drag coefficient gives a number of 0.3971, which is exactly twice the Strouhal number. The calculated Strouhal number is in excellent agreement with the experimental data 0.183 [55-57] (0.18-0.22) and numerical data 0.182 [56], 0.184 [57].

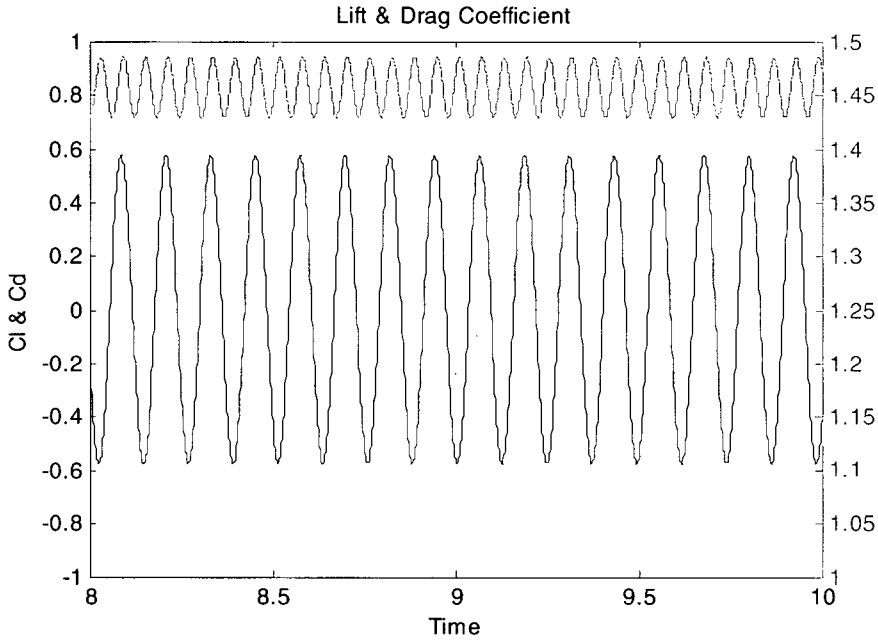

Figure 3.9 Lift and drag coefficients of flow around a cylinder at $Re = 150$

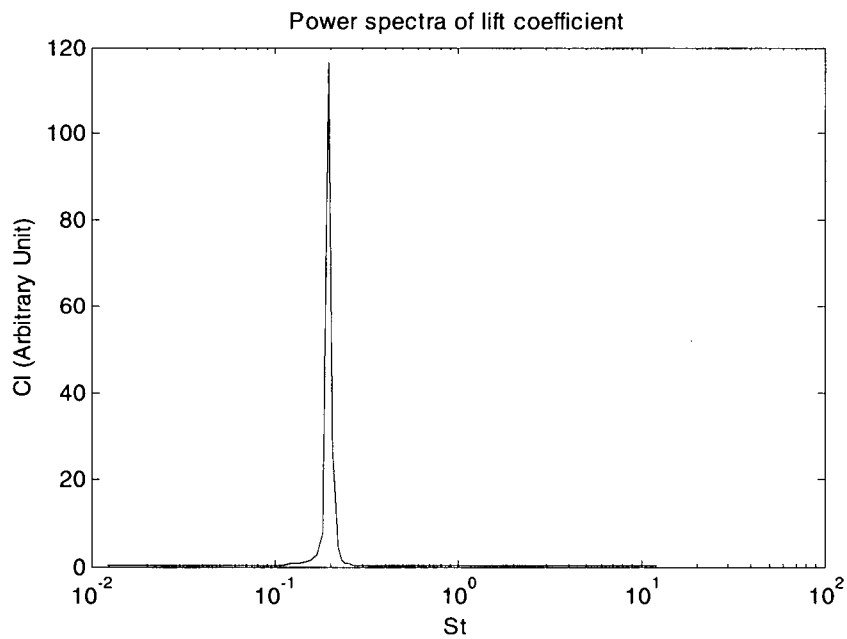

Figure 3.10 Power spectra of lift coefficients of flow around a cylinder at $Re = 150$

Confining a cylinder in a channel not only tends to increase the drag, compared with the flow past a cylinder in an infinite stream, but it also increases the vortex shedding frequency. The confinement in the channel speeds up the processes associated with

vortex shedding [49]. A comparison of drag coefficients and Strouhal numbers at different blockage ratios is given Table 3.2, and this effect is clearly demonstrated.

Blockage Ratio (λ)	0.125	0.0625	0.03125
Drag Coefficient (Cd)	1.649	1.457	1.410
Strouhal Number (St)	0.2177	0.1935	0.1935

Table 3.2 Effect of blockage ratio on drag and Strouhal number at Re = 150

A grid convergence study was performed for both mesh and time step, and for two Reynolds numbers as shown in Table 3.3, Table 3.4 and Figure 3.11. The numbers 45, 90 etc. in the top row refer to the number (45, 90, etc.) of segments on the cylinder surface. We used an unstructured mesh and the total number of cells is given in the brackets. For the time step grid convergence study (second row from bottom), $T/125$ implies that about 125 time steps were used for each period of vortex shedding. For vortex shedding, at least 20 time steps are need for each period. There is always trade-off, however. For a smaller time step, fewer iterations are needed per time step to achieve convergence. For a larger time step, more iterations are needed. It can be seen that the results on coarse grids are very close to the results on fine grids. By comparing results to the finest resolution computations, it is apparent that grid convergence on all important parameters is achieved within 1% provided 70647 cells or more are used, and provided $\Delta t \leq T/125$.

Spatial Grid Convergence ***Re*** **= 150, λ =0.0625**	45 (21265 cells)	90 (40930 cells)	135 (70647 cells)	180 (110072 cells)
Drag Coefficient (Cd)	1.4647	1.4587	1.4584	1.4573
Strouhal Number (St)	0.1935	0.1935	0.1935	0.1935
u/U_o at point 1	0.4793	0.4761	0.4717	0.4703
v/U_o at point 1	0.0006	0.0010	-0.0006	0.0007
u/U_o at point 2	0.8111	0.8077	0.8078	0.8079
v/U_o at point 2	0.3290	0.3344	0.3345	0.3353
Temporal Grid Convergence ***Re*** **= 150, λ =0.0625**	T/125	T/250	T/725	Williamson [55]
Strouhal Number (St), 110072 cells	0.1935	0.1935	0.1935	0.183

Table 3.3 Grid convergence for flow past a single cylinder at Re = 150

Spatial Grid Convergence *Re* = 30, λ =0.0625	20 (15078 cells	45 (21265 cells)	90 (40930 cells)	135 (70647 cells)	180 (110072 cells)
Length of separation bubbles (*L*)	1.087	1.364	1.429	1.446	1.453
x-coordinate of the center of the vortex cores (*a*)	0.436	0.488	0.507	0.511	0.513
y-distance between the vortex cores (*b*)	0.381	0.498	0.501	0.503	0.505
Separation angle (θ)	36.70°	46.20°	48.94°	49.08°	49.22°
Drag coefficent (*Cd*)	2.040	2.065	2.066	2.065	2.064
u/U_o at point 1	0.4143	0.3746	0.3741	0.3700	0.3684
v/U_o at point 1	0.0078	0.0005	0.0010	0.0001	0.0007
u/U_o at point 2	0.7500	0.7457	0.7426	0.7421	0.7417
v/U_o at point 2	0.3782	0.3919	0.3956	0.3955	0.3958

Table 3.4 Grid convergence for flow past a single cylinder at $Re = 30$

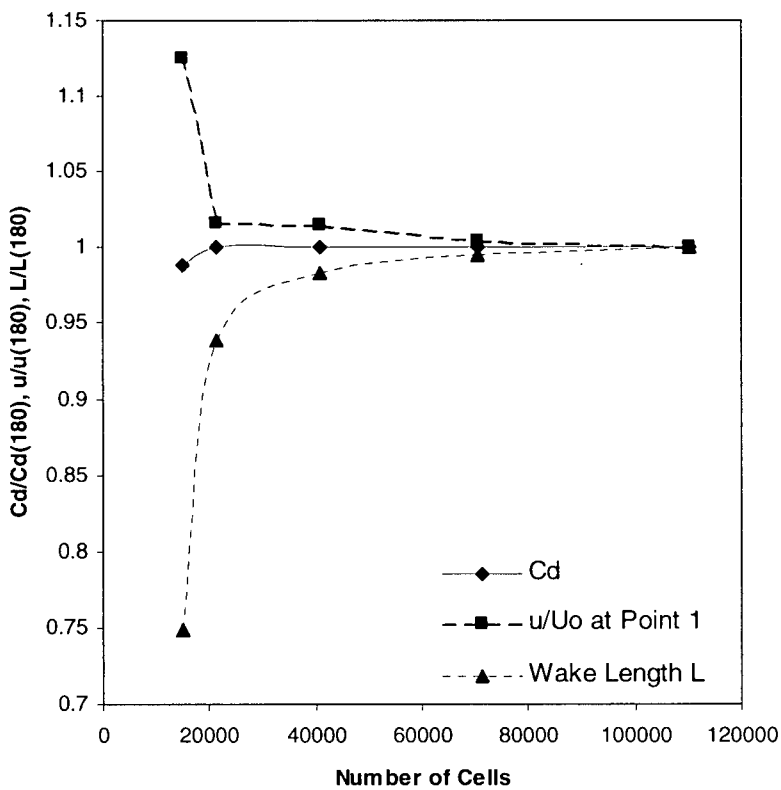

Figure 3.11 Grid convergence for flow past a single cylinder at $Re = 30$

3.3 Flow around two side-by-side cylinders

It is known from experimental studies, numerical simulations and modeling, that the wakes of bluff bodies placed next to one another can interact and create a large variety of phenomena. In particular, the flow around a pair of cylinders exhibits interesting flow patterns due to wake interference. It is very complex and has been studied extensively. The vortices shed from two side-by-side circular cylinders in a uniform cross flow interact dynamically. The individual or combined wake behind the cylinders is therefore different from that behind an isolated cylinder. The gap between the cylinder centers divided by the diameter, g, is known to be a very important parameter. The wake pattern, Strouhal number, and lift and drag coefficients experience serious changes at different values of g. Flow visualization indicates a predominance of anti-phase vortex shedding for gaps between two side-by-side cylinders in the range of 2.0 - 6.0, giving a wake comprising two anti-phase parallel streets in a symmetric form. Such a flow pattern is shown in Figure 3.12 and Figure 3.13, where the gap is 3.0. The Reynolds number based on the free stream velocity and the cylinder diameter is 100. Figure 3.14 gives the lift coefficient of both cylinders and clearly shows the anti-phase oscillation. A Fast Fourier Transform of the lift coefficient gives the vortex shedding frequency in the form of the Strouhal number, $St = 0.1996$, which agrees well with the experimental results [27,40]. It is well known that these two vortex streets are stable and keep the same form for large distances downstream.

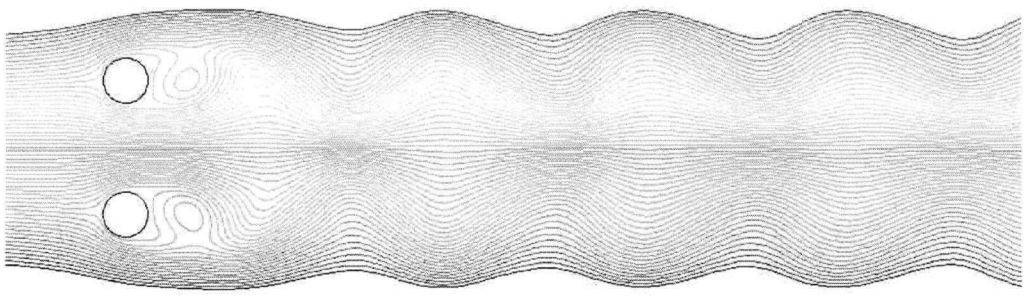

Figure 3.12 Instantaneous stream function of flow past two side-by-side cylinders at $g = 3$, $Re = 100$
Antiphase flow pattern

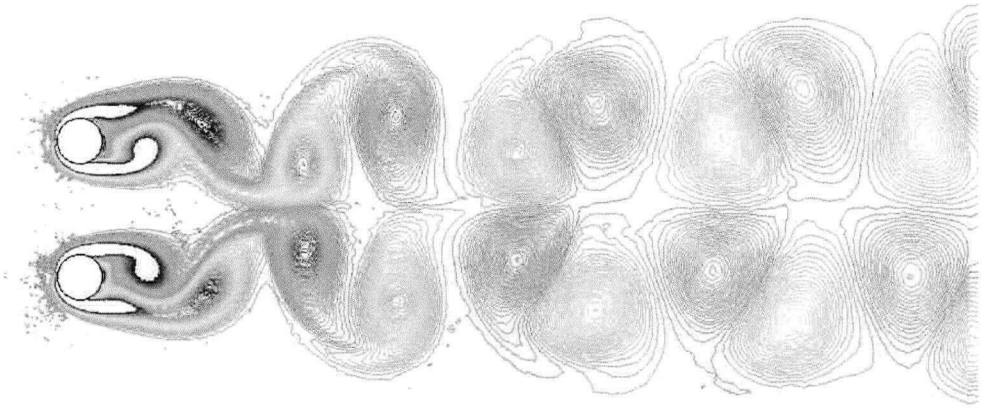

Figure 3.13 Instantaneous vorticity magnitude of flow past two side-by-side cylinders at $g = 3$, $Re = 100$
Anti-phase flow pattern

It is interesting to note that, in the case of flow around two side-by-side cylinders, the predominant frequency of the drag coefficient oscillation is the same as that of the lift coefficient, although there is evidently also a second frequency. Unlike flow past a single cylinder, the drag coefficient fluctuates twice during one period of vortex shedding. The drag coefficient fluctuation and FFT of the drag coefficient are given in Figure 3.15 and Figure 3.16. The FFT shows that two frequencies present, $St = 0.1996$ and $St = 0.3992$, with the predominant frequency being $St = 0.1996$, exactly the same as lift oscillating frequency. The reason that the predominant drag coefficient oscillation has the same frequency as the lift coefficient is that the inner vortex is smaller and weaker than the outer one during the vortex shedding. This observation agrees with Chang and Song's result [41].

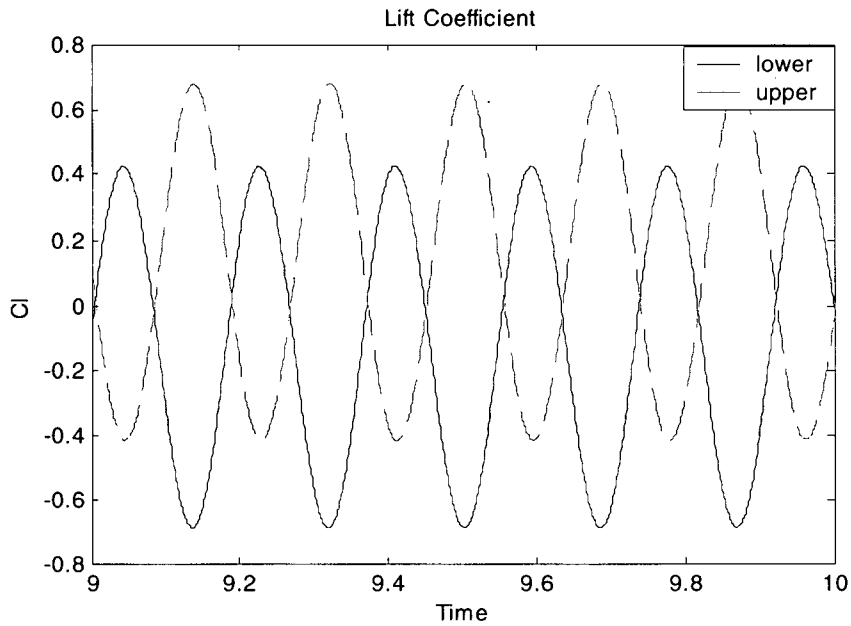

Figure 3.14 Lift coefficients of flow past two side by side cylinders at $g = 3$, $Re = 100$
Anti-phase flow pattern

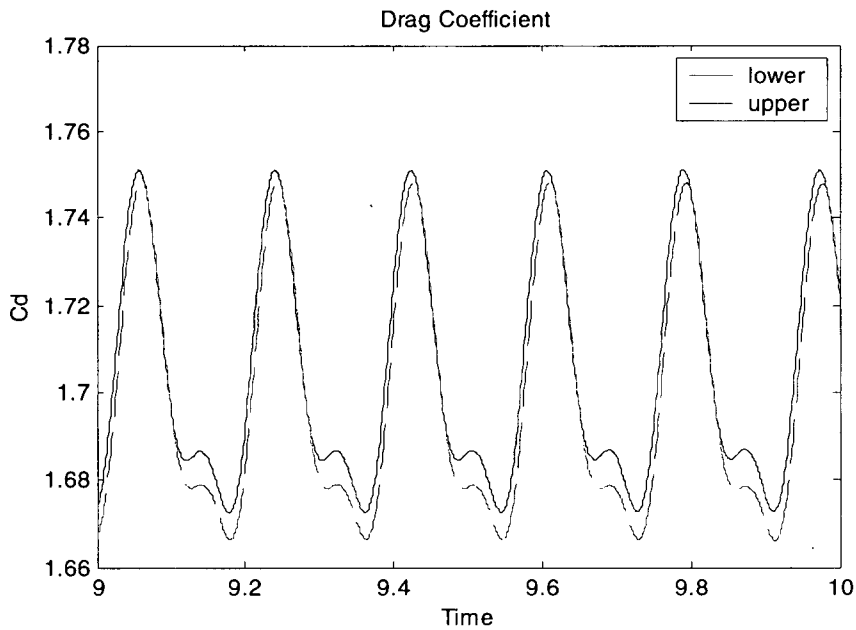

Figure 3.15 Drag coefficients of flow past two side-by-side cylinders at $g = 3$, $Re = 100$
Antiphase flow pattern

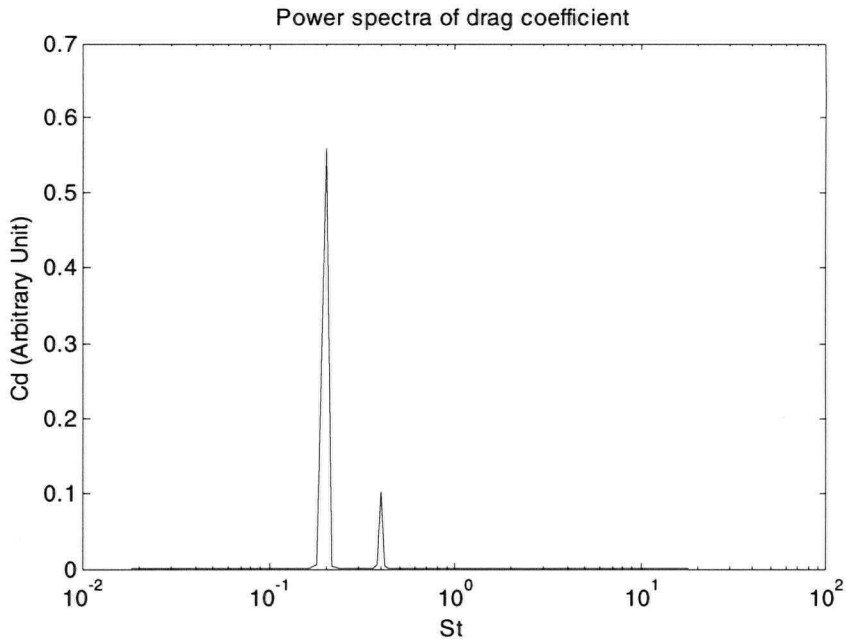

Figure 3.16 Power spectra of drag coefficients of flow past two side-by-side cylinders at $g = 3$, $Re = 100$
Anti-phase flow pattern

It is known from flow visualization [40] and numerical studies [41] that when the gap between two side-by-side cylinders is in the range of 2.0 - 6.0, a wake comprising two in-phase synchronized parallel streets may also form. Unlike anti-phase vortex shedding that is stable and can keep its form for large distances downstream (Figure 3.13), in-phase vortex shedding is not stable and eventually develops into a large-scale single wake. Figure 3.17 and Figure 3.18 clearly show this kind of vortex shedding, where the gap between the two cylinder centers is 3.0.

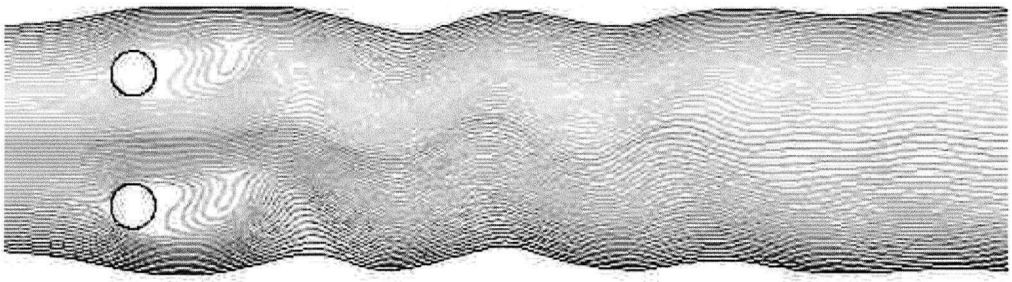

Figure 3.17 Instantaneous stream function of flow past two side-by-side cylinders at $g = 3$, $Re = 100$
In-phase flow pattern

Figure 3.18 Instantaneous vorticity magnitude of flow past two side-by-side cylinders at $g = 3$, $Re = 100$
In-phase flow pattern

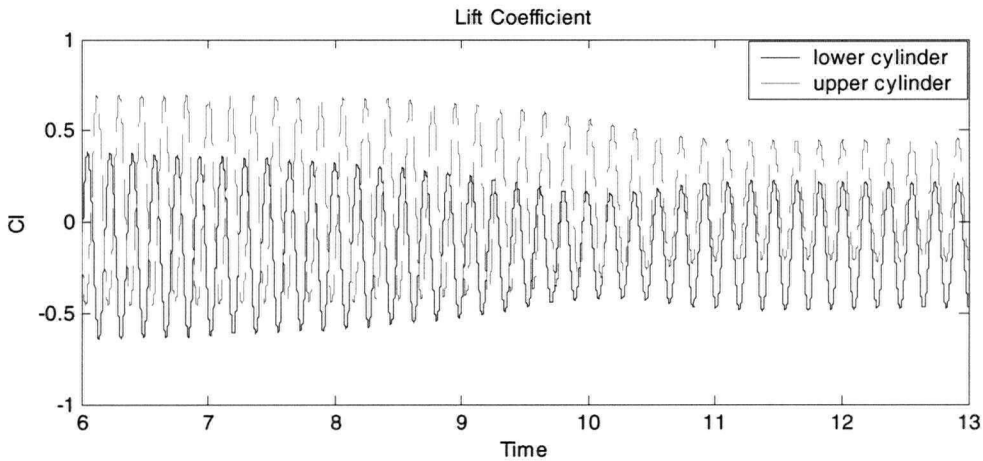

Figure 3.19 Phase shift of lift coefficient from anti-phase to in-phase mode for flow past two side-by-side cylinders at $g = 3$, $Re = 100$

It is worth mentioning that it is possible for the flow to 'flip' from anti-phase shedding to in-phase shedding and vice versa [40,41,45]. It was found that each mode remained stable for many cycles although the flow was capable of changing mode possibly due to perturbations arising during the experiment. There was no exact explanation for what causes the flow to 'flip' from one pattern to the other. Farrant et al. [45] found out that the initial acceleration of the flow typically caused the cylinders to shed anti-phase. However, imposing an oscillatory inflow of similar frequency to the shedding for a short duration caused the in-phase shedding to be established and to continue indefinitely even though the perturbation had ceased many shedding cycles

before. Chang and Song observed the flow drifted with time from anti-phase to in-phase shedding; however, they did not mention what caused the drift. In our calculation, when the two cylinders were placed in the center of the channel, there was only anti-phase shedding; however, when those two cylinders were placed half a cylinder radius off the center, 3.125% relative to the channel width (the channel width is 16*D*), the flow started anti-phase shedding and 'flipped' to in-phase shedding, remaining in-phase thereafter. Our results agree with Farrant et al.'s results [45]. The process of phase change from anti-phase to in-phase shedding is demonstrated in Figure 3.19.

When the gaps between cylinders are smaller than 2.0, but greater than 1.2, a biased flow pattern is observed. The vortex wake behind the cylinders becomes distinctly asymmetric. This kind of asymmetrical flow pattern is characterized by a narrow near-wake region behind one of the cylinders and a wide near-wake behind the other cylinder. Figure 3.20 and Figure 3.21 clearly show this kind of flow pattern, where the gap between the cylinder centers is 1.7 and the Reynolds number based on the free stream velocity and cylinder diameter is 100. The biased flow is clearly illustrated. The individual vortex street only exists in the near wake area and the combined vortices establish a single large wake as if they had originated from a single bluff body. This is due to the fact that the velocity of the gap flow is slow and the 'gap vortices' are weak compared with the case of larger gap size. The pairs of 'gap vortices' from both cylinders are 'squeezed', weakened and amalgamated with the dominant outer vortices. This occurs predominantly on one side of the wake, and in our calculation the gap flow is weakly deflected downwards.

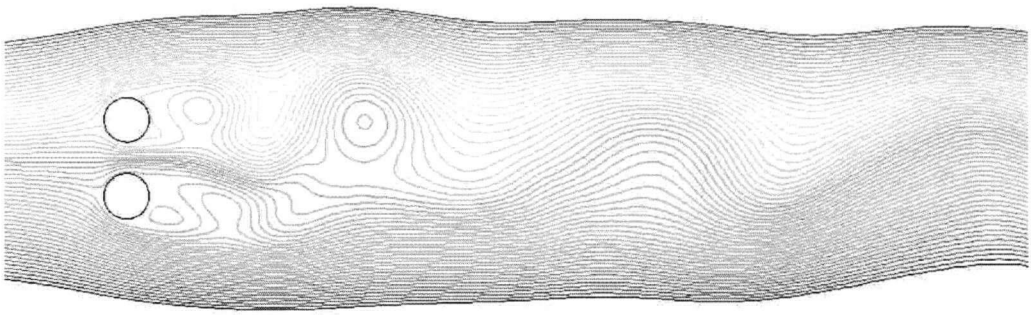

Figure 3.20 Instantaneous stream function of flow past two side-by-side cylinders at $g = 1.7$, $Re = 100$

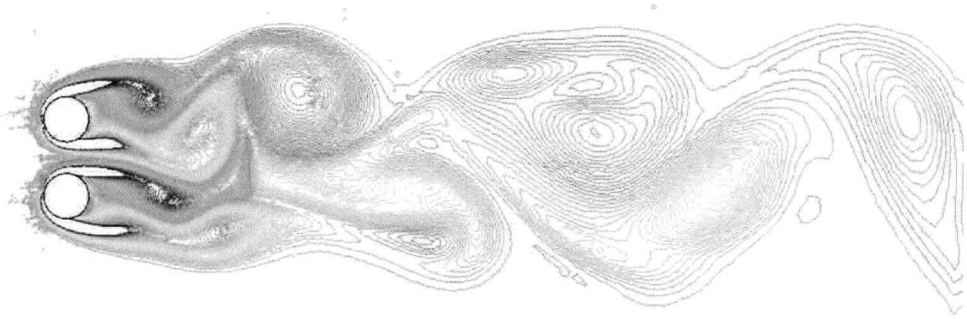

Figure 3.21 Instantaneous vorticity magnitude of flow past two side-by-side cylinders at $g = 1.7$, $Re = 100$

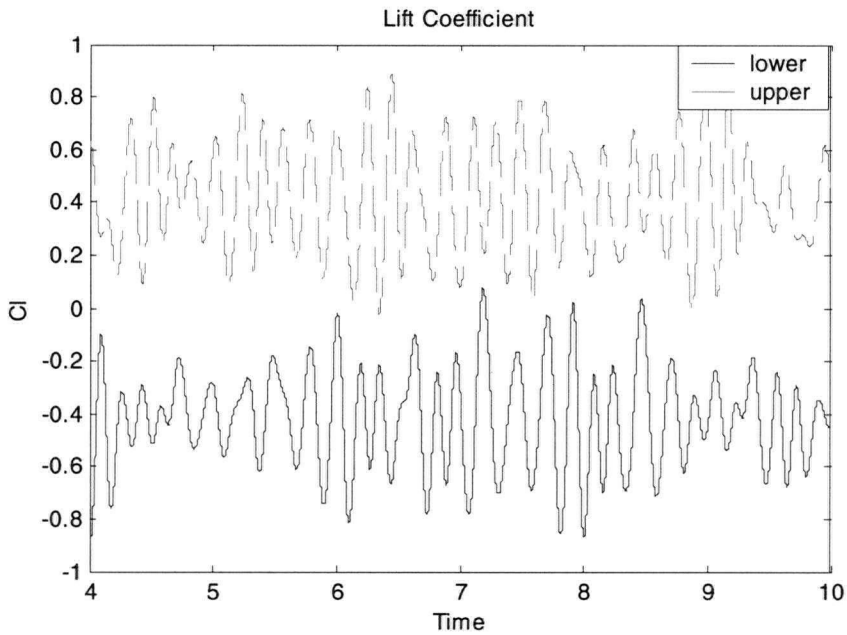

Figure 3.22 Lift coefficients of flow past two side-by-side cylinder at $g = 1.7$, $Re = 100$

It is believed that two dominant vortex shedding frequencies exist, which may result from the narrow and wide wakes behind the two cylinders. The Strouhal numbers are somewhat scattered around the two different values separately. Figure 3.22 shows the oscillation of the lifts of the two cylinders. The lift spectrum exhibits a broad peak, ranging from $St = 0.12$ to $St = 0.23$.

At an even smaller gap between the cylinder centers, i.e., smaller than 1.2, the two cylinders behave in a similar fashion to a single bluff body. A single vortex street is

observed in the combined wake of the two cylinders as shown in Figure 3.23 and Figure 3.24, and the shedding occurs only from the outside of the cylinder pair. The vortex shedding Strouhal number is 0.1089, and is in good agreement with many earlier experimental observations done by Williamson [40], Kim and Durbin [32], Bearman and Wadcock [27], and recent studies by Sumner et al. [35,36].

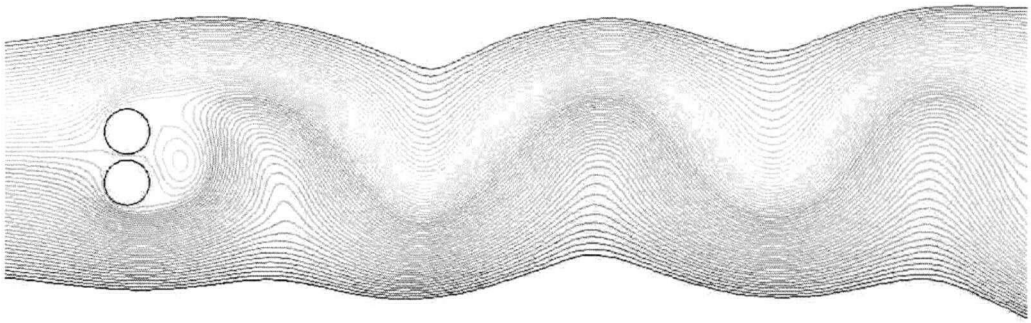

Figure 3.23 Instantaneous stream function of flow past two side-by-side cylinders at g = 1.13, Re = 100

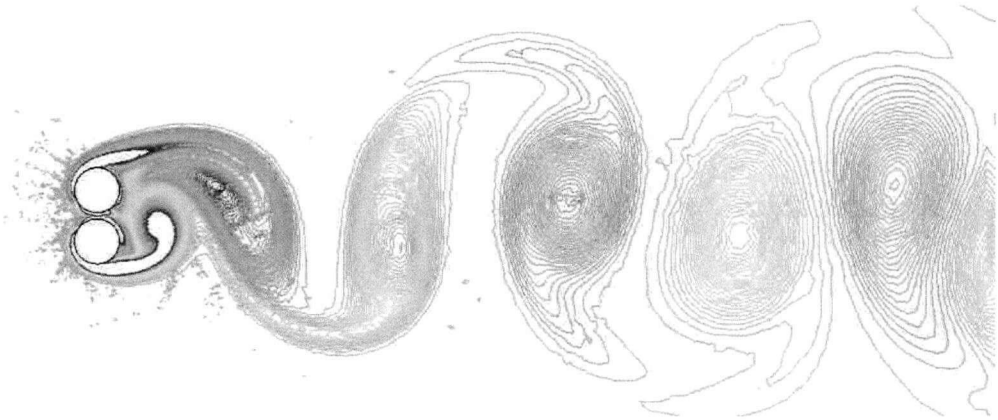

Figure 3.24 Instantaneous vorticity magnitude of flow past two side by side cylinders at g = 1.13, Re = 100

3.4 Flow around one row of cylinders

Studying the flow past a pair of cylinders has laid the foundation for understanding the flow through cylinder arrays. Experimental [28,43] and numerical [42] studies of cylinder arrays have found similar flow patterns to the flow past two side-by-side cylinders. It was shown in Ishigai and Nishikawa's experiments [28] that for moderate

Reynolds numbers and depending on the gap between the cylinders, two types of flow could be observed behind rows of parallel and identical tubes placed perpendicular to an incoming flow. When the distance separating the cylinder axes is more than 2.5 diameters of these cylinders, the vortex shedding from two adjacent cylinders is identical and in anti-phase mode. A typical example of such an oscillatory flow is shown in Figure 3.25, where the gap separating the cylinder axes is 4 and Reynolds number is 100 based on free stream velocity and the cylinder diameter. In order to save computing time, we only calculated six cylinders in one row; anti-phase flow is clearly visible in Figure 3.26 for the four cylinders in the central part of the row. Like the two side-by-side cylinders, these vortex streets are stable and keep the same form for large distances downstream.

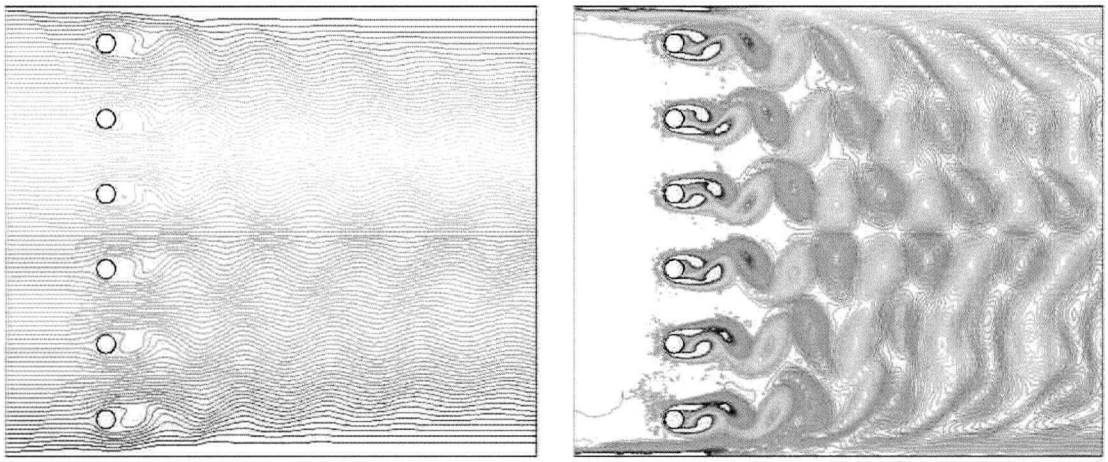

Figure 3.25 Instantaneous stream function and vorticity magnitude of flow past one row of six cylinders in a channel at $g = 4$, $Re = 100$

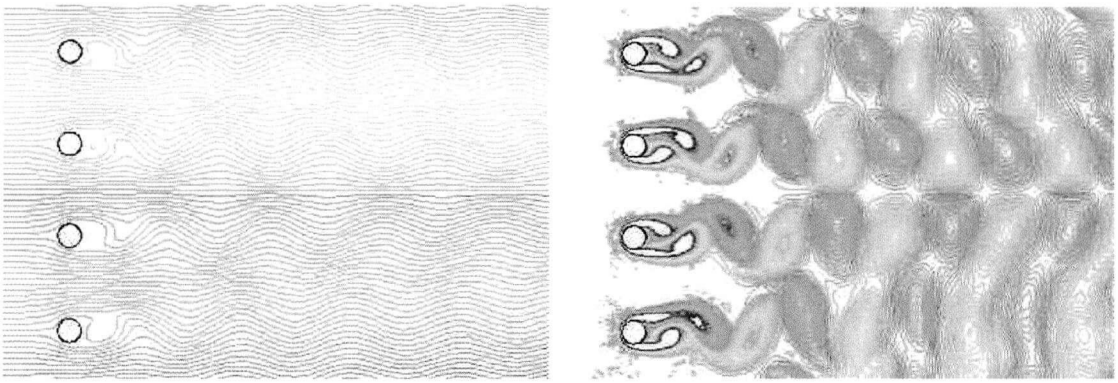

Figure 3.26 Instantaneous stream function and vorticity magnitude of flow past one row of six cylinders in a channel at $g = 4$, $Re = 100$: The four cylinders in the central part

It is interesting to note that when the entire row of cylinders was placed half a cylinder radius off the symmetry position again, another flow pattern occurred. Starting from the smaller gap side, the flow began to synchronize. Figure 3.27 shows that the vortex shedding behind the top three cylinders is in synchronized mode; i.e., in-phase mode, while the vortex shedding behind the bottom four cylinders is in anti-phase mode shown in Figure 3.28. Unlike flow past two side-by-side cylinders, the vortex flow behind the entire row will not shed in a synchronized pattern, i.e., in-phase mode. This is in good agreement with the experimental findings that when the gap separating the cylinder axes is large, the vortex shedding from two consecutive cylinders is in anti-phase mode.

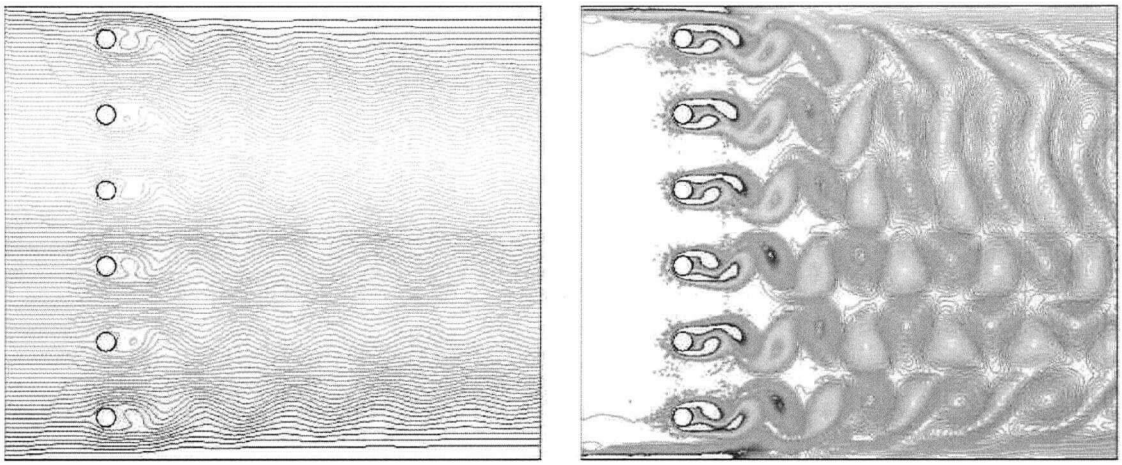

Figure 3.27 Instantaneous stream function and vorticity magnitude of flow past one row of six cylinders in a channel at $g = 4$, $Re = 100$: Combined anti-phase and in-phase mode.

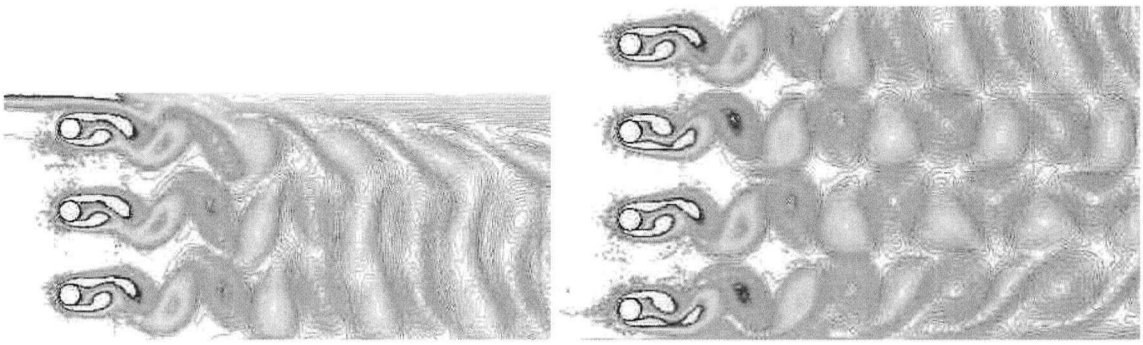

Figure 3.28 Instantaneous vorticity magnitude of flow past one row of six cylinders in a channel at $g = 4$, $Re = 100$: Top three cylinders move in-phase, while bottom four anti-phase.

In contrast to the case $g = 4$, when $g < 2.5$, the jets between the tubes are deviated and the wakes merge to form clusters. The number of wakes inside a cluster has been observed to vary from one to more than ten [42]. In particular, the coupling between the wakes is so strong that the entire flow moves in a synchronized pattern, i.e. in-phase flow pattern. Figure 3.29 shows our simulations of ten cylinders in one row at a center-to-center separation of 1.5 and Reynolds number of 38 based on the free stream velocity (105 based on the velocity between cylinders). The flow behind the ten cylinders moves in one synchronized group.

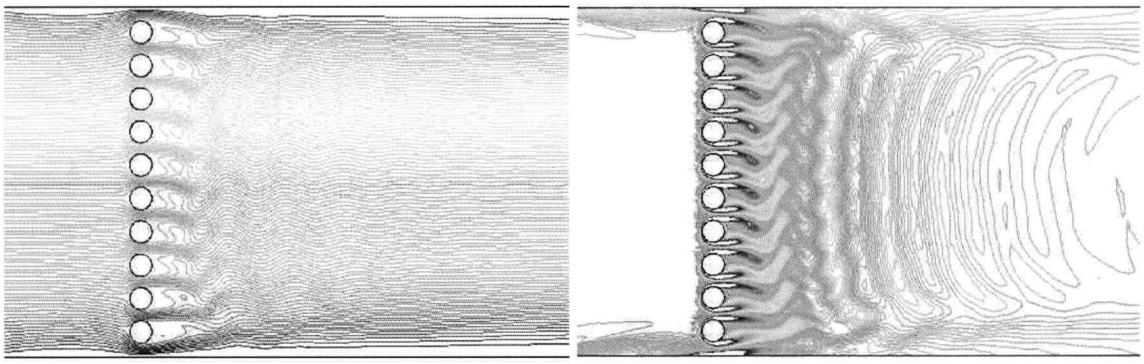

Figure 3.29 Instantaneous stream function and vorticity magnitude of flow past one row of ten cylinders in a channel at $g = 1.5$, $Re = 38$: Synchronized pattern in one group.

Fourteen cylinders were tested with the same pitch and Reynolds number as for the ten cylinders case is depicted. The only difference between ten and fourteen cylinders cases is the gap between the lateral wall and the first cylinder. It is clearly seen from Figure 3.30 that the flow moves in three groups for fourteen cylinders. The upper six cylinders are in one group and the lower six cylinders are in another group, and in both groups in-phase vortex shedding occurs. The central two cylinders are in a separate group showing the biased flow pattern seen in the flow around two side-by-side cylinders. Figure 3.31 is a close-up view of those two cylinders. Recall that changing the gap between the lateral wall and cylinders can trigger the flow to flip from anti-phase to in-phase vortex shedding for two side-by-side cylinders and for one row cylinders as well. The fourteen-cylinder case implies the gap may trigger the flow to cluster, too.

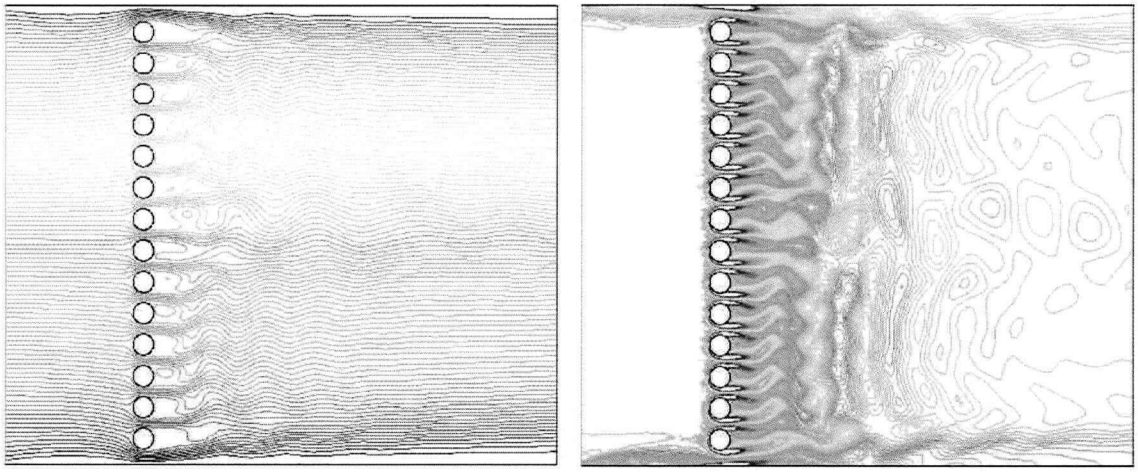

Figure 3.30 Instantaneous stream function and vorticity magnitude of flow past one row of fourteen cylinders in a channel at g = 1.5, Re = 38: Clustering in three groups.

Figure 3.31 Instantaneous stream function and vorticity magnitude of flow past one row of fourteen cylinders in a channel at g = 1.5, Re = 38: Biased flow pattern of the central two cylinders.

Chapter - 4 Flow Through Model Forming Fabrics – Results and Interpretation

As mentioned in the first chapter, the flow through paper machine forming fabrics is three-dimensional and has fibre interactions that create a complex flow that is intractable. To understand the essential flow physics we model the flow through forming fabrics as a two-dimensional, laminar, water flow through cylinder arrays.

In the previous chapter, we have calculated the flow past a single cylinder, then past two side-by-side cylinders, and a single row of identical cylinders. The flow through forming fabrics is simplified to the flow around two rows of unequal-sized cylinders and this chapter discusses these simulations.

4.1 Existing forming fabric: 73x75 triple-layer fabric

It is of vital importance that the fiber distribution in the web be as uniform as possible so that the best paper formation is attained. In order to provide for uniform dewatering, a uniform velocity profile is desired in the cross flow upstream of the fabric. Other researchers, have generally been more interested in the flow patterns *downstream* of cylinder arrays. However, we are interested in the velocity profiles *upstream* of the cylinder arrays, which help determine the fiber distribution and drainage.

4.1.1 Geometry

The following fabric dimensions are based on one of the commercial triple-layer fabric, i.e. 73 x 75 mesh triple-layer fabric, which has two separate layers, each with their own weave and filament diameters [9]:

- Paper side diameters are 0.13 mm for the MD filament and 0.15 mm for the CD.
- CD separation is 0.35 mm for the 0.13 mm filaments.
- The lower layer or machine side diameters are 0.21 mm for the MD filaments and 0.33 mm for the CD.
- CD separation on the machine side is 0.35 mm for the 0.21 mm filaments.

- Average z direction separation between the paper side and machine side layers is about 0.42 mm. In reality this distance is variable within the fabric.

The complicated woven geometry is simplified to two rows of cylinders, as shown in Figure 4.1, with the relevant parameters as d = 0.13 mm, D = 0.21 mm, $G1$ = $G2$ = 0.35 mm, and z = 0.42 mm. Here another parameter, Z = 0.25 mm, the closest separation between the two rows, is introduced. The reason to introduce this surface-to-surface separation, Z, instead of center-to-center distance, z, between the two rows is mainly because of the different diameters of the rows.

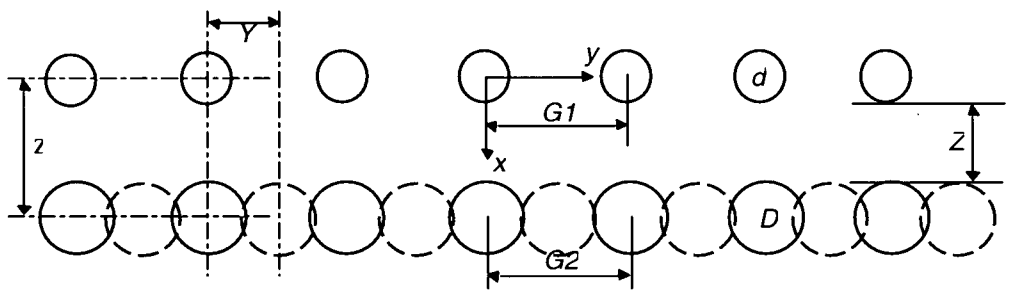

Figure 4.1 Definition of the geometrical parameters of a forming fabric, dashed cylinders represent the offset from in-line arrangement: In-line (solid) and staggered (dashed) arrangements

A real forming fabric, which is about 7 meters wide, has thousands of machine direction filaments. Rather than calculating the flow around so many cylinders, we considered just 8 cylinders in a row and applied a periodic boundary condition at the lateral boundary.

4.1.2 Flow patterns and comparison of different boundary conditions

The two-rows cylinders of diameter ratio D/d = 1.6154, placed in a channel at Reynolds number of about 65 based on the free stream velocity and the first-row cylinder diameter d and at equal gap, $G1$ = $G2$, but at different ratio, $g1$ = $G1/d$ = 2.6923, $g2$ = $G2/D$ = 1.6667, with the separation between the two rows of Z/d = 1, either in-line or staggered was calculated, where d and D are the first-row and the second-row cylinder diameters respectively, $G1$ and $G2$ are the first-row and the second-row cylinder center-to-center spacing respectively, and Z is the surface-to-surface separation between the two rows. The reason to choose surface-to-surface separation instead of center-to-center

between two rows is mainly because of the different diameters. The definition of the geometrical parameters is given in Figure 4.1. The flow pattern of in-line arrangement is shown in Figure 4.2. It demonstrates that there is incomplete vortex shedding behind the first row even at this small separation between the two rows. However, the Karman vortices are not formed; the flow reattached to the second row cylinders because of the confined small area. The two in-line cylinders behave like one slender body. This agrees with the experimental observations of Ishigai et al. [28].

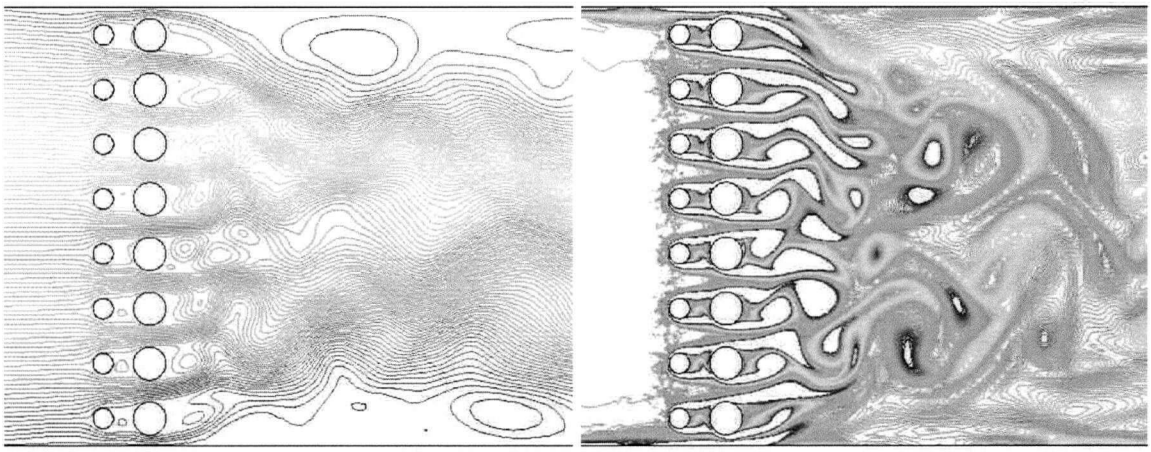

Figure 4.2 Instantaneous stream function and vorticity magnitude of flow past two-rows cylinders in a channel at D/d = 1.6154, $G1$ = $G2$, $g1$ = 2.6923, $g2$ = 1.6667, Z/d = 1, Re = 65: In-line arrangement

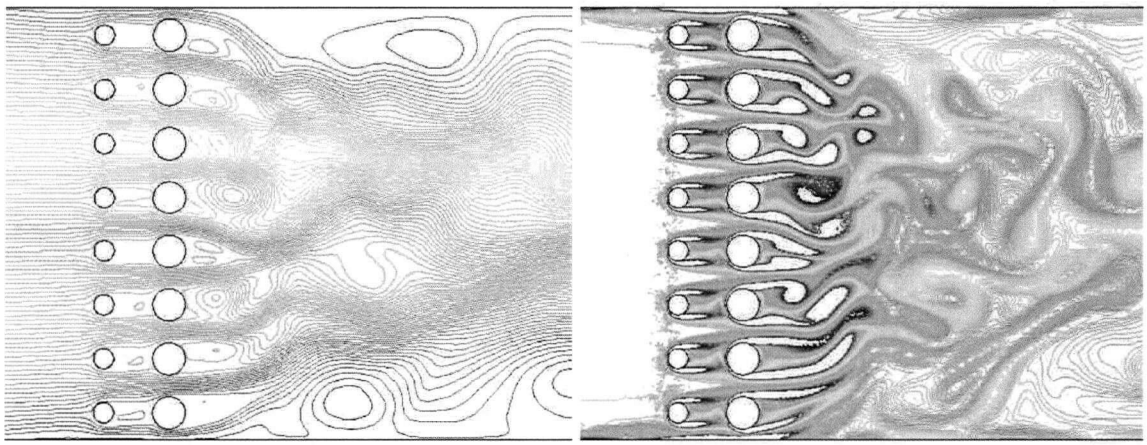

Figure 4.3 Instantaneous stream function and vorticity magnitude of flow past two-rows cylinders in a channel at D/d = 1.6154, $G1$ = $G2$, $g1$ = 2.6923, $g2$ = 1.6667, Z/d = 1.923, Re = 65: In-line arrangement

A similar flow pattern is shown in Figure 4.3 where the separation between the two rows was increased to 1.923. The Karman vortices are almost formed behind the first

row. If the separation is increased further, we can expect that the downstream cylinder will get out of the vortex formation region of the upstream cylinder and the Karman vortices will be formed behind each row. This separation might be a little greater than 2.0 that at this separation for equal-sized cylinders, the Karman vortices are formed behind each row.

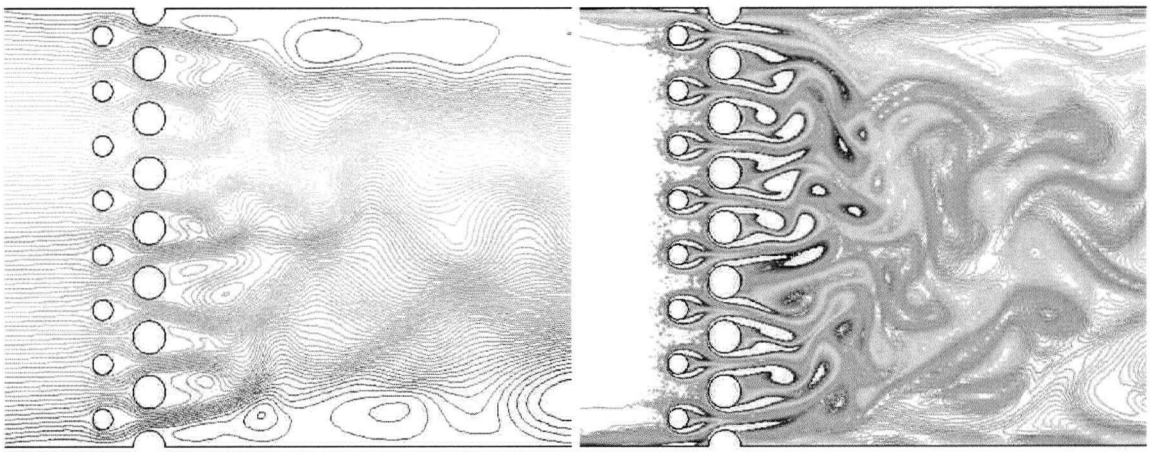

Figure 4.4 Instantaneous stream function and vorticity magnitude of flow past two-rows cylinders in a channel at D/d = 1.6154, $G1$ = $G2$, $g1$ = 2.6923, $g2$ = 1.6667, Z/d = 1, Re = 65: Staggered arrangement

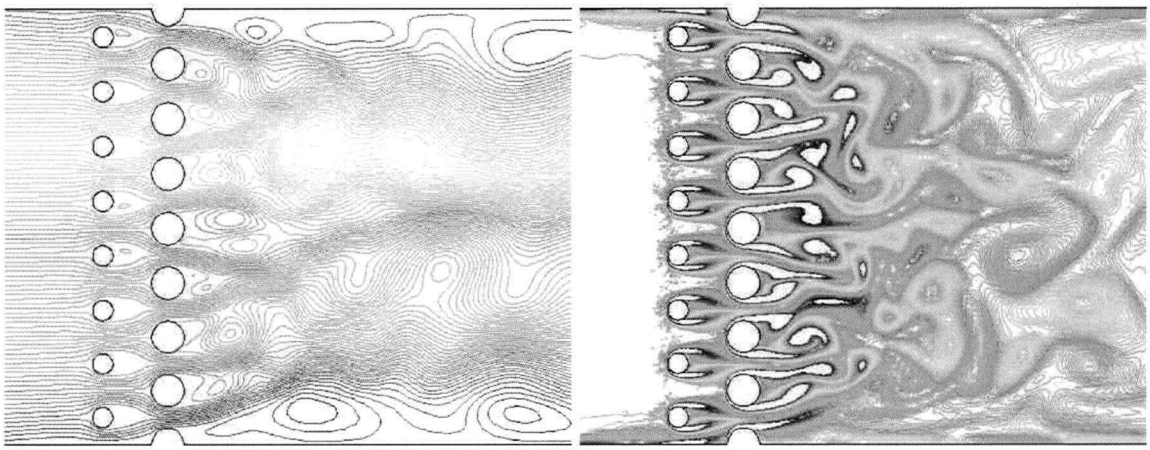

Figure 4.5 Instantaneous stream function and vorticity magnitude of flow past two-rows cylinders in a channel at D/d = 1.6154, $G1$ = $G2$, $g1$ = 2.6923, $g2$ = 1.6667, Z/d = 1.923, Re = 65: Staggered arrangement

Figure 4.4 and Figure 4.5 are the flow patterns for the staggered arrangements. In the upstream row of staggered arrangements, the size of the vortex formation region behind each cylinder is strongly dependent on the separation between the two rows, as can be seen from the stream function graphs. Figure 4.4 is the example of flow patterns with very small vortex formation regions, while Figure 4.5 gives another example of large

vortex formation regions. However, Karman vortices are definitely formed in spite of the very small formation region in Figure 4.5; this phenomenon is confirmed by looking at the velocity oscillations behind the first-row cylinders. Thus unlike in-line arrangements, each cylinder in staggered arrangements sheds Karman vortices.

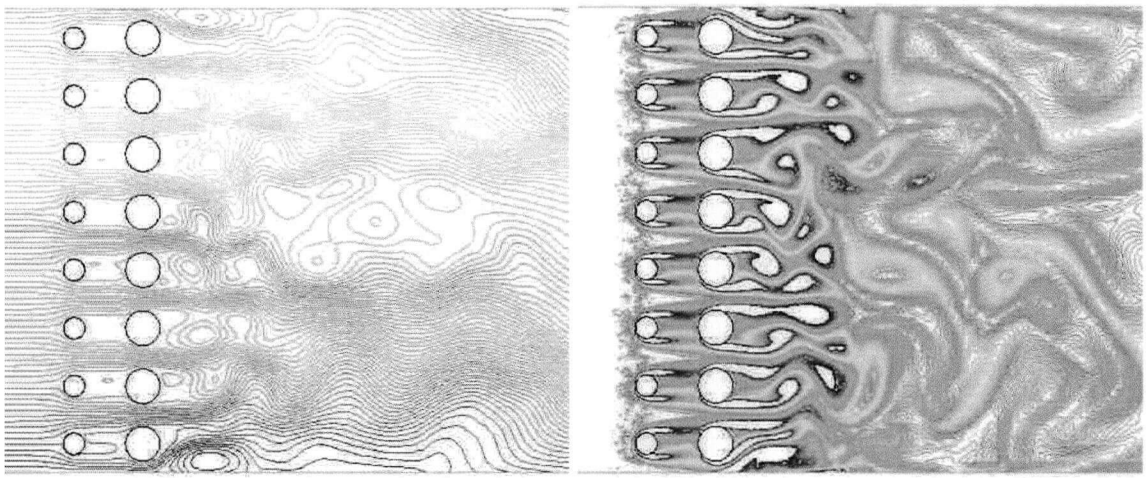

Figure 4.6 Instantaneous stream function and vorticity magnitude of flow past two-rows cylinders at D/d = 1.6154, $G1$ = $G2$, $g1$ = 2.6923, $g2$ = 1.6667, Z/d = 1.923, Re = 65: Periodic lateral boundary condition and in-line arrangement

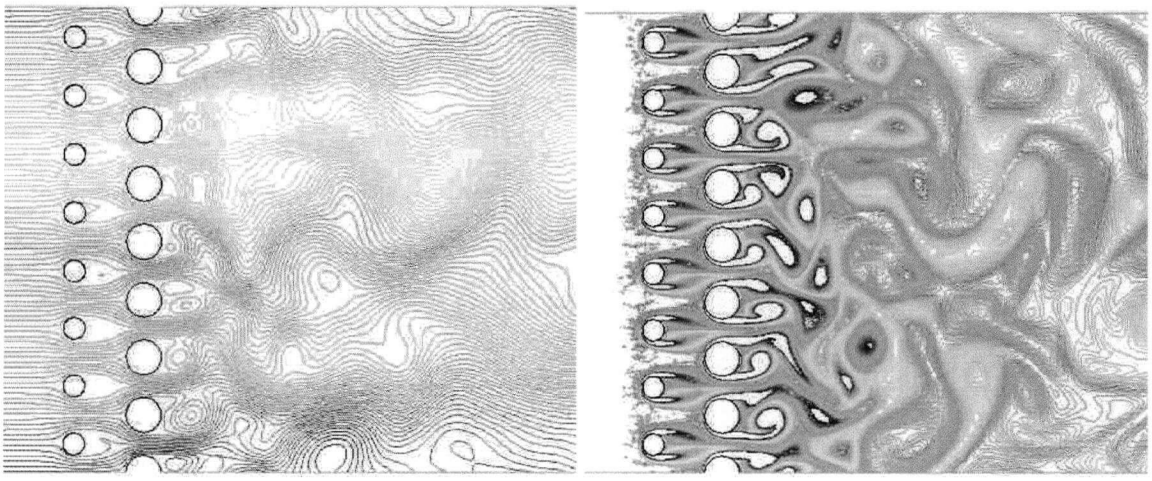

Figure 4.7 Instantaneous stream function and vorticity magnitude of flow past two-rows cylinders at D/d = 1.6154, $G1$ = $G2$, $g1$ = 2.6923, $g2$ = 1.6667, Z/d = 1.923, Re = 65: Periodic lateral boundary condition and staggered arrangement

Because the periodic lateral boundary condition is chosen in the simulations of flow through forming fabrics, a comparison between two types of boundary conditions, i.e., periodic vs. no-slip is conducted. Typical flow patterns are given in Figure 4.6 and Figure

4.7 using periodic lateral boundary conditions for two rows of unequal-sized cylinders in in-line and staggered arrangements. There is no major difference comparing with Figure 4.3 and Figure 4.5 using no-slip wall lateral boundary conditions.

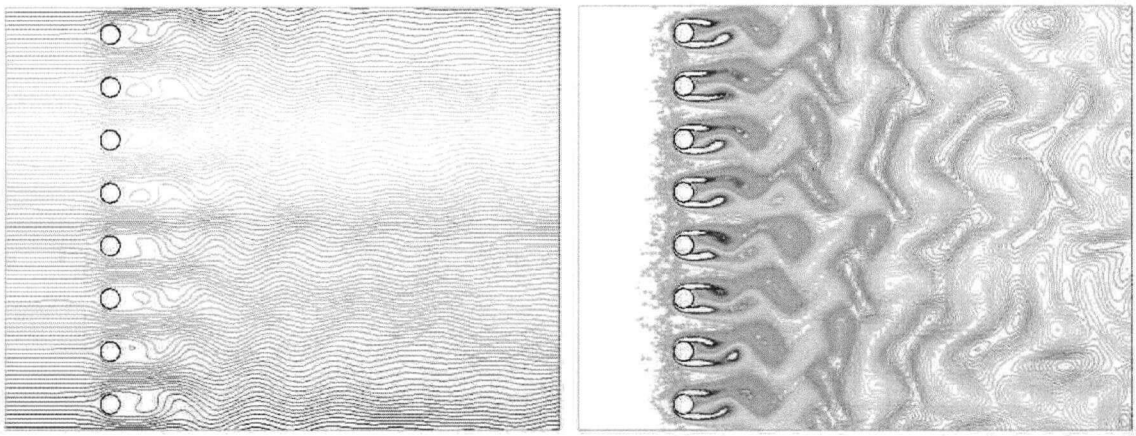

Figure 4.8 Instantaneous stream function and vorticity magnitude of flow past one row of eight cylinders at $g = 2.692$, $Re = 65$: Periodic lateral boundary condition

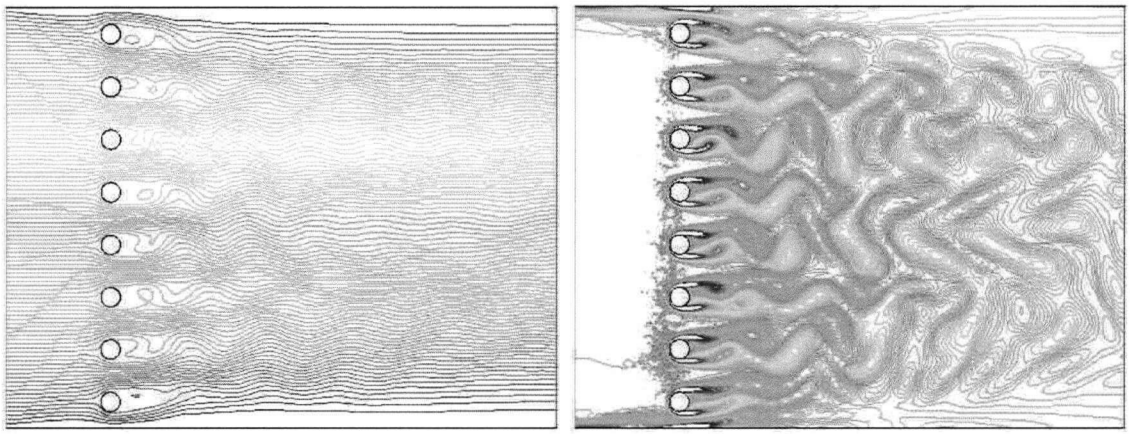

Figure 4.9 Instantaneous stream function and vorticity magnitude of flow past one row of eight cylinders at $g = 2.692$, $Re = 65$: No-slip wall lateral boundary condition, i.e., flow in a channel.

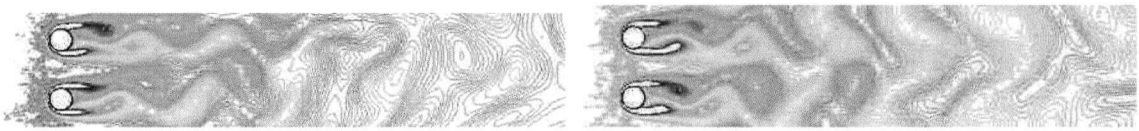

Figure 4.10 Instantaneous vorticity magnitude of flow past one row of eight cylinders at $g = 2.692$, $Re = 65$. Left: Periodic lateral boundary condition; vortex shedding behind the fourth and fifth cylinders from bottom. Right: No-slip wall lateral boundary condition, i.e., flow in a channel; vortex shedding behind the second and third cylinders from bottom.

For a similar reason, a flow pattern comparison between periodic and no-slip boundary conditions is also given in Figure 4.8 and Figure 4.9 for flow around one row of

8 cylinders. It is noted that the periodic boundary condition does not have to induce the synchronized in-phase flow. The boundary conditions only affect the flow near boundaries especially when the number of cylinders is larger. The flow patterns behind inner cylinders are similar for these two boundary conditions. Based on these observations, we may conclude with some assurance that the lateral boundary conditions do not affect the flow near central cylinders.

4.1.3 Velocity profiles upstream of the fabric

Normally a fast-draining fabric with good retention characteristics and without wire marking (shadow marks) is required.

Shadow marking can be considered as topographic marking of the yarn knuckles or drainage marking. Topographical marking is an image of the top surface of a forming fabric in the sheet of a paper caused by fibers following the water flow out of the sheet emphasized by suction, or compression of the sheet against the fabric. Drainage marking means unevenly distributed fines and fillers in the x-y-plane of the sheet according to the drainage channels of a forming fabric. Visible shadow marking often is a combination of both topographical and drainage marking.

For paper grades that are sensitive to shadow marking, a forming fabric with the top side surface made of as small elements or yarn floats as possible needs to be chosen. The floats need to be distributed uniformly. Any diagonal or cross-machine direction lines in the structure can easily cause drainage marking.

Wear resistance of a forming fabric depends on its bottom side structure. The bottom side of a forming fabric is made of as thick and long yarn floats as possible for the paper grade to be produced and for the former type to be used. Initial formation of a paper web becomes uneven if a forming fabric carries uneven amounts of water when the jet hits the fabric. Gap forming is especially sensitive to this.

Forming fabric with a fine paper side surface has proved to show the lowest tendency of fiber bleeding-through. However, fabric designs with a coarse bottom side or wear side easily mark the sheet if drastic drainage occurs like in gap forming. This means a good design requires very fine mesh on the paper side to provide uniform drainage, good retention, and fibre distribution, but very coarse mesh on the machine side to provide fast

drainage, wear resistance, and mechanical support while not causing shadow marking. This commercial triple-layer fabric has the same fine mesh in both paper and machine side so it does not meet this design requirement; however, the tentative design of a forming fabric in next section will fully meet the design requirement.

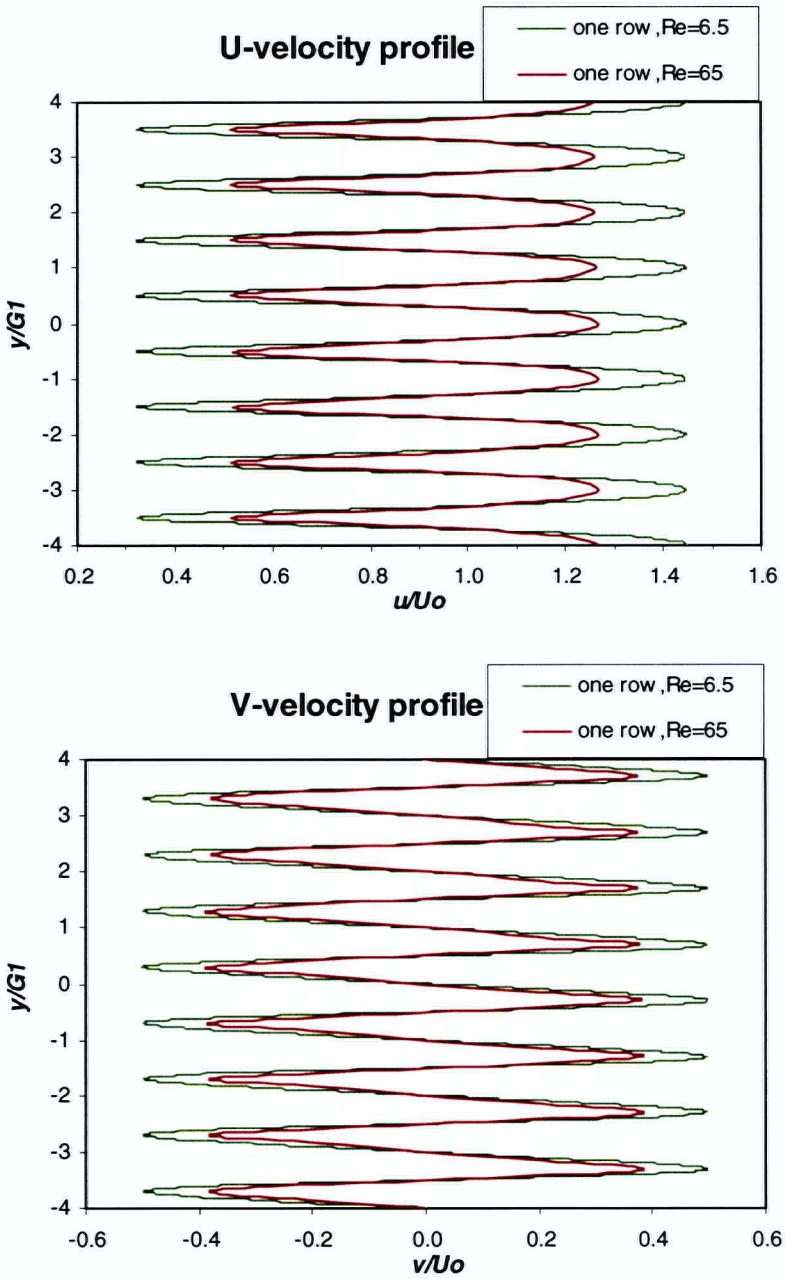

Figure 4.11 U and V velocity profile *d*/4 upstream in front of one row cylinders at *Re* = 65 and *Re* = 6.5

To avoid wire marking (shadow marks), one wishes to have the most uniform velocity profiles upstream in front of the fine row of cylinders. If the coarse bottom side

marks the sheet, its effect must be felt through the alteration of the velocity profile above the top row of cylinders. It is thus appropriate to use the velocity profile in front of one row of cylinders as the reference profile. Figure 4.11 showed the U and V velocity profiles $d/4$ upstream of the row of cylinders for the cases with incoming velocity U_o = 0.5 m/s and U_o = 0.05 m/s respectively, corresponding to Reynolds numbers of Re = 65 and Re = 6.5 based on cylinder diameter, where d is the cylinder diameter.

The reason the calculation is started with a velocity of 0.5 m/s is that this velocity is typical of what happens near jet impingement. At this velocity, the flow is unsteady. Once a fiber mat builds up on the fabric, the velocity through the fabric is much smaller. Therefore, a flow field with a velocity of 0.05 m/s is also calculated. The comparison of effects at these two velocities will be discussed later.

The forming fabric geometry is simplified to two rows of cylinders as shown in Figure 4.1. The velocity profile in upstream of a single row of cylinders is used as the reference profile for the flow through the varying designs examined. Perturbations from the reference flow provide an indication of non-uniformity of drainage and fiber distribution. In particular, the effect of the larger, downstream, structural wires on the upstream velocity profile is examined for varying diameter, pitch and position.

There are several design choices we want to examine. These include the effect of surface-to-surface separation between the two rows, the effect of diameter ratio, the effect of second row spacing between two adjacent cylinders, and the relative position of the two rows of cylinders (offset).

Figure 4.12 and Figure 4.13 show the velocity profile in front of the first row of cylinders for flow around two rows of cylinders and compare with that of flow around one row of cylinders as a function of cylinder offset, $Y/G1$. An unsteady solution is given in Figure 4.12 for Re = 65 and, a steady calculation is shown in Figure 4.13 for Re = 6.5. Both steady and unsteady results show that the flow in front of the first row is not affected by the existence of the second row regardless of the offset. For the three relative positions of the second row, the velocity profiles are overlapping each other and are the exact same as the profile of one row. It is then concluded that there is no shadow marking caused by the machine side mesh for this existing forming fabric.

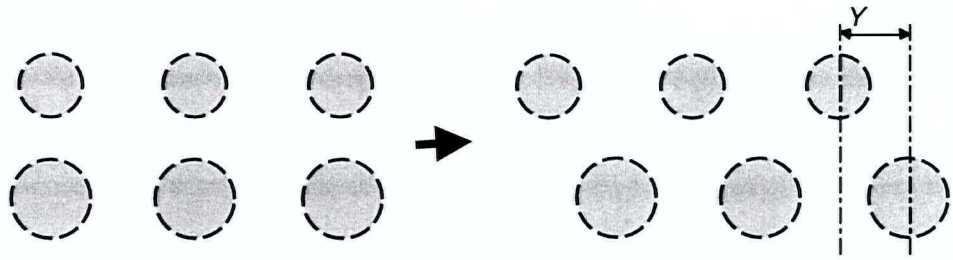

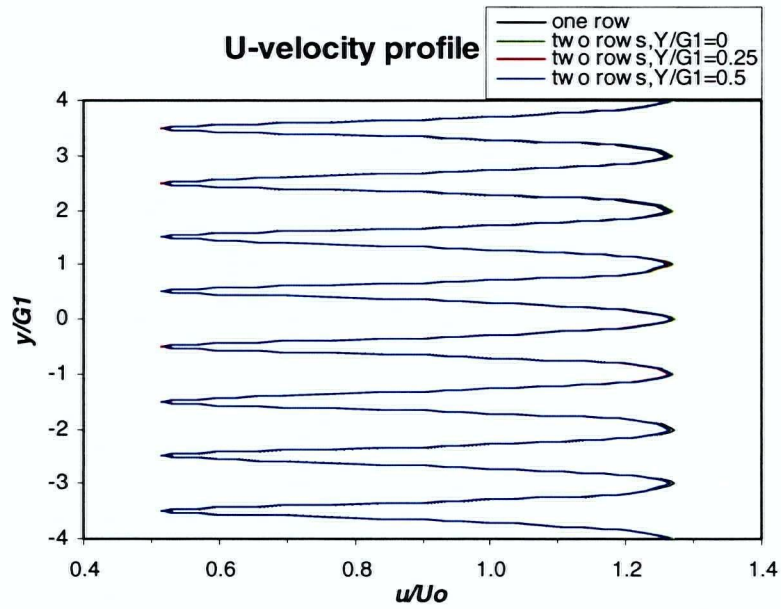

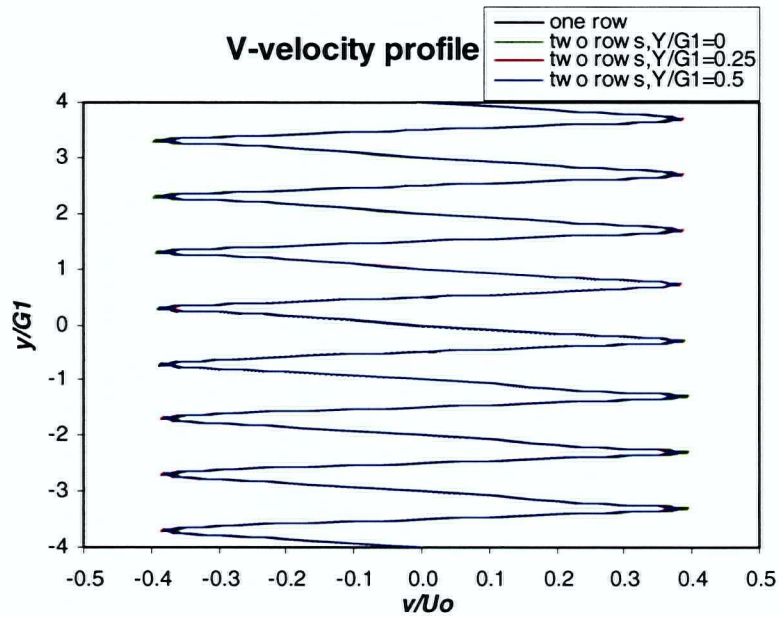

Figure 4.12 U and V velocity profile of unsteady simulation at *Re* = 65, *Z/d* = 1.9, *D/d* =1.6, *G2/G1* = 1
Effect of offset in y direction of the second row

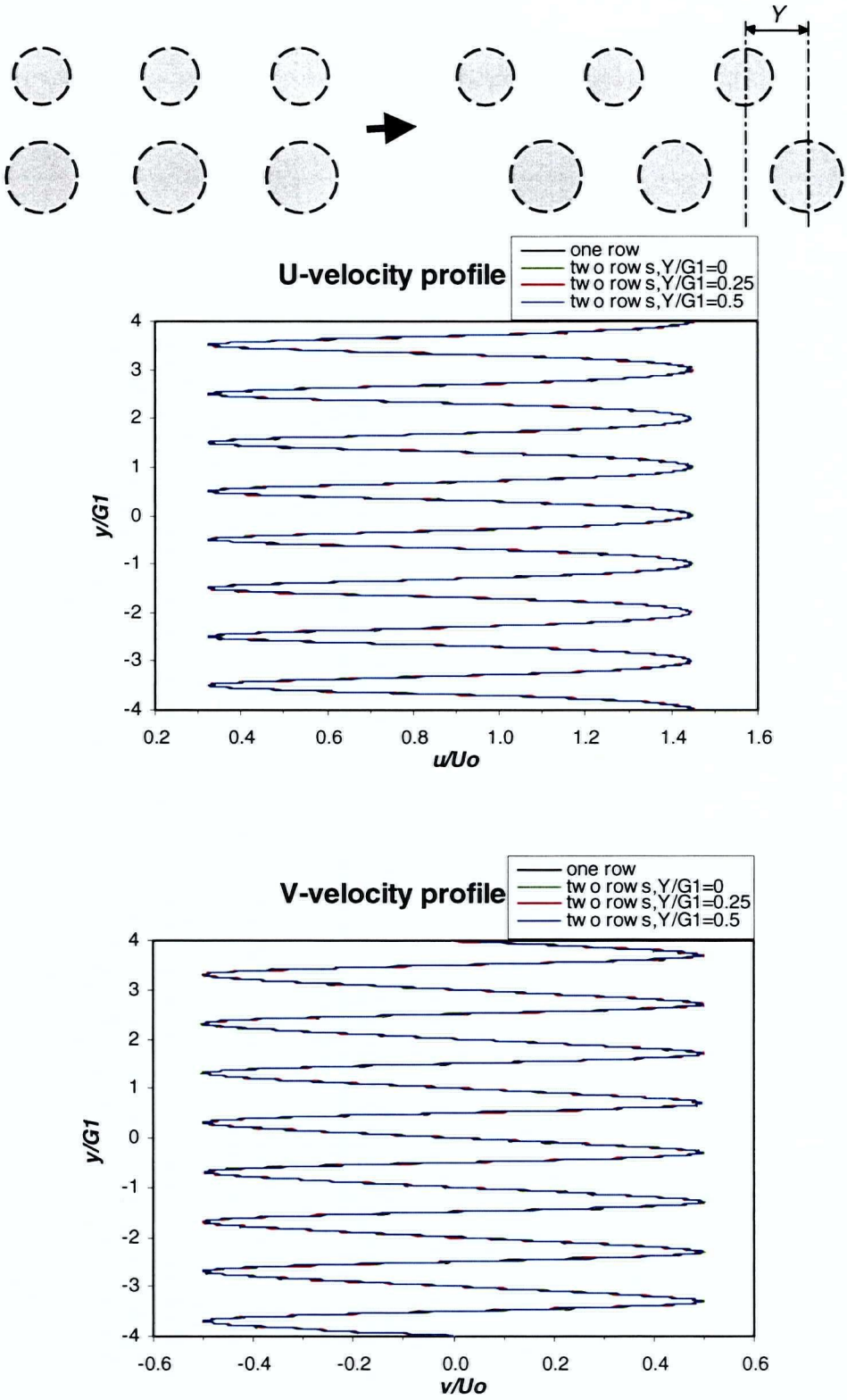

Figure 4.13 U and V velocity profile of steady simulation at *Re* = 6.5, *Z/d* = 1.9, *D/d* =1.6, *G2/G1* = 1
Effect of offset in y direction of the second row

These simulations also demonstrated that the predictions from steady and unsteady calculations provide the same information; therefore, steady calculations are given in the remainder of the thesis. However, unsteady calculations have also been performed to confirm some important findings.

4.1.4 Equal separation for two layers

As shown above, under its current configuration, there is no additional flow variation caused by the machine side mesh for this commercial forming fabric design. However, the question of what fabric design parameters affect flow remains unanswered. To address this question, a systematic study of forming fabric design variables is performed.

There are several parameters examined. The separation between the two rows of cylinders, the diameter of the downstream cylinders, the distance between cylinders in the downstream row (pitch), and the relative transverse position of the two rows of cylinders (offset). The current configuration is modified and simulations are performed to examine the effect of each of these parameters.

4.1.4.1 Effect of offsets at zero gap (z direction separation)

U and V velocity profile of steady simulation at zero separation between two rows is plotted in Figure 4.14 for three offsets in the y direction, given by $Y/G1$ = 0, 0.25 and 0.5. We believe that the z direction separation between the paper side and machine side layers will have the most significant effect on the shadow marking if there is any shadow marking. The closer the two layers, the easier the flow upstream could be altered, thus causing shadow marking. The worst case would be the two layers in close contact with each other, i.e., at zero separation demonstrated in Figure 4.14. It can be seen from Figure 4.14 that the velocity profiles are almost the same as that in front of one-row cylinders; only the magnitude is a little different. The flow upstream is altered by the existence of the second-row, but the velocity profile remains unchanged. It is assumed that this small perturbation would not cause any shadow marks.

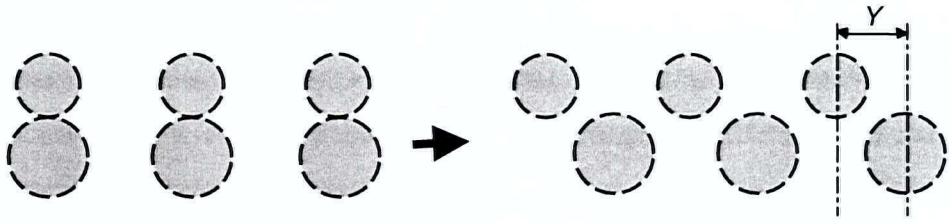

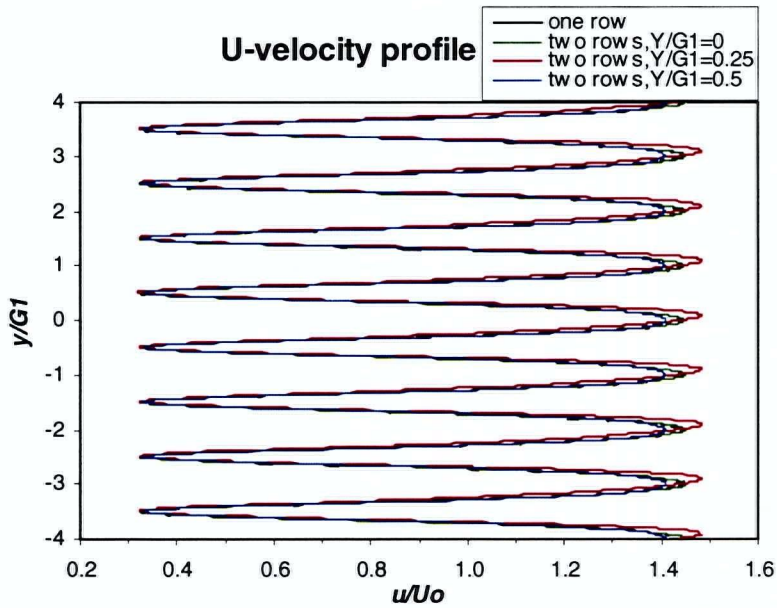

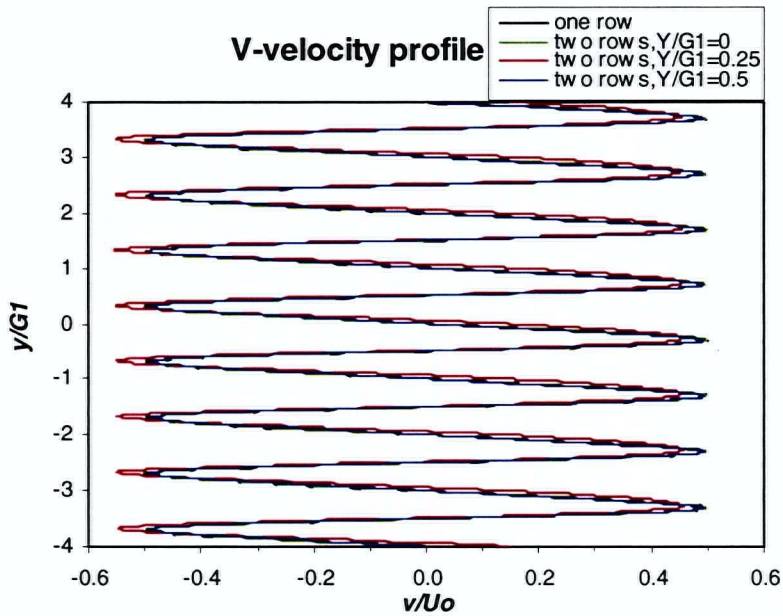

Figure 4.14 U and V velocity profile of steady simulation at $Re = 6.5$, $Z/d = 0$, $D/d = 1.6$, $G2/G1 = 1$
Effect of zero separation between two rows and offset in y direction of the second row

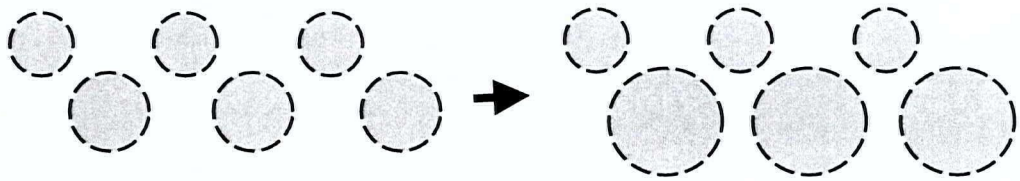

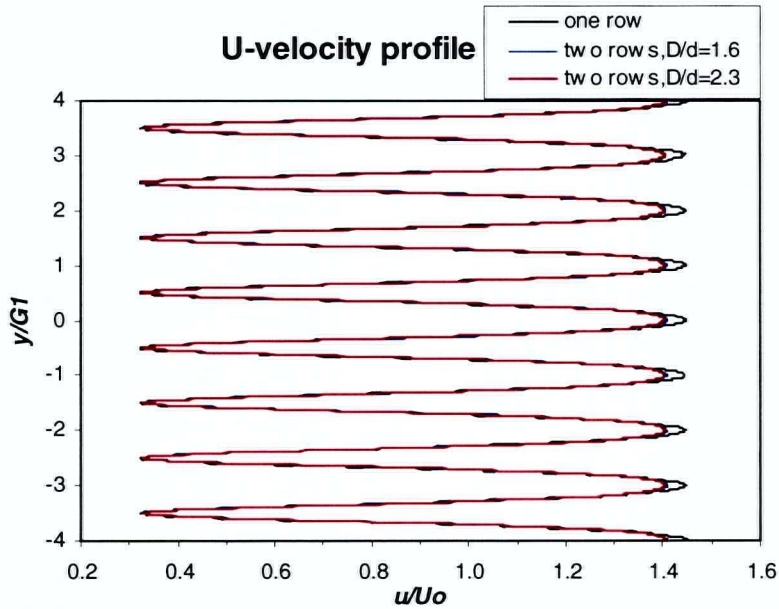

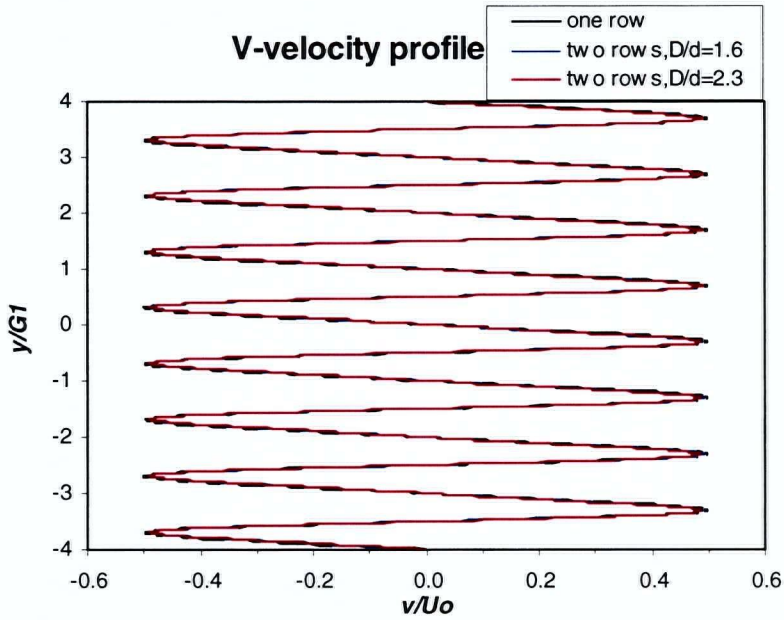

Figure 4.15 U and V velocity profile of steady simulation at $Re = 6.5$, $Z/d = 0$, $Y/G1 = 0.5$, $G2/G1 = 1$
Effect of zero separation and diameter ratio between two rows

4.1.4.2 Effect of diameter ratio at zero gap (z direction separation)

Small changes in diameter ratio do not have much of an impact on the velocity profile, as can be seen from Figure 4.15, where the diameter ratio was changed from 1.6 to 2.3 while keeping other parameters unchanged. It can be concluded that as long as the forming fabric has fine mesh in both paper and machine sides, changes in z direction separations of two layers, diameter ratios, or offsets between two layers appear to have little impact on the velocity profiles upstream in front of the first row. This design does not have any issue of shadow marking, though it is not economic.

4.1.5 Unequal separation for two layers

In the above section, the second row spacing between two adjacent cylinders is unchanged. It represents both fine mesh in the paper side and the machine side. The conclusion is that changes of other parameters, such as z direction separations of two layers, diameter ratios, or offsets between two layers appear to have little impact on the velocity profiles upstream in front of the first row. In this section, the second row spacing is increased and so is the cylinder diameter. They represent a fine mesh in the paper side and a coarse mesh in the machine side. Some representative dimensions for this hypothetical modification of the commercial triple-layer fabric are:

- Paper side diameters of 0 .13 mm for MD filaments (*d* is unchanged)
- CD separation of 0.35 mm (*G1* is unchanged)
- Machine side diameters of 0.39 mm or 0.30 mm for the MD filaments (diameter ratio, *D/d*, impact will also be considered)
- CD separation, *G2*, on the machine side of 0.56 mm or 0.70 mm (effect of different CD separations of the machine side layer will take into account)
- z direction separation (surface-to-surface), *Z/d*, changing from zero to a point where there would be no effect.

It should be noted that the arrangement of the paper side layer (upstream layer) is unchanged; the changes are all made in the machine side layer (downstream layer) so that it becomes a coarser mesh. The definition of the geometrical parameters is given in

Figure 4.1. As before, the effect of design changes is assessed in terms of the perturbation of the upstream fluid velocity profile from a single row of cylinders.

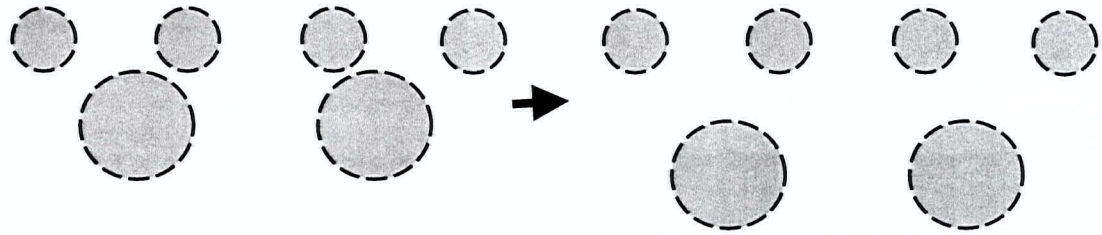

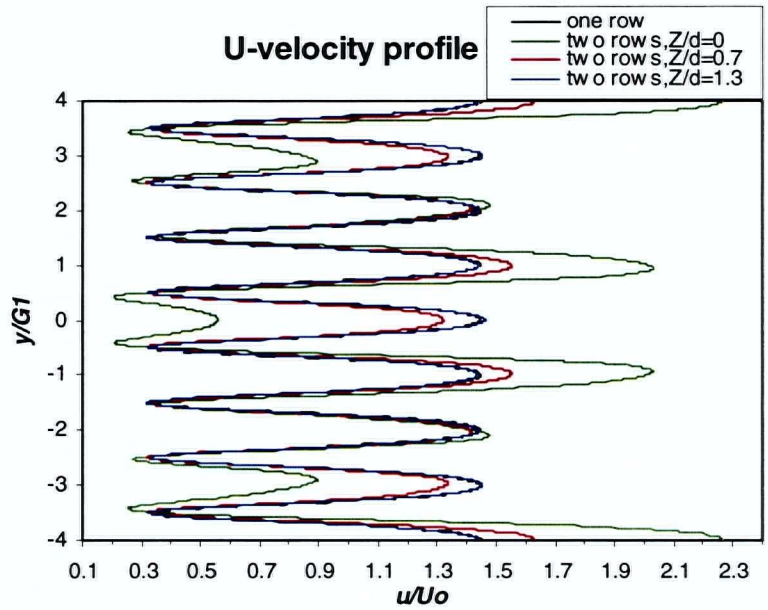

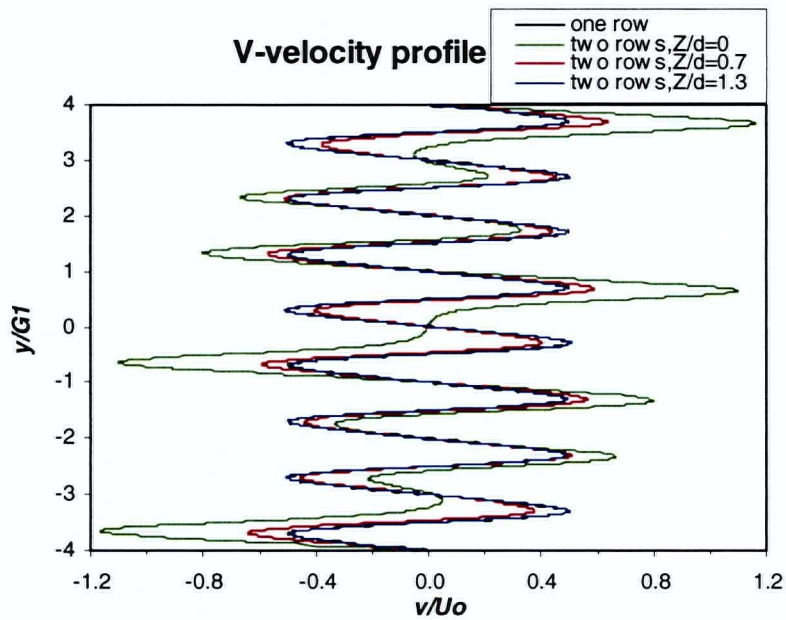

Figure 4.16 U and V velocity profile of steady simulation at $Re = 6.5$, $D/d = 3$, $G2/G1 = 1.6$
Effect of z direction separation between two layers

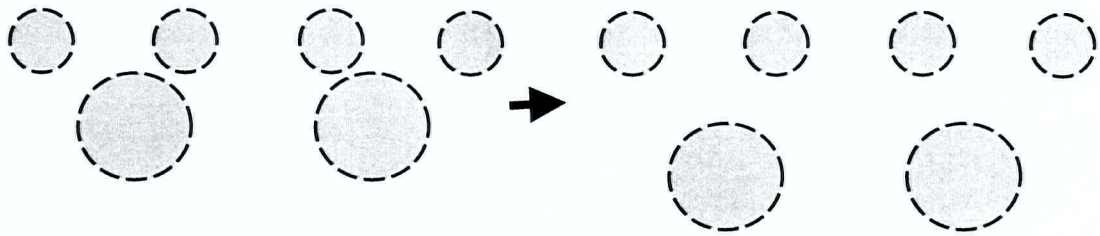

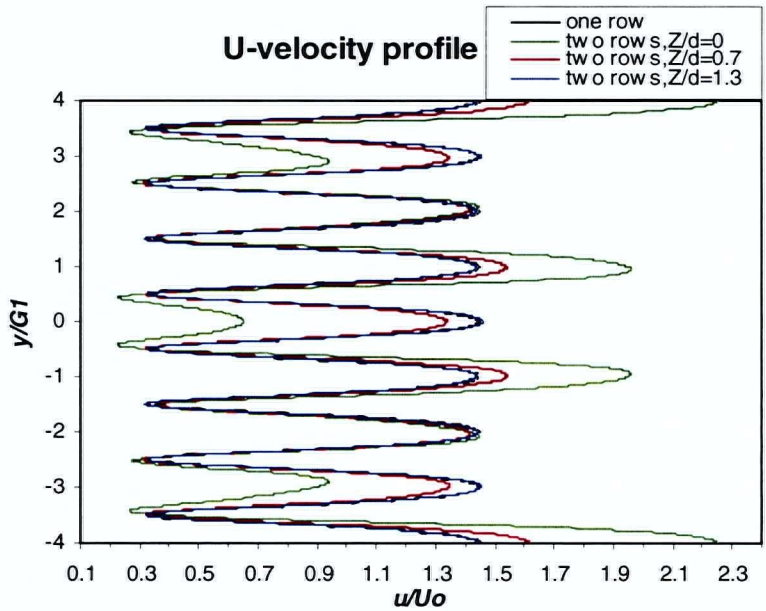

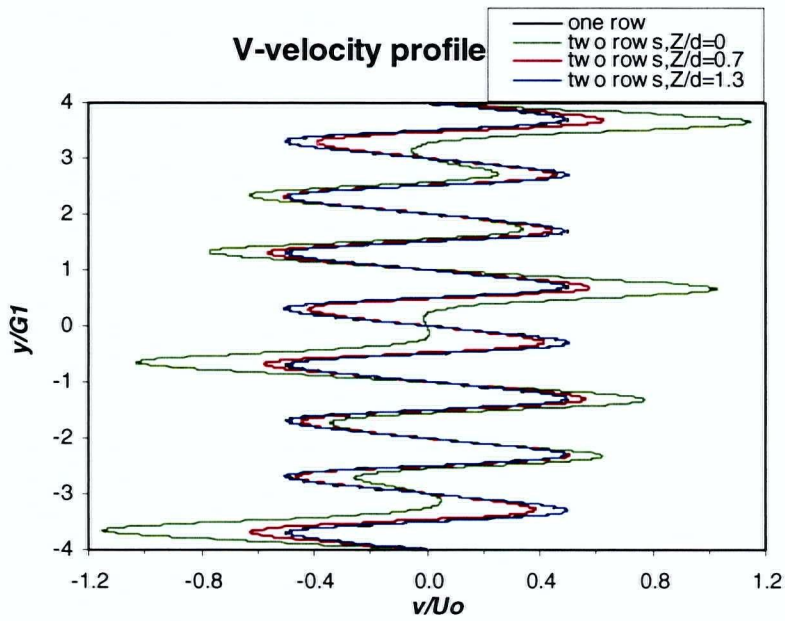

Figure 4.17 U and V velocity profile of steady simulation at *Re* = 6.5, *D/d* =2.3, *G2/G1* = 1.6
Effect of z direction separation between two layers

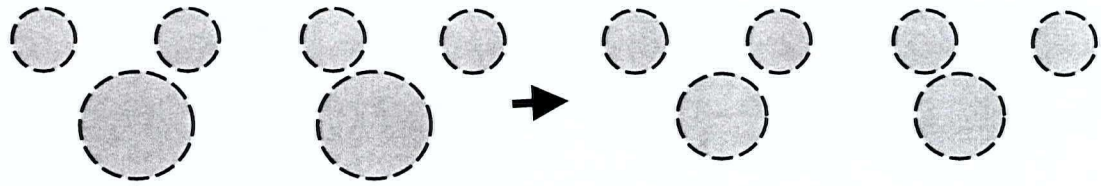

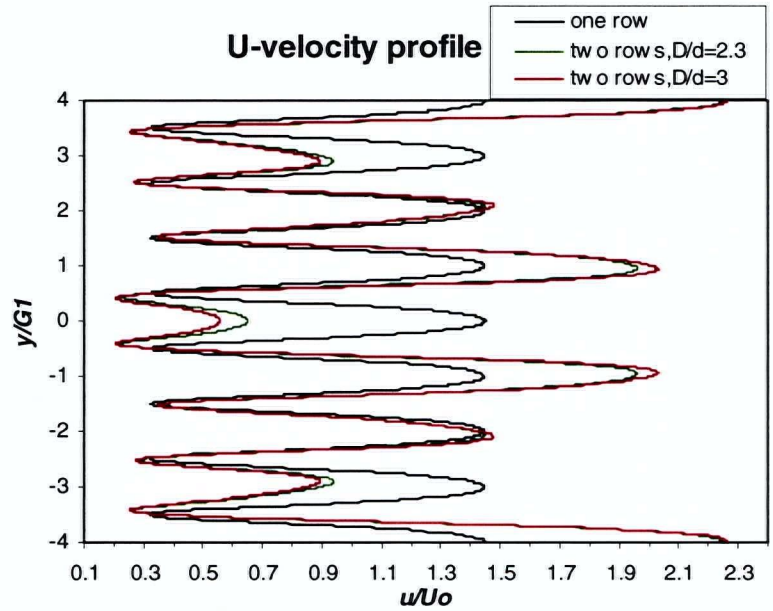

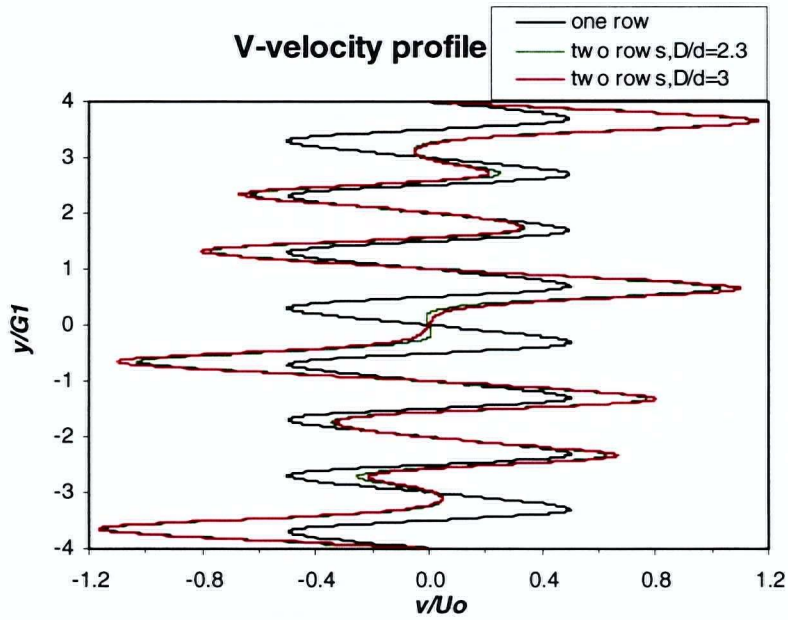

Figure 4.18 U and V velocity profile of steady simulation at Re = 6.5, Z/d =0, $G2/G1$ = 1.6
Effect of zero z direction separation between two layers and comparison of two diameter ratios

4.1.5.1 Effect of gap (z direction separation) and diameter ratio

The U and V velocity profiles in front of the upstream row of cylinders are given at Re = 6.5, for the downstream cylinder (machine side) diameters of 0.39 mm in Figure 4.16, and for the downstream cylinder (machine side) diameters of 0.30 mm in Figure 4.17. When the z direction separation between the two layers is zero, a dramatic change in the flow upstream appears as shown in Figure 4.16 and Figure 4.17. As this separation is increased to 0.17 mm, corresponding to Z/d = 1.3, the impact on the velocity profile disappears. This result confirms our understanding that the z direction separation between the paper side and machine side layers would have the most significant effect on shadow marking if there is any. It is obviously true that if the second row is moved far apart from the first row, the flow upstream in front of the first row cannot be affected.

One final point from these two figures (Figure 4.16 and Figure 4.17) should be noted that the diameter ratio seems to have little impact on the velocity profiles. A comparison of two diameter ratios is shown in Figure 4.18, where the velocity profiles from the two diameters are almost overlapping each other. It points out that the changes of machine side filaments diameter do not have a significant impact on the flow upstream.

4.1.5.2 Effect of pitch

When the CD separation, $G2$, on the machine side is another different constant, the impact on the flows upstream is similar. Figure 4.19 shows the U and V velocity profiles of steady simulation at Re = 6.5 for two different CD separations of the machine side layers of 0.56 mm and 0.70 mm respectively. It is clearly shown that although the profiles are different, they have a similar pattern and the magnitude of changes from that of one-row cylinders is almost equal.

4.1.5.3 Effect of Reynolds number

The unsteady results are shown in Figure 4.20, where Re = 65, D/d =2.3, $G2/G1$ = 1.6. The z direction separation between two layers is varied from zero to 1.3d. The velocity profiles are similar to the steady simulation illustrated in Figure 4.17 for the same configuration of forming fabric except the incoming velocity is increased from U_o = 0.05 m/s corresponding to Reynolds number of Re = 6.5 to U_o = 0.5 m/s corresponding

to Re = 65. Figure 4.21 compares velocity profiles from unsteady computation with that from steady calculation at zero separation between the two layers. It clearly indicates that the shape of the velocity profiles is similar; however, the magnitude of changes is different. At a higher flow speed, the flow upstream is less sensitive to the downstream objects than that at a lower speed. It is because that at a higher speed, the flow is more convective; downstream effects do not propagate as far upstream. At a z direction separation between the paper side (upstream) and machine side (downstream) layers of $0.7d$, there is no impact of the machine side (downstream) layer on the flow upstream, while for the steady solution at the same separation the flow upstream undergoes significant changes.

In reality, the flow velocity decreases as the fiber mat accumulates on the forming fabric. This velocity changes from roughly 0.8 m/s to less than 0.1 m/s. The shadow marking usually forms at the initial stage of the fiber accumulation. The simulation at a higher speed corresponding to the early stage of paper formation gives a more realistic estimate of the impact on the wire marking (shadow marks); whereas, a more conservative estimate is given by the steady simulation.

In this section, a systematic study of the geometry design choices for an existing forming fabric was conducted. The initial commercial triple-layer geometry showed very little perturbation of the fluid velocity profile upstream of a single layer (single row) of cylinders. Under its current configuration, there is no shadow marking caused by the machine side mesh. The effect of several design changes were examined through simulation, such as the z direction separation between the paper side and machine side layers, the diameter ratio of two-row cylinders, the second row spacing between two adjacent cylinders, and the relative position of the two rows of cylinders (offset). Three conclusions are reached. First, when the forming fabric has a fine mesh in both paper and machine sides, changes in z direction separations of two layers, diameter ratios, or offsets between two layers appear to have little impact on the velocity profiles upstream. Second, when the fabric has a fine mesh on the paper side and a coarse mesh on the machine side, the z direction separation between the paper side and the machine side layers has the most significant effect on the shadow marking. Finally, the unsteady simulation at a

higher speed corresponding to the early stage of paper formation gives a more realistic estimate of the impact on the shadow marking.

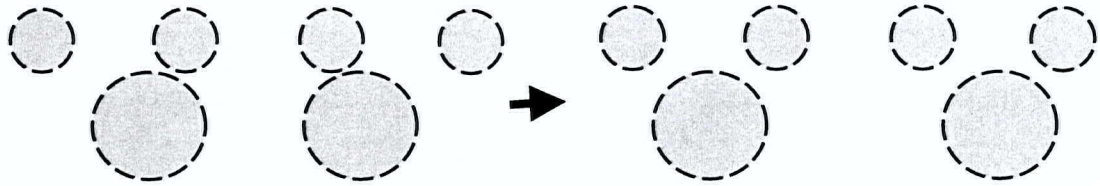

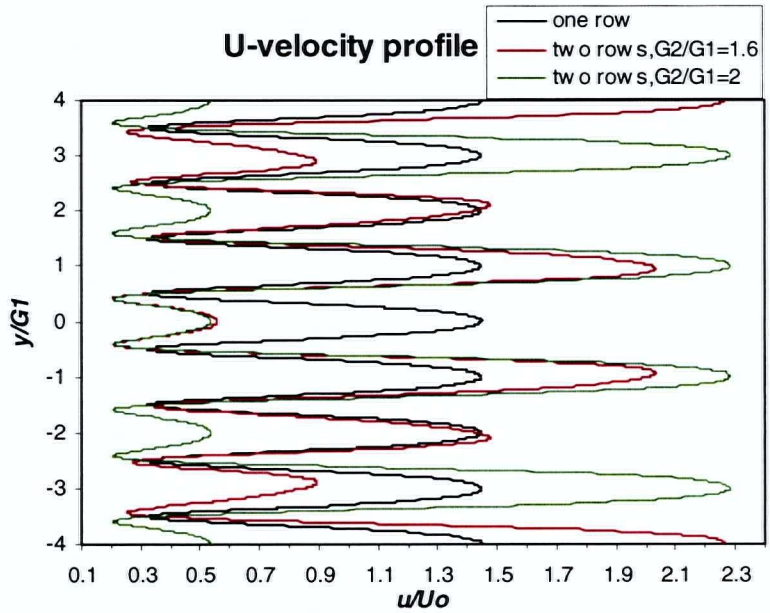

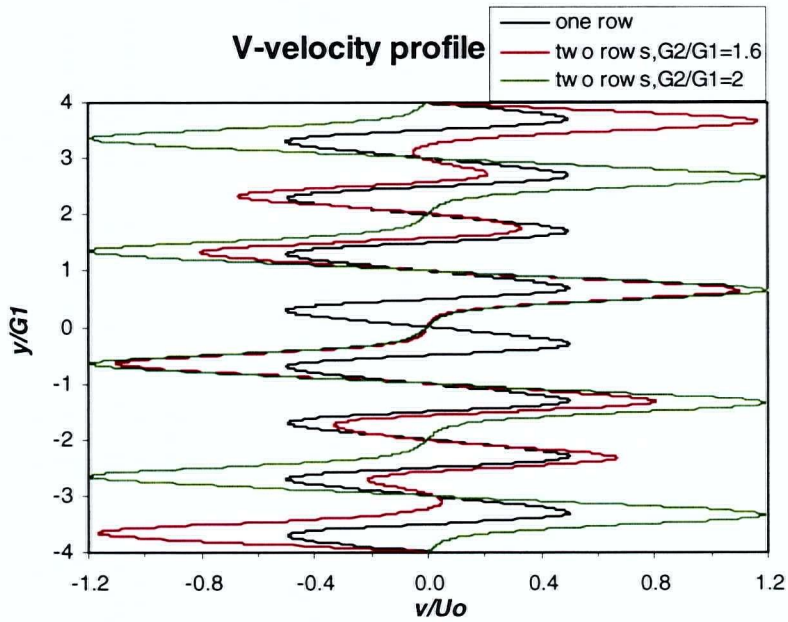

Figure 4.19 U and V velocity profile of steady simulation at $Re = 6.5$, $Z/d = 0$, $D/d = 3$
Effect of different CD separations of two layers

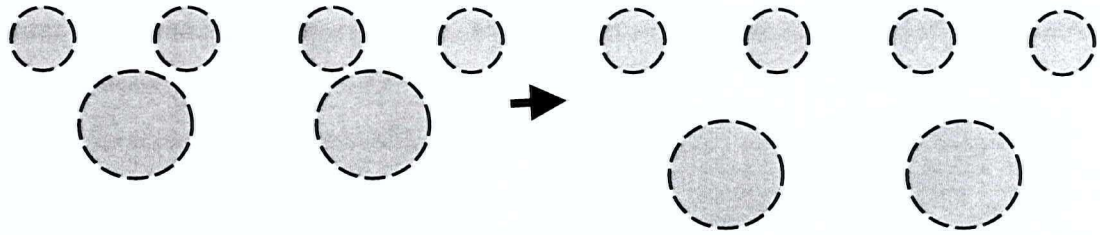

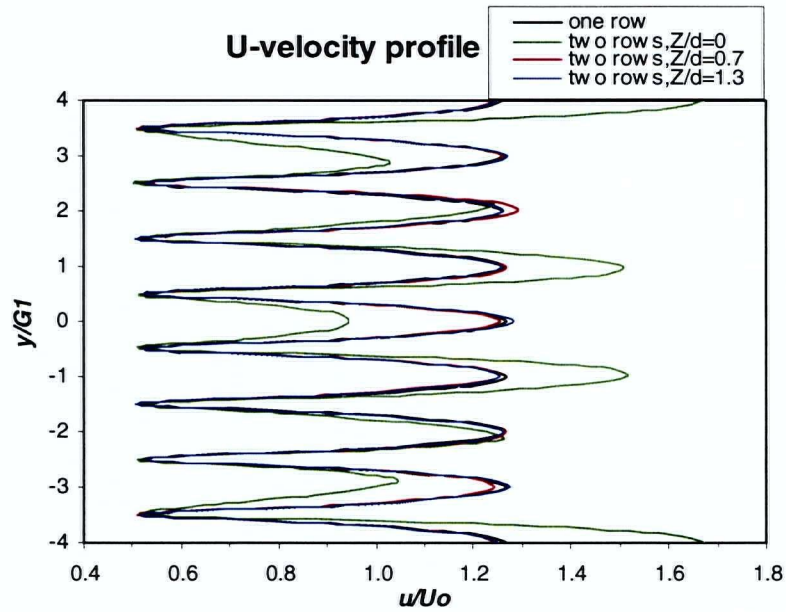

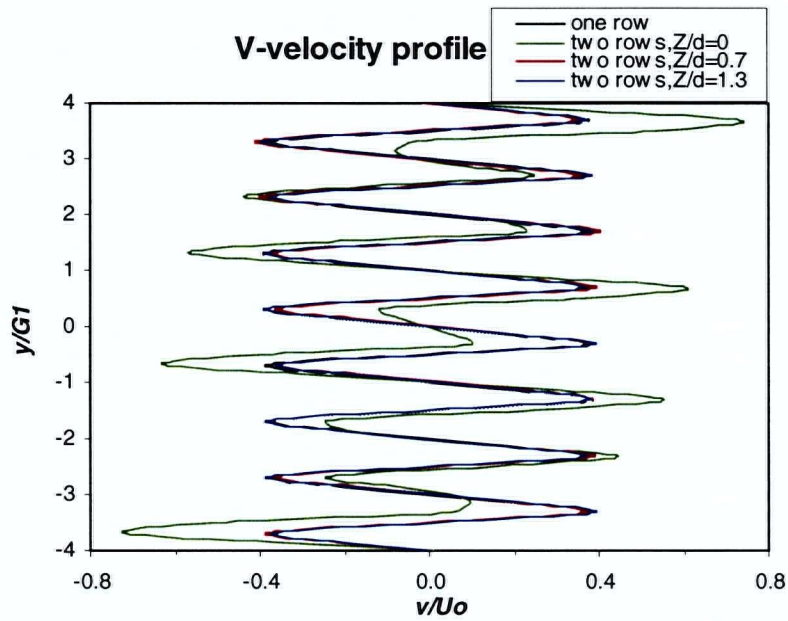

Figure 4.20 U and V velocity profile of unsteady simulation at Re = 65, D/d =2.3, $G2/G1$ = 1.6
Effect of z direction separation between two layers

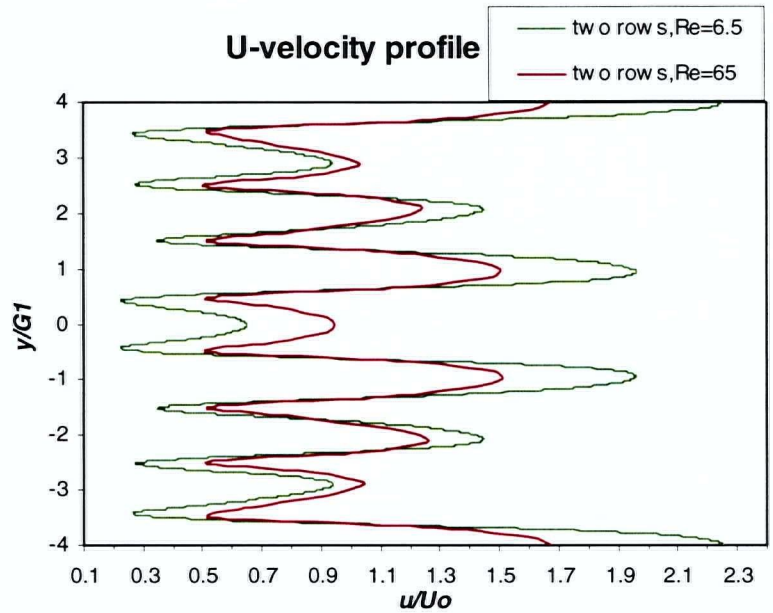

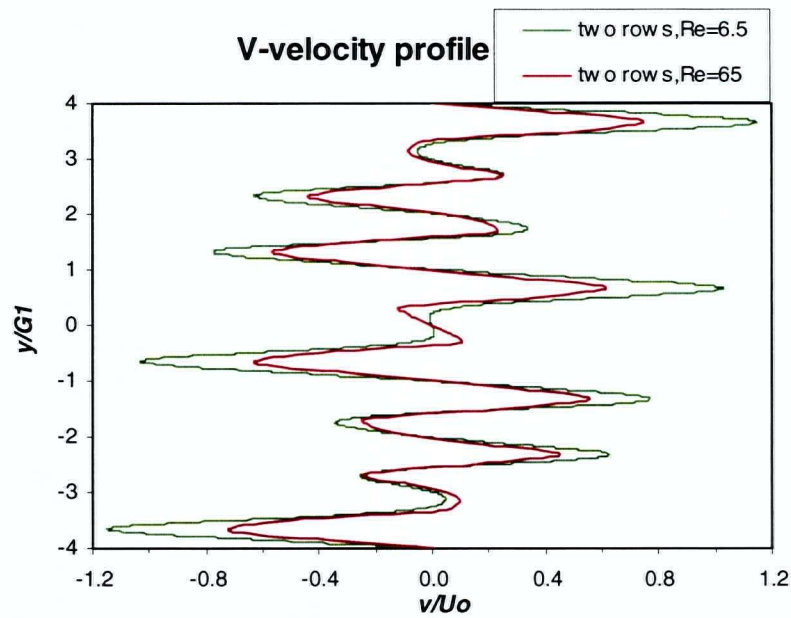

Figure 4.21 U and V velocity profile of steady and unsteady simulation at $Z/d = 0$, $D/d = 2.3$, $G2/G1 = 1.6$
Steady vs. unsteady, effect of Reynolds numbers

4.2 Tentative design

In this section we will simulate a hypothetical triple-layer scenario that would be of interest to forming fabric manufacture. This would be a very fine paper side mesh in

close z direction proximity to a very coarse mesh machine side layer. This hypothetical triple-layer fully meets the design requirements. Some representative dimensions for one such arrangement would be [9]:

- Paper side diameters of 0 .11 mm for both MD and CD filaments
- CD separation of 0.25 mm
- Machine side diameters of 0.35 mm for the MD filaments and 0.40 mm for the CD
- CD separation on the machine side of 0.55 mm
- Average z direction separation of 0.30 mm

The relevant geometrical parameters for this fabric shown in Figure 4.1 are:

$d = 0.11$ mm

$D = 0.35$ mm or $D/d = 3.182$

$G1 = 0.25$ mm or $g1 = G1/d = 2.273$

$G2 = 0.55$ mm, or $g2 = G2/D = 1.571$, $G2/G1 = 2.2$

$z = 0.30$ mm corresponding to $Z = 0.07$ mm or $Z/d = 0.6364$

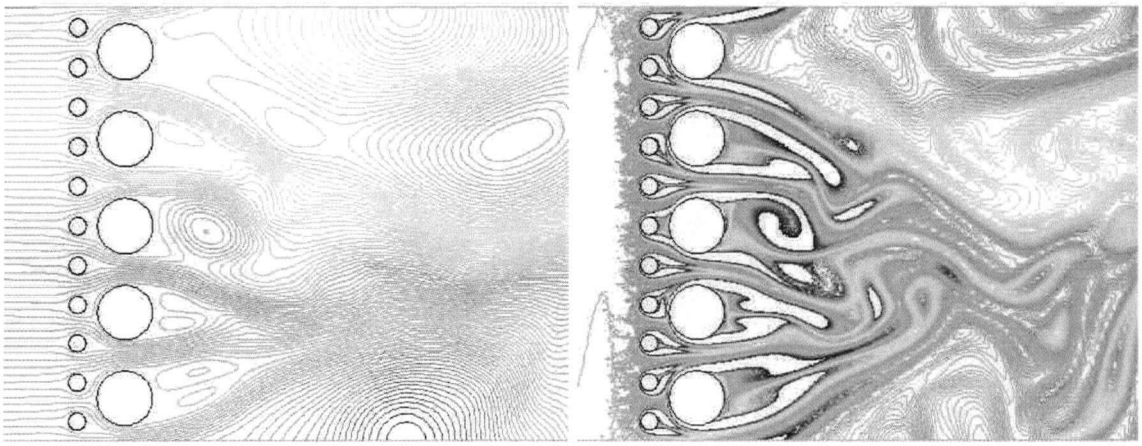

Figure 4.22 Instantaneous stream function and vorticity magnitude of flow through two rows cylinders at $Re = 55$, $Z/d = 0.6364$, $D/d = 3.182$, $G2/G1 = 2.2$: Periodic lateral boundary condition

One of the conclusions from the previous section was that when the fabric has a fine mesh on the paper side and a coarse mesh on the machine side, the z direction separation between the paper side and machine side layers has the most significant effect on the shadow marking. To find out shadow marking effect of this fabric configuration simply

requires finding out the z direction separation between two layers at which the effect diminishes. Figure 4.23 shows an unsteady simulation at current configuration at $Re = 55$ corresponding to incoming velocity $U_o = 0.5$ m/s. It can be seen that there is only a modest effect shown at a higher incoming flow speed. The corresponding wake pattern is also given in Figure 4.22.

4.2.1 Effect of gap

The steady solution is given in Figure 4.24 for the same configuration. As expected, at a lower incoming flow speed, the flow upstream is more sensitive to the existence of the second row than at a higher speed. This also confirms the findings of previous section. When z direction separation between the two layers is increased to 0.40 mm, i.e., $Z/d = 1.545$, the flow upstream is totally undisturbed.

4.2.2 Effect of variable pitch

Figure 4.25 gives the velocity profiles at $Z/d = 1.545$ but with a variable spacing between the adjacent cylinders in the second row, i.e., $G2$ is not a constant value. It represents a slight error occurred when manufacturing the fabric. The largest $G2/d$ is 6.5 and the smallest one is 4.3. The velocity profiles undergo visible changes. The asymmetric geometry appears to play an important role and introduces more complicated phenomenon. This kind of error should be avoided or otherwise the z direction separation between the two layers should be increased to eliminate the impact on flow upstream. As this separation is increased to $6d$, the velocity profiles closely match such that the differences are negligible as shown in Figure 4.25. Because these extra variations on velocity profile were brought by the irregularity in the downstream fabric, it might be appropriate to relate the z direction separation to the largest spacing between two adjacent cylinders in the downstream row. As a rough rule of thumb, provided the fine layer is more than L upstream of the coarse layer, where L is the scale of the largest irregularity in the downstream fabric (e.g. the width of two grouped filaments), then the flow above the fine layer is unaffected by the coarse layer. For this case, $L = 6.5d$.

In summary, because unsteady simulation at a higher speed corresponding to the early stage of paper formation gives a more realistic estimate of the impact on the shadow marking, and because the unsteady solutions of this hypothetical triple-layer fabric show that there is no disturbance to the flow upstream, the configuration of the fabric might work.

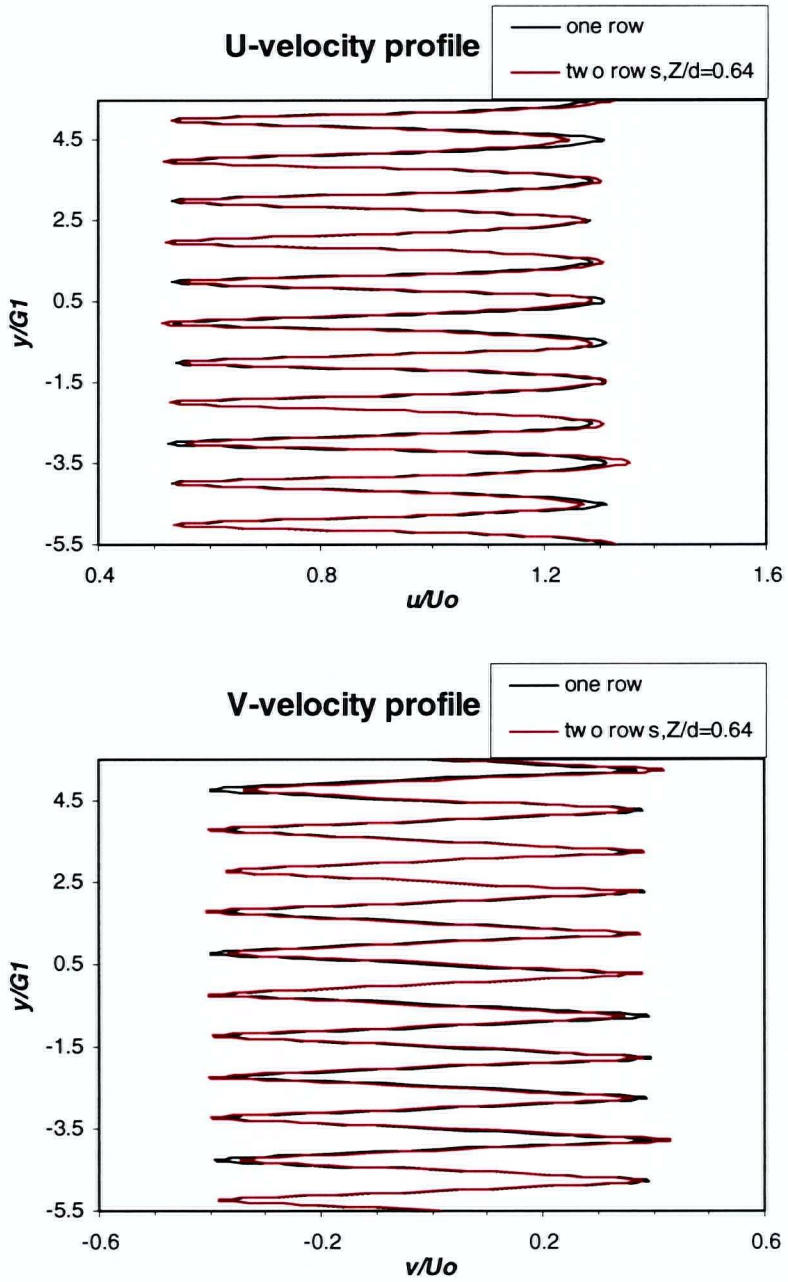

Figure 4.23 Velocity profile of unsteady simulation at $Re = 55$, $Z/d = 0.6364$, $D/d = 3.182$, $G2/G1 = 2.2$

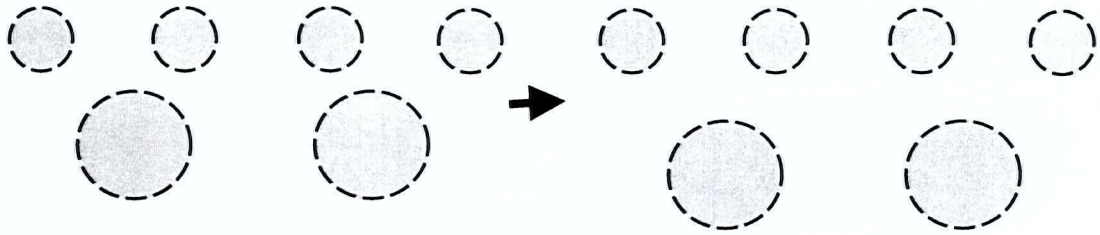

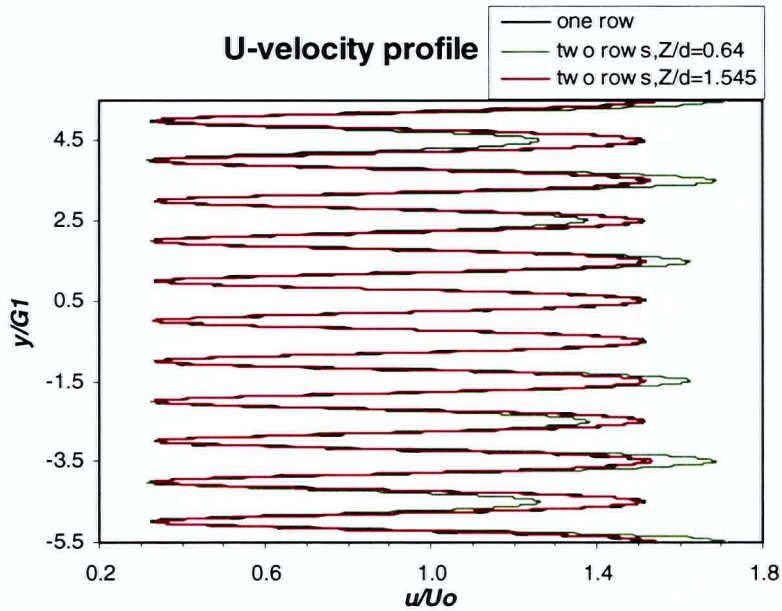

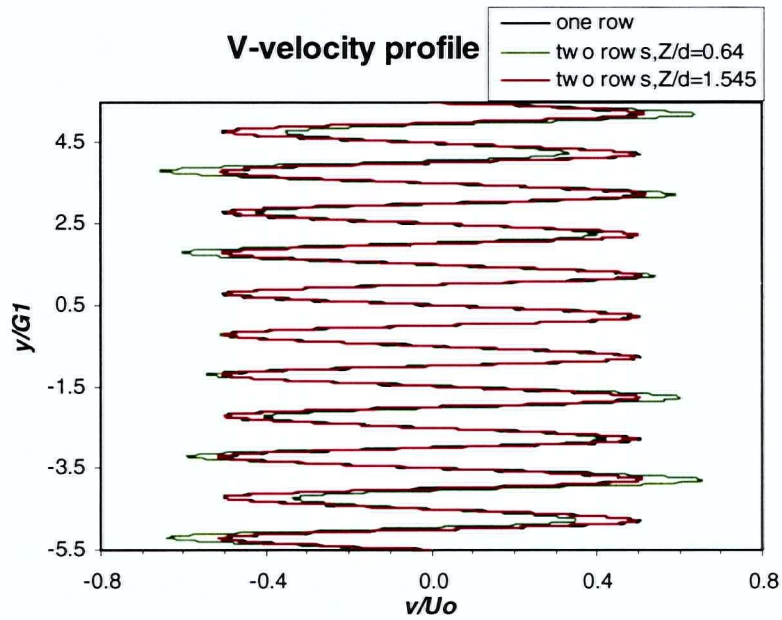

Figure 4.24 Velocity profile of steady simulation at *Re* = 5.5, *D/d* =3.182, *G2/G1* = 2.2

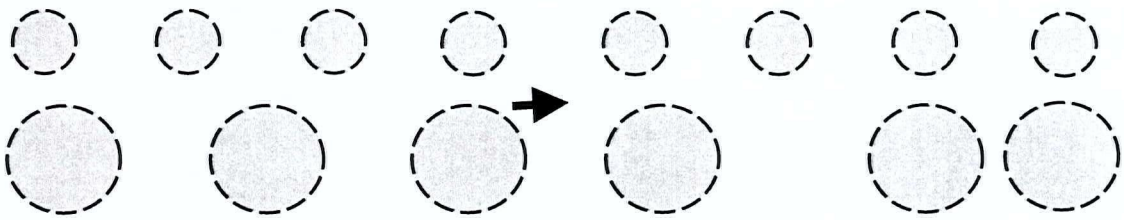

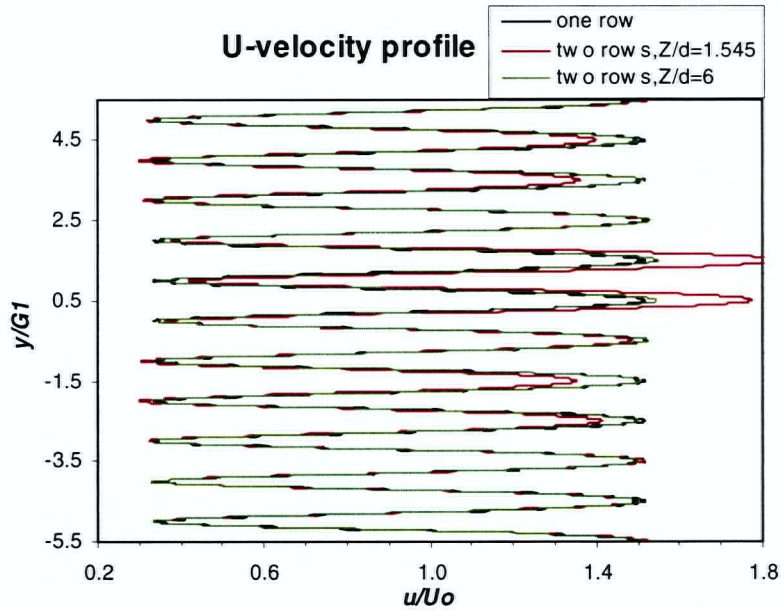

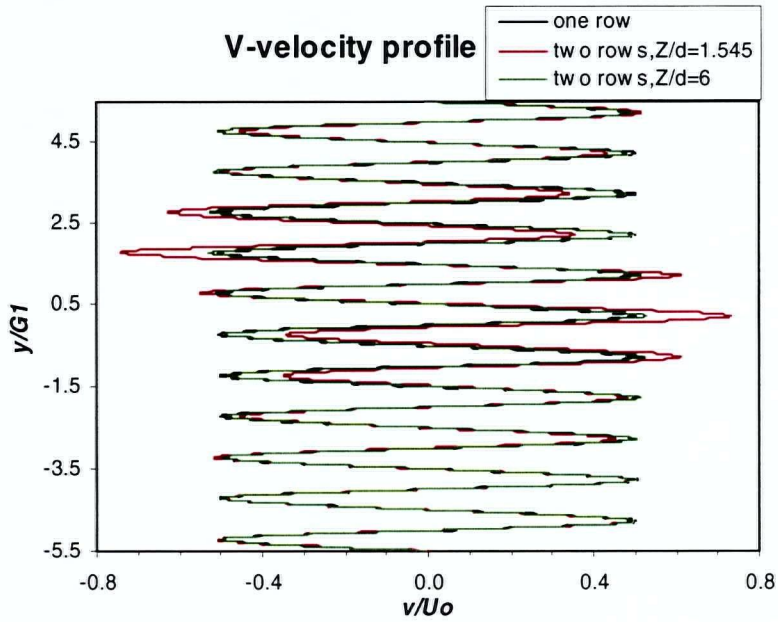

Figure 4.25 Velocity profile of steady simulation at *Re* = 5.5, *Z/d* = 1.545, *D/d* =3.182, a variable *G2*

Chapter - 5 Conclusions and Recommendations for Future Work

In summary, a computational model has been applied for the first time to study the flow details through paper machine forming fabrics. The details of the forming fabric structure affect drainage and paper qualities such as shadow marks. The forming fabric structure was modeled as cylinder arrays and two-dimensional laminar simulations were performed. The results give some indication of the conditions under which the support filament structure may affect the paper shadow marking and the uniform drainage.

5.1 Conclusions

As a result of the simulations performed, the following conclusions can be drawn:

1. When the forming fabric has fine mesh in both paper and machine sides, changes in z direction separations of two layers, diameter ratios, or offsets between two layers appear to have little impact on the velocity profiles upstream. Thus under the current configuration of the commercial 73 x 75 mesh triple-layer fabric, the machine side mesh does not cause flow perturbations that could cause shadow marking.
2. When the fabric has a fine mesh on the paper side and a coarse mesh on the machine side, the z-direction separation between the paper side and the machine side layers has the most significant effect on the shadow marking. The critical z direction separation between two layers, at which the effect diminishes, is thus becoming an important parameter of the design of the forming fabric. At or above the critical z direction separation, the flow upstream in front of the paper side layer cannot be disturbed by the machine side layer, and thus will not cause shadow marking. This critical separation is generally not greater than $2d$, where d is the diameter of filaments on the paper side layer.
3. The unsteady calculation at a higher speed corresponding to the early stage of paper formation will give a more realistic estimate of the impact on the shadow marking than the steady simulation at a lower speed does; whereas a more

conservative estimate is given by the steady flow simulation. Also steady simulations give the same trend of impact on the flow upstream as the unsteady simulations, and make it possible to have the same results by using steady simulations instead of unsteady ones. The unsteady calculation of the hypothetical triple-layer fabric under the proposed configuration showed only a modest impact on the flow upstream of the paper side layer caused by the machine side layer. Therefore, the design parameters are confirmed.

4. Unequal CD separation of the machine side layer plays a negative role in shadow marking. The CD separation of the machine side layer should be kept as constant as possible, or otherwise a larger z direction separation between the two layers is required to eliminate the impact on flow upstream. As a rough rule of thumb, provided the fine layer is more than L upstream of the coarse layer, where L is the scale of the largest irregularity in the downstream fabric (e.g. the width of two grouped filaments), then the flow above the fine layer is unaffected by the coarse layer.

5.2 Recommendations for future work

The simplified two-dimensional laminar model of the flow through paper machine forming fabrics has been applied for the first time and some observations are useful to the design of the forming fabrics. However, an experimental study is preferred to validate this model. A PIV (Particle Image Velocimetry) technique will be employed to visualize the flow through cylinder arrays. The pressure drop across the cylinder arrays that relates to the pressure difference across the forming fabric will be measured as well by a differential pressure transducer. A schematic drawing of the test section is shown in

Figure 5.1. The PIV system will provide both qualitative information about the flow field (separation, inter-cylinder jets, etc.) in the region around the cylinders, and quantitative details of the velocity profiles in front of the first-row of cylinders. The velocity profiles will then be compared with the computational results as validation.

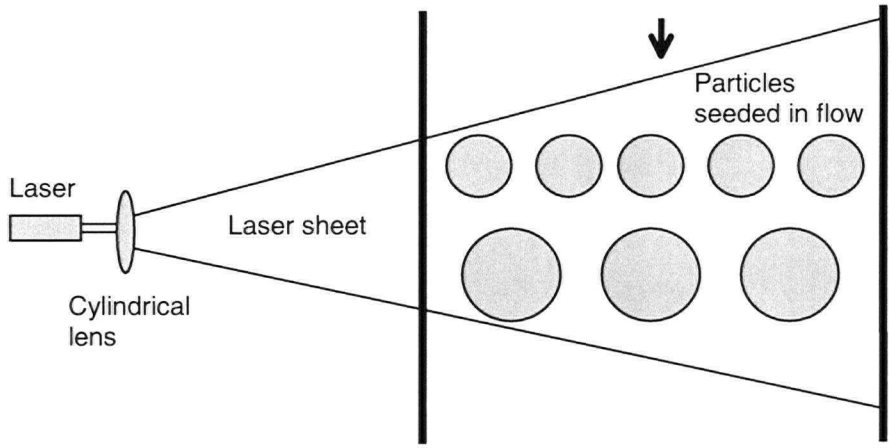

Figure 5.1 Schematic diagram of experimental test setion

A three-dimensional CFD model should be developed. Two-dimensional simulations are less computationally expensive to perform and a lot of useful information can be acquired. However, there are several limitations of this two-dimensional model. First, no information on the machine direction flow can be learned from the two-dimensional simulations. Second, and probably the greatest drawback of the simplified two-dimensional model, is that the CD filaments are neglected. The CD filaments are in close contact with the paper side layer and will have the most significant impact on the flow upstream in front of the paper side layer. Third, because the CD filaments are not considered and the difference between a double-layer and a single-layer fabric is the CD filaments configuration, the two-dimensional model cannot distinguish single-layer fabrics from double-layer ones or different triple-layer fabrics among many configurations of CD filaments. Thus a three-dimensional model is desired. It would be very time consuming to perform such a three-dimensional simulation due to the complex geometry of the fabric. Once the three-dimensional model is developed, it also becomes possible to investigate the effect of different angles of incidence of the flow approaching the forming fabric which is important at the jet impingement region.

References

1. H. Paulapuro, "Papermaking part 1, Stock preparation and wet end," *Papermaking Science and Technology*, **Book 8**, Fapet Oy, Finland, 2000.
2. G. A. Smook, *Handbook for pulp & paper technologists*, Second Edition, Angus Wilde Publications Inc., Vancouver, Bellingham, 1994
3. B. Norman, "On the mechanisms of dewatering in twin-wire and press section," *Nordic Pulp and Paper Research J.*, 1987, pp. 39-42.
4. B. Nordstrom and B. Norman, "Effects on paper properties and retention of the proportion of roll dewatering during twin-wire roll-blade forming of TMP," *J. Pulp and Paper Science*, **22(8)**, 1996, pp. J283-J289.
5. S. I. Green, "Analytical and computational modelling of twin wire blade forming," *Journal of Pulp and Paper Science*, **23(7)**, 1997, pp. J353-J357.
6. S. I. Green, R.H. Zhao, and R. J. Kerekes, "Pressure distribution between forming fabrics in blade gap formers: Blades of finite width and fabrics of finite stiffness," *Journal of Pulp and Paper Science*, **24(2)**, 1998, pp. 60-67.
7. S. Zahrai and F. H. Bark, "On the fluid mechanics of twin wire blade forming in paper machines," *Nordic Pulp and Paper Research J.*, 1995, pp. 245-252.
8. B. Heinola, R. Kilpelainen, J. Schlegel, and L. Maarve, "The influence of forming fabrics on the retention and drainage on gap formers," *Pulp and Paper Canada*, **98(6)**, 1997, pp. 67-70.
9. D. Johnson, AstenJohnson Inc., personal communications.
10. J. Timonen and M. Kataja, "Fluid dynamics and paper making," *Pulp and Paper Technology Review*, 2000, pp. 10-11.
11. S. Green and R. Kerekes, "Modeling the flow through a forming fabric," *NSERC grant proposal*, 2001.
12. K. R. McCumsey, "Drainage interactions between the headbox, forming fabric(s), dewatering elements, and their impact on converting operations," *TAPPI J.*, **1(6)**, 2002, pp. 9-11.

13. M. A. Paradis, J. M. Genco, D. W. Bousfield, J. C. Hassler, and V. Wildfong, "Determination of drainage resistance coefficients under known shear rate," *TAPPI J.*, **1(6)**, 2002, pp. 12-18.

14. R. B. Bird, W. E. Stewart, and E. N. Lightfoot, *Transport Phenomena*, Wiley Press, New York, 1960, pp. 200.

15. W. E. Duplantis and S. I. Green, "Measurements of fibre mat permeability with a new device," *Journal of Pulp and Paper Science*, **28(7)**, 2002, pp. 240-244.

16. J. H. Jong, W. D. Baines and I. G. Currie, "Experimental characteristic of forming fabric and fabre mat," *Journal of Pulp and Paper Science*, **25(3)**, 1999, pp. 95-99.

17. P. M. Moretti, "Flow induced vibrations in arrays of cylinders," *Ann. Rev. Fluid Mech.*, **25**, 1993, pp. 99-114.

18. S. Granger and M. P. Paidoussis, "An improvement to the quasi-steady model with application to cross-flow-induced vibration of tube arrays," *J. Fluid Mech.*, **320**, 1996, pp. 163-184.

19. D. S.-K. Ting, D. J. Wang, S. J. Price and M. P. Paidoussis, "An experimental study on the fluidelastic forces for two staggered circular cylinders in cross-flow," *J. Fluids and Structures*, **12**, 1998, pp. 259-294.

20. K. Nakagawa, K. Kishida and K. Igarashi, "Vortex-induced oscillation and lift of yawed circular cylinders in cross-flow," *J. Fluids and Structures*, **12**, 1998, pp. 759-777.

21. S. Ziada and A. Oengoren, "Flow periodicity and acoustic resonance in parallel triangle tube bundles," *J. Fluids and Structures*, **14(2)**, 2000, pp. 197-219.

22. Y. Zhou, Z. J. Wang, R. M. C. So, S. J. Wu, and W. Jin, "Free vibrations of two side-by-side cylinders in a cross-flow," *J. Fluid Mech.*, **443**, 2001, pp. 197-229.

23. G. Stanescu, A. J. Fowler, and A. Bejan, "Optimal spacing of cylinders in free-stream cross-flow forced convection," *Int. J. Heat Mass Trans.*, **39(2)**, 1996, pp. 311-317.

24. J. W. Scholten and D. B. Murray, "Heat transfer and velocity fluctuations in a staggered tube array," *Int. J. Heat and Fluid flow*, **19**, 1998, pp. 233-244.

25. E. Buyruk, "Numerical study of heat transfer characteristics on tandem cylinders, inline and staggered tube banks in cross-flow of air," *Int. Comm. Heat Mass Transfer*, **29(3)**, 2002, pp. 355-366.

26. S. Ishigai, E. Nishikawa, K. Nishmura and K. Cho, "Experimental study on structure of gas flow in tube banks with tube axes normal to flow (Part I: Karman vortex flow around two tubes at various spacings)," *Bulletin of JSME*, **15,** 1972, pp. 949-956.

27. P. W. Bearman and A. J. Wadcock, "The interaction between a pair of circular cylinders normal to a stream," *J. Fluid Mech.*, **61(3)**, 1973, pp. 499-511.

28. S. Ishigai and E. Nishikawa, "Experimental study of structure of gas flow in tube banks with tube axes normal to flow (Part II: On the structure of gas flow in single-column, single-row, and double-rows tube banks)," *Bulletin of JSME*, **18(119)**, 1975, pp. 528-535.

29. M. M. Zdravkovich, "Review of flow interference between two circular cylinders in various arrangements," *ASME J. Fluids Eng.*, **99**, 1977, pp. 618-631.

30. M. Kiya, M. Arie, H. Tamura and H. Mori, "Vortex shedding from two circular cylinders in staggered arrangement," *ASME J. Fluids Eng.*, **102**, 1980, pp.166-173.

31. T. Nishimura, A "Flow across tube banks," *Encyclopedia of Fluid Mechanics –flow Phenomena and Measurement*, **1** (ed. N.P. Cheremisinoff), 1986, pp. 763-785. Gulf.

32. H. J. Kim and P. A. Durbin, "Investigation of the flow between a pair of circular cylinders in the flopping regime," *J. Fluid Mech.*, **196**, 1988, pp.431-448.

33. Y. Ohya, A. Okajima and M. Hayashi, "Wake interference and vortex shedding," *Encyclopedia of Fluid Mechanics – Aerodynamics and compressible flow*, **8** (ed. N.P. Cheremisinoff), 1989, pp. 322-389. Gulf.

34. D. R. Polak and D. S. Weaver, "Vortex shedding in normal triangular tube arrays," *J. Fluids Struct.*, **9**, 1995, pp. 1-17.

35. D. Sumner, S. S. T. Wong, S. J. Price, and M. P. Paidoussis, " Fluid behaviour of side-by-side circular cylinders in steady cross-flow," *J. Fluids Struct.*, **13(3)**, 1999, pp. 309-338.

36. D. Sumner, S. J. Price, and M. P. Paidoussis, "Flow-pattern identification for two staggered circular cylinders in cross-flow," *J. Fluid Mech.*, **411**, 2000, pp. 263-303.

37. Y. Zhou, R. M. C. So, M. H. Liu, and H. J. Zhang, "Complex turbulent wakes generated by two and three side-by-side cylinders," *Int. J. Heat Fluid Flow*, **21(2)**, 2000, pp. 125-133.

38. H. J. Zhang and Y. Zhou, "Effect of unequal cylinder spacing on vortex streets behind three side-by-side cylinders," *Physics of Fluids*, **13(12)**, 2001, pp. 3675-3686.

39. N. K. -R. Kevlahan and J. M. Ghidaglia, "Computation of turbulent flow past an array of cylinders using a spectral method with Brinkman penalization," *Eur. J. Mech. B*, **20(3)**, 2001, pp. 333-350.

40. C. H. K. Williamson, "Evolution of a single wake behind a pair of bluff bodies," *J. Fluid Mech.*, **159**, 1985, pp. 1-18.

41. K. S. Chang and C. J. Song, "Interactive vortex shedding from a pair of circular cylinders in a transverse arrangement," *Int. J. Numerical Methods in Fluids*, **11**, 1990, pp. 317-329.

42. M. J. Braun and V. V. Kudriavtsev, "Fluid flow structures in staggered banks of cylinders located in a channel," *ASME J. Fluids Eng.*, **117**, 1995, pp. 36-44.

43. P. Le Gal, I. Peschard, M. P. Chauvre, and Y. Takeda, "Collective behavior of wakes downstream a row of cylinders," *Physics of Fluids*, **8(8)**, 1996, pp. 2097-2106.

44. I. Peschard and P. Le Gal, "Coupled wakes of cylinders," *Physical Review Letters*, **77(15)**, 1996, pp. 3122-23125.

45. T. Farrant, M. Tan and W. G. Price, " A cell boundary element method applied to laminar vortex shedding from circular cylinders," *Computers & Fluids*, **30**, 2001, pp. 211-236.

46. *FLUENT 6.0 User's Guide*, Vol. 5, Fluent Inc., Lebanon, NH, 2001

47. J. P. Vandoormaal and G. D. Raithby, "Enhancements of the SIMPLE method for predicting incompressible fluid flows," *Numerical Heat transfer*, **7**, 1984, pp. 147-163.

48. R. I. Issa, "Solution of implicitly discretized fluid flow equations by operator splitting," *J. Comput. Phys.*, **62**, 1986, pp. 40-65.

49. J. H. Ferziger and M. Peric, *Computational Methods for Fluid Dynamics*, Second Edition, Springer, Berlin, New York, 1999.

50. H. V. Patankar, *Numerical heat transfer and fluid flow*, Hemisphere, Washington D.C., 1980.

51. Frank M. White, *Viscous Fluid Flow,* Second Edition, McGraw-Hill, New York 1991.

52. H. J. Lugt, *Vortex flow in nature and technology*, John Wiley & Sons, New York, 1983.

53. M. Coutanceau and R. Bouard, "Experimental determination of the main features of the viscous flow in the wake of a circular cylinder in uniform translation. Part1. Steady flow," *J. Fluid Mech.,* **79(part 2)**, 1977, pp. 231-256.

54. E. M. Saiki and S. Biringen, "Numerical simulation of a cylinder in uniform flow: Application of a virtual boundary method," *J. Comput. Phys.*, **123**, 1996, pp. 450-465.

55. C. H. K. Williamson, "Oblique and parallel modes of vortex shedding in the wake of a circular cylinder at low Reynolds number," *J. Fluid Mech.*, **206**, 1989, pp. 579-627.

56. C. Liu, X. Zheng and C. H. Sung, "Preconditioned multigrid methods for unsteady incompressible flows," *J. Comput. Phys.*, **139**, 1998, pp. 35-57.

57. M. C. Lai and C. S. Peskin, "An immersed boundary method with formal second-order accuracy and reduced numerical viscocity," *J. Comput. Phys.*, **160**, 2000, pp. 705-719.